

**THE RESPONSE OF HAGAFELLSJÖKULL VESTARI
GLACIER, ICELAND, TO FUTURE CLIMATE
SCENARIOS COMPUTED WITH A DYNAMIC GLACIER
FLOWLINE MODEL COUPLED TO A DEGREE-DAY
MASS BALANCE MODEL**



MARK PICKETT

MAGDALENE COLLEGE

JUNE 2009

SCOTT POLAR RESEARCH INSTITUTE

UNIVERSITY OF CAMBRIDGE

LENSFIELD ROAD

CAMBRIDGE

“This dissertation is submitted for the degree of Master of Philosophy”

DECLARATION

This dissertation is the result of my own work and includes nothing which is the outcome of work done in collaboration except where specifically indicated in the text.

The dissertation is no more than 20,000 words in length excluding the acknowledgements, declaration, list of references, tables, captions and appendices.

THE RESPONSE OF HAGAFELLSJÖKULL VESTARI GLACIER, ICELAND, TO FUTURE CLIMATE SCENARIOS COMPUTED WITH A DYNAMIC GLACIER FLOWLINE MODEL COUPLED TO A DEGREE-DAY MASS BALANCE MODEL

MARK PICKETT

JUNE 2009

ABSTRACT

A dynamic glacier flowline model is coupled to a degree-day mass balance model with the purpose of modelling the response of Hagafellsjökull vestari glacier to future climate change scenarios. The degree-day mass balance model is calibrated using mass balance measurements for the period 1997-2007. The temperature and precipitation input for the calibration is provided by a combination of ERA-40 reanalysis data and local weather station records. The calibrated model shows good agreement with the measured mass balances ($r^2 = 0.95$, RMSE = 0.68 m w.e.).

The flowline model is then calibrated against the 2007 surface profile extracted from a DEM constructed from LiDAR data. During calibration the model is run from 1997 to 2007 with the mass balance input provided by the calibrated degree-day model. A number of changes had to be made to the model in order to achieve a good fit with the reference profile. These included a parameterisation of the basal mechanisms of movement (i.e. sliding and deformation of the bed) which was forced by the calculation of water flux at the base; and the introduction of a uniform basal melt rate. The calibrated model calculates the 2007 ice surface profile with an RMSE of 4.41 m. The need to introduce a basal melt rate of 0.8 m yr^{-1} suggests the presence under the glacier of a significant source of geothermal energy.

A range of climate scenarios are imposed on the finalised model to predict the glacier's behaviour between 2007 and 2109. In the 'worst-case' scenario the glacier will lose almost 80% of the 2007 ice volume over the next century. If there is no future climate change relative to the 1978-2007 30-year averages for temperature and precipitation, by 2109 the glacier will lose 30% of the 2007 ice volume and the glacier front will retreat by just over 5 km from its 2007 position.

ACKNOWLEDGEMENTS

I would like to thank Finnur Pálsson of the Science Institute at the University of Iceland for providing access to the data that the team at the University of Iceland have collected. This included data for the bed topography and 1997 ice surface of Langjökull ice cap; the time series of winter, summer and net mass balance measurements; the automatic weather station data for the two locations on Hagafellsjökull vestari recorded in the summer of 2006; and the other useful maps and figures that were provided that have assisted in making this project a success.

I would like to thank Tony Payne of the School of Geographical Sciences at the University of Bristol for providing the original ice flow model Matlab code.

Additionally, I would like to thank Cameron Rye and Gareth Rees of the Scott Polar Research Institute at the University of Cambridge; Cameron for his providing and then assisting in the processing of the ERA-40 reanalysis data and Gareth for providing the Langjökull 2007 LiDAR digital elevation model and his instruction in the use of the ImageJ software package.

Last but not least, I would like to thank Neil Arnold of the Scott Polar Research Institute at the University of Cambridge firstly for providing the initial components of the Matlab code but mainly for his helpful advice and assistance throughout the course of this project.

TABLE OF CONTENTS

TITLE PAGE	1
DECLARATION	2
ABSTRACT	3
ACKNOWLEDGEMENTS	4
TABLE OF CONTENTS	5
LIST OF TABLES	8
LIST OF FIGURES	9
1 INTRODUCTION	15
1.1 Glaciers and Climate	15
1.2 Previous Work	16
1.3 Objectives of the study	20
1.4 The study area	21
1.4.1 Iceland	21
1.4.2 Langjökull ice cap	22
1.4.3 Hagafellsjökull vestari glacier	24
2 THE HAGAFELLSJÖKULL VESTARI FLOWLINE	26
2.1 Constructing digital elevation models	26
2.2 Determination of the glacier flowline	28
2.3 Extracting profiles along the flowline	28
2.4 Determination of glacier width	31
3 THE MASS BALANCE MODEL	33
3.1 Choosing the mass balance model	33
3.2 The degree-day calculation	33
3.3 Collation and processing of the meteorological input data	35
3.4 The Matlab calculation	37
4 MASS BALANCE MODEL – CALIBRATION	38
4.1 Determination of model parameters	38
4.1.1 Determining the temperature lapse rate	38
4.1.2 Determining the precipitation gradient	39

4.1.3	Determining σ	41
4.2	Establishing the degree-day factors	42
4.2.1	Initial calibration	45
4.2.2	'Reverse engineering' the temperature lapse rate	46
4.2.2.1	Jóhannesson (1997), Blöndujökull / Kvíslajökull glacier, Iceland	47
4.2.2.2	Jóhannesson (1997), Illviðrajökull glacier, Iceland	47
4.2.3	Arbitrary values of temperature lapse rate	48
4.2.3.1	Average of studies on glaciers from neighbouring Hofsjökull ice cap	48
4.2.3.2	Lowest value from studies on glaciers from neighbouring Hofsjökull ice cap	48
4.3	The finalised mass balance model parameter values	50
5	MASS BALANCE MODEL – SENSITIVITY ANALYSIS	51
5.1	Sensitivity analysis	51
5.1.1	Sensitivity to temperature lapse rate	51
5.1.2	Sensitivity to the precipitation gradient	55
5.1.3	Sensitivity to snow threshold temperature	56
5.1.4	Sensitivity to σ gradient	56
5.2	Conclusions from sensitivity analysis	56
6	THE DYNAMIC GLACIER MODEL	58
6.1	Basic equations	58
6.2	The Matlab calculation	59
6.3	The default ice flow model parameters	63
7	THE DYNAMIC GLACIER MODEL – CALIBRATION	64
7.1	Glen's flow law coefficient, A	64
7.2	Calibration methodology	65
7.3	Initial investigations with A	65
7.4	Sectioning the transect	68
7.5	Linking ice flow to water flux	70
7.6	Geothermal heating – the missing link?	73
8	THE RESPONSE OF HAGAFELLSJÖKULL VESTARI GLACIER TO FUTURE CLIMATE CHANGE SCENARIOS	80
8.1	Climate change scenarios	80

8.2	Processing and interpolating scenario data	81
8.3	Trends in the scenario data	82
8.4	Results and interpretation	84
9	CONCLUSIONS	87
	LIST OF REFERENCES	90
	APPENDICES	97
	Appendix 1	97
	Appendix 2	118

LIST OF TABLES

- Table 4.1 Example degree-day model parameter values taken from a selection of studies based on Nordic glaciers.
- Table 4.2 Table displaying the wide range of temperature lapse rates that were calculated using either the AWS data from sites L01 and L05 or a combination of the AWS and ERA-40 data.
- Table 4.3 Example degree-day factors (for ice (DDF_i) and snow (DDF_s)) taken from studies on other glaciers in Nordic countries.
- Table 4.4 Model parameters used during initial determination of degree-day factors for snow and ice.
- Table 4.5 Elevations (m a.s.l.) of the measurement locations used in the calibration of the mass balance model and how they changed over time. (Source: F. Pálsson)
- Table 4.6 Finalised mass balance model parameter values.
- Table 5.1 Parameter values used in sensitivity analysis.
- Table 6.1 Default parameters used in the ice flow model.
- Table 6.2 Time taken to complete 10 year run (balance years 1997-1998 to 2006-2007) given changing values of δt . Other parameters constant at $A = 6.8e-15 \text{ s}^{-1} (\text{kP})^{-3}$ and $\delta x = 100 \text{ m}$.
- Table 6.3 Default parameters to be used in the calibration of the ice flow model and throughout the rest of the study.
- Table 7.1 Recommended values of flow parameter A at different temperatures and $n = 3$. (Source: Paterson, 1994)
- Table 7.2 Finalised ice flow model parameters. These parameters will remain unchanged for the modelling of glacier behaviour to future climates.

LIST OF FIGURES

- Figure 1.1 The steps in the relation between the position of a glacier's terminus and the climate. After Meier (1965). (Source: redrawn from Paterson (1994).
- Figure 1.2 Location map of Iceland showing ice caps, the volcanic zone and the central volcanoes (Source: Björnsson, 2002)
- Figure 1.3 Map of Langjökull ice cap with 50 metre contours (grey), boundaries of glacier drainage basins (red), and the remaining extent of ice cap (blue). In addition, the thick blue line through Hagafellsjökull vestari glacier delineates the glacier's flow line (Source: F. Pálsson, personal communication)
- Figure 1.4 Oblique aerial photograph of Hagafellsjökull vestari showing the lobate nature of the glacier's lower slopes. Photo taken on 20th June 1999 looking north from the southern margin of Langjökull ice cap (Source: Sigurðsson and Williams, 2008)
- Figure 2.1 Bed topography of Langjökull ice cap and surrounding area. This is a 100 m cubic interpolation of the original 400 m gridded data. The extent of Hagafellsjökull vestari (HV) is superimposed for reference.
- Figure 2.2 1997 surface topography of Langjökull ice cap at 100 m spatial resolution. The extent of Hagafellsjökull vestari (HV) is superimposed for reference. The raw data for this DEM was based upon dGPS skidoo track runs over the ice cap and provided by the University of Iceland. There are some irregularities at the boundaries of the DEM that it is believed by the author relate to initial processing and interpolation of the dGPS data (note in particular the northern boundary), however, this does not affect the area of interest for this study.
- Figure 2.3 Hill shaded image showing coverage of the LiDAR 2007 data for Langjökull ice cap. The extent of Hagafellsjökull vestari (HV) is superimposed for reference. (Source: SPRI, no date)
- Figure 2.4 Comparison of the Hagafellsjökull vestari flowline as determined by the University of Iceland team (a) and the author's simplified approximation (b). Contours indicate 1997 ice surface.

- Figure 2.5 Profiles along the flowline for the 1997 surface and bed topography provided by the University of Iceland, and the 2007 surface provided by the SPRI. In addition, the 2007 surface after the necessary correction had been performed is also shown.
- Figure 2.6 Representation of the glacier's width at the ice surface in 1997. These widths, in conjunction with the 1997 ice thicknesses, are used by the model as reference data from which updated widths are calculated as the model run progresses and the ice thickness changes.
- Figure 3.1 Image displaying positions of the chosen ERA-40 data grid point (ERA-40) and the Stafholtsey weather station (SWS) relative to Hagafellsjökull vestari (HV) (Image source: Google Maps)
- Figure 3.2 Graph illustrating the good correlation between ERA-40 and real world Stafholtsey weather station temperature data. In order to merge the Stafholtsey data with the ERA-40 data correction factors were applied.
- Figure 4.1 Map detailing sites of measured mass balance on Langjökull ice cap. Mass balance data covering the balance years 1997 through to 2007 were used in the calibration of the mass balance model. Only data from sites along or nearest to the flowline were utilised (L01-07). Data from AWS set up at L01 and L05 over the summer of 2006 was also used in the calibration of the model. (Source: F. Pálsson, personal communication)
- Figure 4.2 Measured winter balance against elevation (▲) for mass balance years 1996-1997 (a) and 1997-1998 (b) using data from sites L01 to L07. Black lines show line of best fit calculated through simple linear regression. The equation solving the line of best fit and the related coefficient of determination (R^2) are also shown for each example.
- Figure 4.3 Basic rules that were followed in the calibration of the mass balance model. The degree-day factors were amended for the next model run based on the distribution of data points from the preceding run. The ultimate goal being to have all points plotted on the dashed, central line.

- Figure 4.4 Measured and modelled net mass balance for the balance years 1996-1997 to 2006-2007 with $DDF_s = 0.0101 \text{ m w.e. } ^\circ\text{C}^{-1} \text{ d}^{-1}$ and $DDF_i = 0.00873 \text{ m w.e. } ^\circ\text{C}^{-1} \text{ d}^{-1}$. Orange line shows calculated linear regression relationship.
- Figure 4.5 Measured and modelled net mass balance for the balance years 1996-1997 to 2006-2007 with temperature lapse rate at $0.0046 \text{ } ^\circ\text{C m}^{-1}$ and degree day factors taken from a study of Illviðrajökull glacier (Jóhannesson, 1997). Orange line shows calculated linear regression relationship.
- Figure 4.6 Measured and modelled net mass balance for the balance years 1996-1997 to 2006-2007 with $DDF_s = 0.00694 \text{ m w.e. } ^\circ\text{C}^{-1} \text{ d}^{-1}$, $DDF_i = 0.00822 \text{ m w.e. } ^\circ\text{C}^{-1} \text{ d}^{-1}$ and temperature lapse rate of $0.0053 \text{ } ^\circ\text{C m}^{-1}$. Orange line shows calculated linear regression relationship.
- Figure 5.1 Percentage change from the default values over elevation for both positive degree-days and the fraction of precipitation that falls as snow given a percentage change in the temperature lapse rate.
- Figure 5.2 (a) Probability density functions for temperature for elevations of 471 m a.s.l. (broken lines) and 1335 m a.s.l. (continuous lines) given mean monthly temperature at 2 m a.s.l. of $1.68 \text{ } ^\circ\text{C}$, temperature lapse rate of $0.0053 \text{ } ^\circ\text{C per m}$ and $\pm 20\%$, and σ as a function of elevation (as per section 4.1.3). (b) Positive degree-days represented graphically from probability density functions in (a). Integration between 0°C and $\infty^\circ\text{C}$ will give number of positive degree-days for this month (October 1996).
- Figure 5.3 Probability density functions for temperature for elevations of 471 m a.s.l. (broken lines) and 1335 m a.s.l. (continuous lines) given mean monthly temperature at 2 m a.s.l. of $1.68 \text{ } ^\circ\text{C}$, temperature lapse rate of $0.0053 \text{ } ^\circ\text{C per m}$ and $\pm 20\%$, and σ as a function of elevation (as per section 4.1.3). Black dashed line denotes snow threshold temperature (1°C) and fraction of area under a curve to the left of this line is the fraction of precipitation that will fall as snow.
- Figure 5.4 Net mass balance gradients for mass balance year 1996-1997 modelled with different temperature lapse rates.

Figure 5.5 Net mass balance gradients for mass balance year 1996-1997 modelled with different precipitation gradient rates.

Figure 6.1 Ice surface profile plot illustrating the 'step' artefacts (along the section indicated by orange arrow) being generated by the ice flow model. Green arrows indicate both the initial bed over-deepening and subsequent hummocky terrain. This profile is the result of a 10 year run (balance years 1997-1998 to 2006-2007) with $A = 6.8\text{e-}15 \text{ s}^{-1} (\text{kPa})^{-3}$ and δt 1 year.

Figure 6.2 Ice surface profile plots illustrating the reduction in 'step' artefacts being generated by the ice flow model as δt is reduced (fractions indicate fractions of a year). Profiles are offset for easier viewing. All profiles are a result of a 10 year run (balance years 1997-1998 to 2006-2007) with $A = 6.8\text{e-}15 \text{ s}^{-1} (\text{kPa})^{-3}$ and $\delta x = 100 \text{ m}$.

Figure 7.1 Screenshot of the ice model calibration graphical user interface. (1) The balance year of the data that the surface profile window (2) and mass balance gradient window (7) are displaying. Within the surface profile window is also found the current modelled surface profile (black line (3)); the 2007 measured profile (blue line (4)); the bed topography (green line (5)); the section of the profile that is ice free (pink line (6)); information pertaining to both chosen parameter values for this particular run (Flow coefficient, Basal melt rate, Meltwater factor) and the time the run was initiated but also the RMSE of the current profile against the 2007 profile; and the region of the profile that has a snow free surface after the mass balance model is run (red line along x axis (11)). (8) is the glacier metrics window and displays calculated ice volume (green), glacier length (blue) and the size of the glacier accumulation zone (red) for each year of the model run. (9) buttons to start and stop the model run and to close the GUI window.

Figure 7.2 Plotted modelled 2007 surface profiles when $A = 6.8 \times 10^{-15} \text{ s}^{-1} (\text{kPa})^{-3}$ (a); $A = 10.0 \times 10^{-15} \text{ s}^{-1} (\text{kPa})^{-3}$ (b); $A = 20.0 \times 10^{-15} \text{ s}^{-1} (\text{kPa})^{-3}$ (c). None of these runs approached an acceptable fit and had RMSE values of 11.22 m, 11.56 m and 19.75 m respectively.

- Figure 7.3 Plotted modelled 2007 surface profiles with sectioned transect. In (a) the values of the flow law coefficient are $A = 2.4 \times 10^{-15}$, 10.0×10^{-15} , $10.0 \times 10^{-15} \text{ s}^{-1} (\text{kPa})^{-3}$ and the RMSE = 10.20 m. In (b) the coefficients are $A = 5.0 \times 10^{-15}$, 13.0×10^{-15} , $25.0 \times 10^{-15} \text{ s}^{-1} (\text{kPa})^{-3}$ and RMSE = 13.55.
- Figure 7.4 Plotted modelled 2007 surface profiles produced with new water flux model. In (a) $\lambda = 0.15$ and $A_0 = 6.8 \times 10^{-15} \text{ s}^{-1} (\text{kPa})^{-3}$ resulting in a RMSE = 9.71 m. In (b) $\lambda = 0.25$ and $A_0 = 5.0 \times 10^{-15} \text{ s}^{-1} (\text{kPa})^{-3}$ resulting in a RMSE = 9.44 m.
- Figure 7.5 Approximation of the cumulative net mass balance for the glacier over the balance years 1996-1997 to 2006-2007 (blue line). Additionally plotted is the difference between the cumulative net mass balance profile and the 2007 measured profile (red dotted line). In this model run the ice flow model was disabled and the only input was the net mass balance for each point as calculated by the mass balance model.
- Figure 7.6 Map detailing the situation of ice caps Langjökull and Hofsjökull relative to the volcanic zone and the central volcanoes within it. Of particular note is the central volcano under the southern part of Langjökull which Hagafellsjökull vestari (HV) overlies. (Source: adapted from Björnsson, 2002)
- Figure 7.7 Long-lived small depressions on Mýrdalsjökull ice cap which are result of long-lived, low magnitude geothermal heat sources. Their diameter is of the same magnitude as the ice thickness and according to Jarosch and Guðmundsson (2007) they are the “most common type of ice surface depression in Iceland”. (Source: Jarosch and Guðmundsson, 2007)
- Figure 7.8 Extract from 2007 surface DEM LiDAR that has then been hill-shaded. The image would suggest that there is a high degree of ‘pitting’ on much of the glacier surface (particularly within orange box). 1997 margin of Hagafellsjökull vestari outlined for reference (blue).
- Figure 7.9 (a) Plotted modelled 2007 surface profile produced with finalised model. $A_0 = 5.3 \times 10^{-15} \text{ s}^{-1} (\text{kPa})^{-3}$, $\lambda = 0.2$ and basal melt rate = $0.8 \text{ m w.e. yr}^{-1}$. Resulting RMSE = 4.41 m. (b) Plot of model error along the profile. There is no indication of major bias in the profile with positive and negative errors occurring along its full length. The sum of errors for all 184 available pairs is only +11.4 m.

Figure 8.1 Graphic providing a qualitative description of the IPCC emission scenarios (Source: adapted from IPCC (2001))

Figure 8.2 Temperature change from the 1961-1990 average over time for the month of January given climate change scenario A2. Triangles (▲) denote points of known data. The only reasonable method for interpolation between these points was through the calculation of simple linear relationships between successive points (red lines). This process was performed for all months for temperature data and the combined annual change for precipitation data for each climate scenario.

Figure 8.3 Annual temperature change (a) and annual precipitation change (b) from the 1961-1990 average against time for each of the IPCC climate change scenarios. Underlying data was calculated by the ECHAM5 global circulation model.

Figure 8.4 Change in the length (a) and volume (b) of Hagafellsjökull vestari glacier over time relative to length and volume as at 2007. Graphs are given for each of the IPCC climate scenarios and also the 1961-1990 and 1978-2007 30-year averages. (N.B. 'steps' in (a) are due to the models 100 m resolution of glacier length).

Figure 8.5 Comparison of glacier surface profiles as at the end of their respective model runs (year 2109). The modelled 2007 surface profile (black dashed line) is included for reference.

1 INTRODUCTION

1.1 Glaciers and Climate

It is now accepted without question that glaciers and climate are inextricably linked. However, it was only as recently as the 1940s, and the work of Matthes, that a direct connection between glaciers and climate was established (Tangborn, 1980). It was further work, first by Ahlmann and then by Nye (*in* Tangborn, 1980) and Hoinkes (1968), that managed to clearly demonstrate definite relationships between climate, energy exchange, mass balance, and the dynamic response of glaciers. These relationships can be represented in the simple flow chart, Figure 1.1, below.

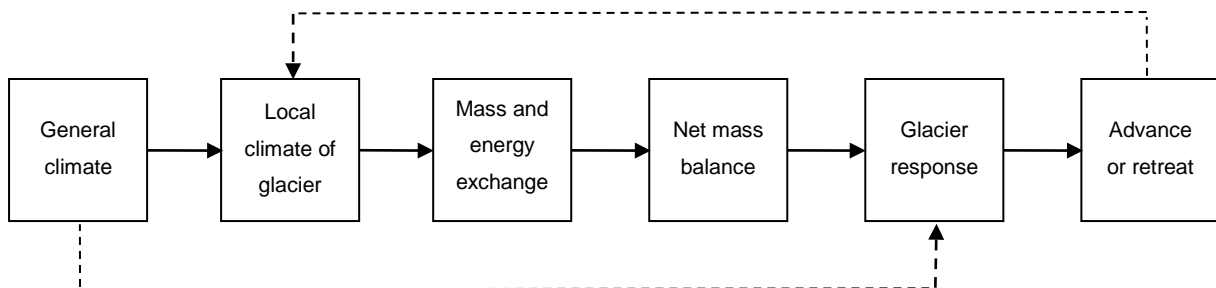


Fig. 1.1 The steps in the relation between the position of a glacier's terminus and the climate. After Meier (1965). (Source: redrawn from Paterson (1994))

The dashed lines in Figure 1.1 indicate a few of the further connections that exist such as climate changing the ice temperature and therefore the flow of the glacier without affecting the mass balance, and the feedback on local climate from changes to glacier properties like glacier extent or the surface albedo (Paterson, 1994). It was deduced that the feedback loops between these factors can be used to explain the current state and behaviour of a glacier in response to the climate of the present and the recent past (Tangborn, 1980).

As a result of this intimate relationship between climate and glacier behaviour, glaciers are considered to be high-confidence indicators of air temperature change and thus have been the subject of many studies into changing climate. A considerable advantage of glaciers over much larger bodies of ice (specifically the Greenland and Antarctic ice sheets) is their far shorter dynamic response time. This is the time in which a body of ice takes to reach equilibrium with climate and whilst it is estimated that the present-day response time of the Greenland ice sheet is some 3,000 years, the response time of a valley glacier is of the order of a few centuries or even decades (Bamber and Payne, 2004). Given this short response

time, Oerlemans (1994) was able to use historical records of glacier length collated by the World Glacier Monitoring Service to derive an independent estimate of global temperature change over the previous century. This value of +0.66 K is sandwiched by the more recently derived values of the Intergovernmental Panel on Climate Change (IPCC) of +0.6 K (for the period 1901-2000) and +0.74 K (for the period 1906-2005) (IPCC, 2007). Oerlemans (2005) repeated this process with a more comprehensive database of glaciers (169 compared to the 48 of the 1994 study) and achieved very similar results for the 20th century global temperature change. Such results demonstrate the great potential afforded by glacier monitoring and study.

Recent research has also highlighted the disproportionate impact that valley glacier and ice cap melt is having on global sea-level. Whilst only 3% of the planet's ice is found outside of the Antarctic and Greenland ice sheets, between 2003 and 2008 it accounted for 60% ($1.1 \text{ mm} \pm 0.25 \text{ mm yr}^{-1}$) of the sea-level rise attributed to ice melt (Meier et al, 2007). In addition, whilst between 1993 and 2003 only 40% of sea-level rise has been attributed to melting ice, between 2003 and 2008 the figure is estimated to be 75-85% (Cazenave et al, 2008) highlighting the increasing importance of ice mass loss, and in particular loss from glaciers and ice caps, on global sea-level. This is a clear demonstration of how, while the two major ice sheets have the potential to dramatically affect our lives in the future, smaller bodies of ice are already starting to do so and that it is essential that monitoring programmes and research on them continues.

1.2 Previous Work

Whilst in recent years the importance of long-term glacier monitoring programmes as tools for understanding and quantifying the climate-glacier relationship has been realised, many of the long standing monitoring programmes were initiated for more prosaic reasons. These include hydropower production (e.g. Tangborn, 1984), local or regional water supply (e.g. Kulkarni et al, 2004) and even tourism (Oerlemans, 1997). As a result, many of the monitoring programmes are situated close to population centres for whom the glaciers are of particular local importance. Others that are established purely for scientific research are quite often chosen for their ease of access. As a result, the glaciers that have been studied in great detail are not truly representative of the glacier population as a whole. Indeed, the most comprehensive data set of parameters of glacier regime (inclusive of mass balance measurements) to date is found in Dyurgerov (2002) but even this collection of 280 time-series datasets represents less than 0.5% of the recognised world population of glaciers. To compound the representation issue, within the available record there is large geographical

bias as demonstrated in Oerlemans (2005) where 93 of the 169 glaciers in this ‘global’ study were situated in the European Alps.

One can use the available data to study the relationship between glaciers and climate with varying degrees of complexity. For example, at the simplest end of the scale, Hoinkes (1968) produced an empirical relationship between glacier growth and the frequency of different types of weather. Progressing from this, initial work into linking climate with individual glaciers employed basic regression techniques and related the mass balance of glaciers to meteorological parameters (e.g. Tangborn (1980) and Letreguilly (1988)). However, one of the most widely used methods in which mass balance is calculated from meteorological input is the degree-day method successfully developed by Braithwaite (1981, 1985) and used and developed further in many studies since (e.g. Reeh, 1991; Laumann and Reeh, 1993; Guðmundsson et al, 2003b; Braithwaite and Raper, 2007; Hughes and Braithwaite, 2008). At its most basic, a positive degree-day model relates melt rate to air temperature through empirical regression. However, as melting only occurs above 0 °C and as this will only happen for certain periods of any given mass balance year, determining the best measure of air temperature is not so simple. An elegant solution to this problem is to calculate the *sum* of positive degree-days such that,

$$S = \sum_i \alpha_i T_i \quad (1.1)$$

where T_i is mean daily temperature and $\alpha_i = 1$ if $T_i \geq 0$ °C (Paterson, 1994). Braithwaite (1985) devised a method for calculating S from mean monthly temperatures and Laumann and Reeh (1993) did the same for mean annual temperatures. Whilst both methods make assumptions about the distribution of temperature over time, these two methods drastically reduce the data input requirements thus making this method very accessible. Once the sum of positive degree-days is known, a regression coefficient (or degree-day factor) can be calculated through calibration with measured mass balances. This method can be refined further through the use of separate degree-day factors for both snow and ice given that snow melts more slowly than ice at a given temperature.

Whilst the positive degree-day method is able to estimate ablation, in order to produce a value of net mass balance accumulation need also be calculated. Whilst studies of Greenland could make the assumption that all precipitation would be as snow (e.g. Reeh, 1991), in other situations a significant proportion would be as rain and thus not contribute to the accumulation mass. A solution for this was devised by Laumann and Reeh (1993) which,

using a similar technique to the positive degree-day methodology above, calculates the proportion of time for which the temperature is below a certain *snow threshold* value. Using the assumption that precipitation is evenly distributed over time, one can then apportion the accumulation from the known total precipitation.

Given that these techniques produce empirical relationships between mass balance and just two meteorological parameters (temperature and precipitation) it is possible to use them without the need for in situ data. The assumption is that data collected at a nearby weather station will closely approximate that experienced at the glacier surface once corrections for change in elevation, and possibly also correction factors for orientation and distance from the data source (e.g. Jóhannesson et al, 1995), have been made. This assumption was tested to the extreme in Rasmussen and Conway (2001) who accurately modelled the mass balance of the South Cascade Glacier in the United States using meteorological data collected by a radiosonde roughly 300 km away. Techniques like this would in theory enable researchers to stop continuous, long-term field study programmes at a few sites and instead carry out more limited field studies at many sites acquiring data purely for ground truthing and calibration. Being able to generate accurate mass balance values from remote rather than in situ meteorological sources has obvious logistical advantages but in addition, being able to parameterise the surface mass balance in terms of a few widely available meteorological variables allows an estimation of the mass balance record back to whenever the records began (e.g. Bøggild et al, 1994). A degree-day model has even been used to reverse-engineer the Pleistocene climate in Greece through the knowledge of historical glacier extent and modern day degree-day factors (Hughes and Braithwaite, 2008). Taking the logical step, with climate change scenarios typically given in terms of temperature and precipitation changes, degree-day modelling is an ideal vehicle for testing the impact on mass balance of future climates (e.g. Laumann and Reeh, 1993).

Whilst most studies using the degree-day methodology employ constant degree-day factors for snow and ice, work by Braithwaite (1995) suggests that in reality they are subject to a whole range of factors that are not accounted for in such models. Guðmundsson et al (2003a) support the notion of Braithwaite but also found that degree-day factors can actually remain remarkably stable even when underlying factors in the energy-balance vary greatly. Their results indicate that this stability is in part due to a cancelling of several independent trends in the energy-balance components. Whilst this lends support to the use of positive degree-day models, Guðmundsson et al (2003a) do note that should the relative timing of these trends alter (say with a warming climate) a degree-day model would not be able to account for the change whereas an energy-balance model would. However, in order to run

an energy-balance model and represent in more detail physical processes involved in accumulation and ablation at a point on a glacier, the knowledge of a large number of variables is required. These can include short-wave radiation, long-wave radiation, surface albedo, wind speed and direction, air and surface temperatures, humidity and precipitation (Laumann and Reeh, 1993). This has been done successfully (e.g. Arnold et al, 1996; Anslow et al, 2008) but the demanding data requirements can make this energy-balance modelling approach highly impractical. Whilst energy-balance modelling is the only viable option for accurately modelling mass balance on the hourly to daily time scale and at a high spatial resolution, degree-day modelling is the obvious choice for a project such as this, being as it is of a far greater temporal scale and of reasonably low spatial resolution.

However, van der Veen (2002) has demonstrated the limitations of both degree-day and energy-balance modelling in an analysis of a study by Huybrechts and de Wolde (1999) in which the dynamic response of the Greenland and Antarctic ice sheets was modelled based upon differing climate warming scenarios. Taking into consideration just the parameter uncertainty in the calculation of mass balance (at 95% confidence ranges), Van der Veen (2002) demonstrated how all three warming scenarios could seemingly result in a *lowering* of sea-levels. Hock (2003) provides a comprehensive review of degree-day models and their limitations with particular reference to their use in mountainous areas that goes into a degree of detail beyond the scope of this study. However, I am confident that for the purposes of this small-scale study the use of degree-day modelling is acceptable in accuracy and, as noted by Hubbard (2006), on occasions there is no alternative.

Thus far the work highlighted has focussed on the modelling of a glacier's mass balance but in order to determine the advance or retreat of a glacier one must also model the physical processes that act on the ice itself causing it to deform and move. Whilst the flow chart in Figure 1.1 is simple the reality is far from it with there actually being myriad feedback loops in effect that are not shown in addition to a range of mechanisms of movement working within the ice (creep and thrusting), at the ice-bed interface (sliding, regelation and enhanced basal creep), and in many cases within the bed substrate itself (deformation of subglacial material, and this material can itself slide over a rigid underlayer) (Knight, 1999). Some examples of feedback loops include the ice thickness - mass balance feedback, nonlinearities arising from complicated geometry, the dependence of ablation on glacier geometry, and the coupling between debris cover, ice flow and ablation (Oerlemans, 1989).

Physically based ice flow models have gone some of the way to account for such mechanisms. These dynamic models attempt to match over time a known behaviour of a

glacier (such as the position of the glacier terminus or longitudinal profile) whilst being forced by mass balance measurements (e.g. Schlosser, 1997). Such models can range from the relatively simple one-dimensional (flowline) models (e.g. Huybrechts et al, 1989; Stroeven et al, 1989) in which each flow mechanism is not modelled explicitly but rather all are accounted for in one or two terms, to the highly complex three-dimensional ice-dynamics models which are then coupled to further models simulating other aspects of the glacial system such as hydrology and isostasy thus forming a model suite (e.g. Flowers et al, 2008). Whilst wanting to represent the glacier system chosen for this project as accurately as possible, the complexities inherent in three-dimensional ice-dynamic modelling place it outside the scope of this project and instead a one-dimensional flowline model will be the basis for physically modelling ice flow.

1.3 Objectives of the study

The overall aim of this study is to simulate the response of Hagafellsjökull vestari glacier to a range of future climate scenarios using a calibrated dynamic ice-flow model with integrated degree-day mass balance model. This can be broken down into a set of subsidiary objectives needed to fulfil this aim:

- 1) The first objective is to review the Matlab scripts of the ice-flow model and degree-day calculation provided by N.S. Arnold (person communication) and to adapt them for use in this project, making additions and adjustments as and when required as the project progresses.
- 2) The second objective is to generate digital elevation models of Langjökull bed topography and 1997 ice surface using the raw data provided by F. Pálsson and from these extract profiles along the flow line of Hagafellsjökull vestari glacier.
- 3) The third objective is to collate temperature and precipitation records for a location as close as possible to Hagafellsjökull vestari glacier for 1997 to 2007, the time period over which mass balance measurements were collected on Langjökull and which have been provided by F. Pálsson.
- 4) The fourth objective is to establish all parameters required for the degree-day mass balance model including determination of the degree-day factors for both snow and ice through calibration with the measured mass balance record.

5) The fifth objective is to calibrate the ice-flow model through comparison to a 2007 ice surface profile of Hagafellsjökull vestari glacier extracted from a digital elevation model generated from LiDAR data and provided by G. Rees (personal communication). The ice-flow model will be forced by the newly calibrated degree-day mass balance model.

6) The sixth objective is to take the finalised model and to run it a century into the future whilst forcing it with different climate scenarios (including three utilised in the IPCC reports) to simulate the glacier's response.

This study uses the 11 years of mass balance measurements and GPS and radio-echo sounding surveys collected and performed on Langjökull by the University of Iceland. Whilst modelling work already utilising parts of this data has been performed on the Langjökull ice cap as a whole, both historically (e.g. Flowers et al (2008) reconstruction of ice cap variation and climate conditions in the Holocene and, in addition, specifically during the Little Ice Age (Flowers et al, 2007)) and predictively (modelled response of Vatnajökull, Hofsjökull and Langjökull ice caps to climate change (Björnsson et al, 2006)), as yet, no modelling has been carried out specifically focussing on Hagafellsjökull vestari.

This study will also be using a digital elevation model of Langjökull produced from airborne LiDAR altimetry data collected in the summer of 2007 by the NERC ARSF. This forms part of a dataset being used by the Scott Polar Research Institute (SPRI) to analyse patterns of surface elevation change across the ice cap. Preliminary results indicate that there are marked spatial variations in elevation changes across the icecap reflecting spatial variations in surface mass balance, moderated by changes in ice dynamics (SPRI, unpublished). The presence of spatial variation adds weight, I believe, to the argument that it is a worthwhile exercise to investigate specific parts of the ice cap in greater detail.

1.4 The study area

1.4.1 Iceland

Iceland is situated in the North Atlantic close to the Arctic Circle between latitudes 63°23'N and 66°32'N and longitudes 13°30'W and 24°32'W. The total area of the country is 103,100 km² and the average height above sea level is 500 m (Einarsson, 1984). At any one time the weather type differs considerably from one part of the country to the other due to topography

and wind direction but the climate of Iceland could generally be described as maritime with cool, dry summers and mild, wet winters (Einarsson, 1984).

Presently, ice covers roughly 11,200 km² (10%) of the total area of Iceland and 60% of this ice overlies Iceland's active volcanic zone (Figure 1.2) (Björnsson, 2002). The four largest ice caps in Iceland (Vatnajökull (8,100 km²), Langjökull (925 km²), Hofsjökull (925 km²), and Mýrdalsjökull (600 km²)) are all either situated within or partially overlie this volcanic zone, however, known volcanic eruptions under the ice caps have been limited to Vatnajökull and Mýrdalsjökull over the last millennium (Björnsson, 2002).

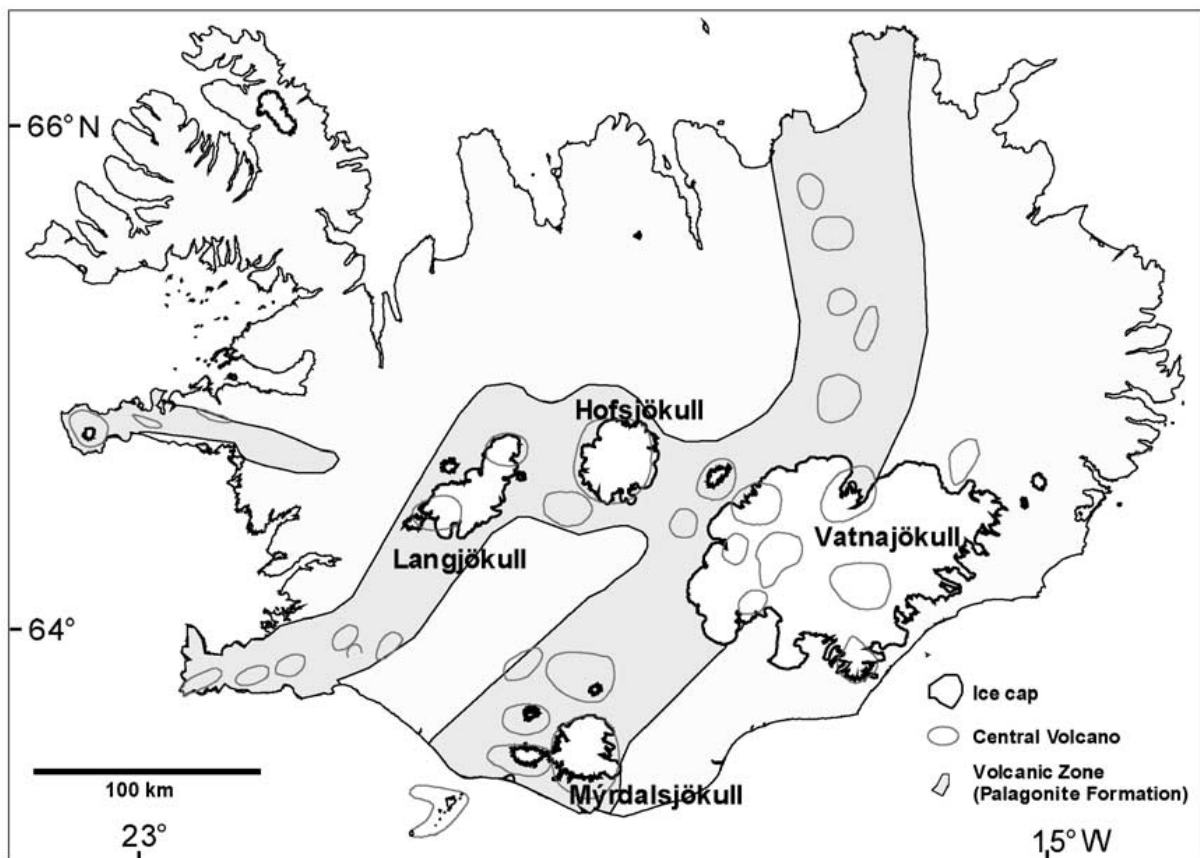


Fig. 1.2 Location map of Iceland showing ice caps, the volcanic zone and the central volcanoes (Source: Björnsson, 2002)

1.4.2 Langjökull ice cap

Langjökull is the most westerly of the four largest ice caps (centred at 64°40'N 20°15'W) and the third largest by ice volume (190 km³ (Björnsson et al, 2006)). It ranges in elevation from 450 to 1,450 m a.s.l. with an average of 900 m a.s.l., and presently has a maximum ice thickness of 580 m (Guðmundsson et al, 2003a; Björnsson et al, 2006). The ice cap is

believed to be resting upon deformable sediments (Hart, 1995) and is drained by 11 outlet glaciers (Figure 1.3). It is believed that a significant part of the glacial meltwater drains directly into the groundwater aquifer (Sigurdsson, 1990 *in* Guðmundsson et al, 2003a).

The outlet glaciers of Langjökull can be split into non-surgings and surging. Non-surgings are located on the steep western and eastern slopes whilst the two surge-type glaciers are found in the south (Björnsson et al, 2003). The surge-type glaciers (Hagafellsjökull vestari and Hagafellsjökull eystri) are characterised by shallow surface gradients (2.9° and 2.7° respectively) when compared to the average for 45 non-surge type Icelandic glaciers (mean and median surface slopes of 11.8° and 7° respectively) (Björnsson et al, 2003).

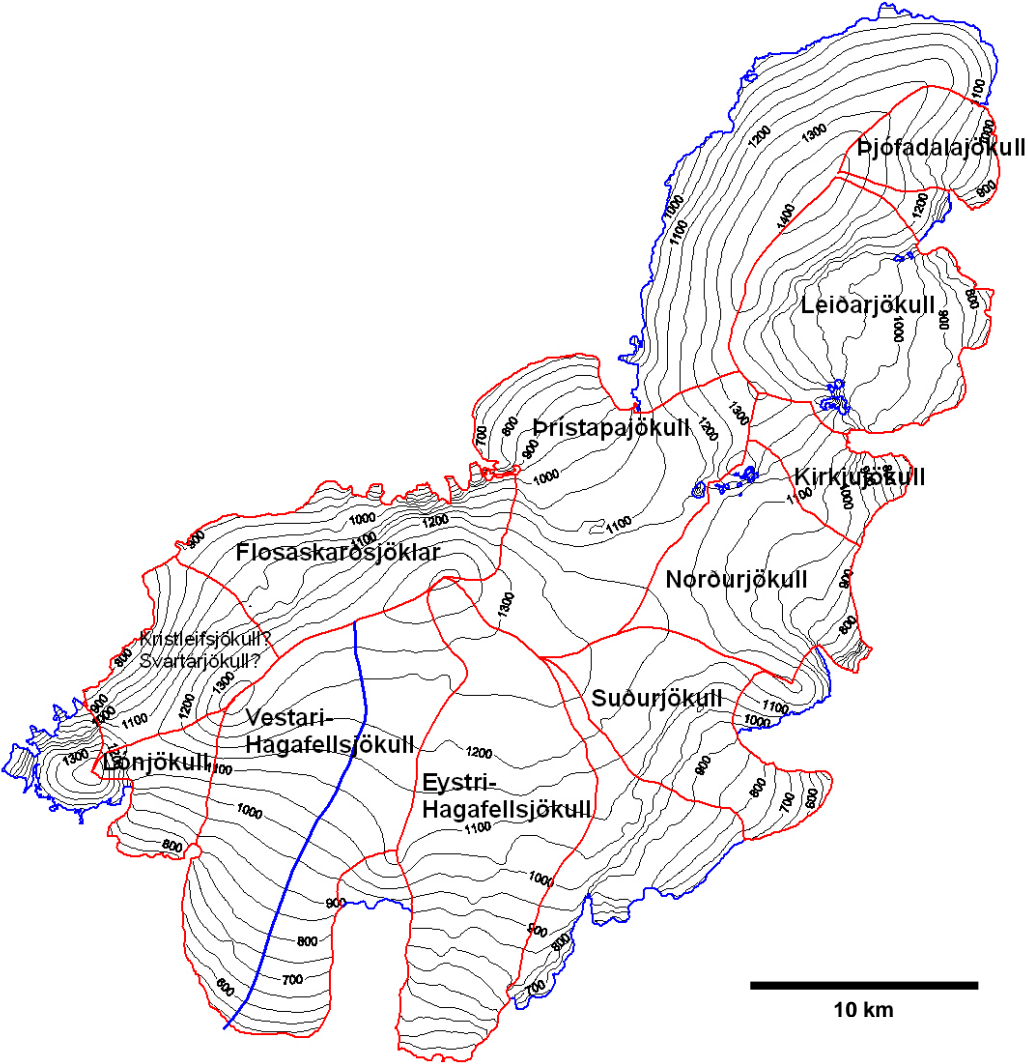


Fig. 1.3 Map of Langjökull ice cap with 50 metre contours (grey), boundaries of glacier drainage basins (red), and the remaining extent of ice cap (blue). In addition, the thick blue line through Hagafellsjökull vestari glacier delineates the glacier's flow line (Source: F. Pálsson, personal communication)

Surges have been recorded for Hagafellsjökull vestari in 1970 and 1980, and Hagafellsjökull eystri in 1974, 1980 and 1999. It is believed that previous to 1970 there was a period of quiescence for at least 40 years for both glaciers (Björnsson et al, 2003). Whilst the two drainage basins are divided by the Hagafell ridge there is evidence to suggest that their surge behaviour is linked. Whilst concurrent surges have only been officially recorded once (1980), from summer 1997 to autumn 1998 the surface velocity of Hagafellsjökull vestari accelerated from 50 to 250 m yr⁻¹ in a zone 4 to 12 km from the glacier front, but then suddenly dropped back again. Björnsson et al (2003) propose that an “incipient surge in the western branch aborted, while a surge of eastern Hagafellsjökull that had begun around the same time continued”.

1.4.3 Hagafellsjökull vestari glacier

Hagafellsjökull vestari (alternatively known as ‘Hagafellsjökull’, ‘Hagafellsjökull vestri’, ‘Vestri-Hagafellsjökull’ and ‘Vestari-Hagafellsjökull’ (Sigurdsson and Williams, 2008)) is the subject glacier for this study. It is a surge-type glacier approximately 20 km in length and with a mean surface slope of 2.9°C. In combination with the neighbouring Hagafellsjökull eystri glacier, it drains most of the southern sector of the ice cap. The margin of Hagafellsjökull vestari is lobate (Figure 1.4) with an approximate surface slope of 3.8° (Eyre et al, 2005), and it extends over a large Holocene basalt lava field (Hart, 1995).



Fig. 1.4 Oblique aerial photograph of Hagafellsjökull vestari showing the lobate nature of the glacier's lower slopes. Photo taken on 20th June 1999 looking north from the southern margin of Langjökull ice cap (Source: Sigurdsson and Williams, 2008)

The ice is believed to be temperate throughout. At the time of their fieldwork (summers of 1999 and 2000), Eyre et al (2005) encountered the widespread presence of moulins implying that meltwater is able to reach the glacier bed freely. They also located a large (~20 m wide) drainage conduit at the margin adjacent to their study area, however, as previously noted, Sigurðsson (1990 *in* Guðmundsson et al, 2003a) believes that a significant part of the meltwater from Langjökull ice cap as a whole drains directly into the groundwater aquifer.

Whilst the last recorded surge event occurred in 1980, there was a period of accelerated surface velocity in a zone 4 to 12 km from the glacier front between summer 1997 and autumn 1998 (Björnsson et al, 2003).

2 THE HAGAFELLSJÖKULL VESTARI FLOWLINE

In order to produce surface profiles along the flowline of Hagafellsjökull vestari on which to base the reference inputs for the model, a number of operations were performed on both the raw data (provided by F. Pálsson) for the 1997 surface and bed topography and also the digital elevation model (DEM) of Langjökull (produced by the SPRI) of the 2007 surface.

2.1 Constructing digital elevation models

The University of Iceland provided raw data for both the bed topography of Langjökull and the surrounding area and also the 1997 surface of Langjökull. Both were in ASCII format (x-lambert193, y-lambert193, z-surface (m a.s.l.) values) with the bed topography at 400 m spatial resolution and the 1997 surface at 100 m spatial resolution. Using Matlab this data was processed into grids to enable construction of the DEMs. In addition, the bed topography was then converted to 100 m spatial resolution through cubic interpolation and ‘snapped’ to the same grid as the 1997 surface.

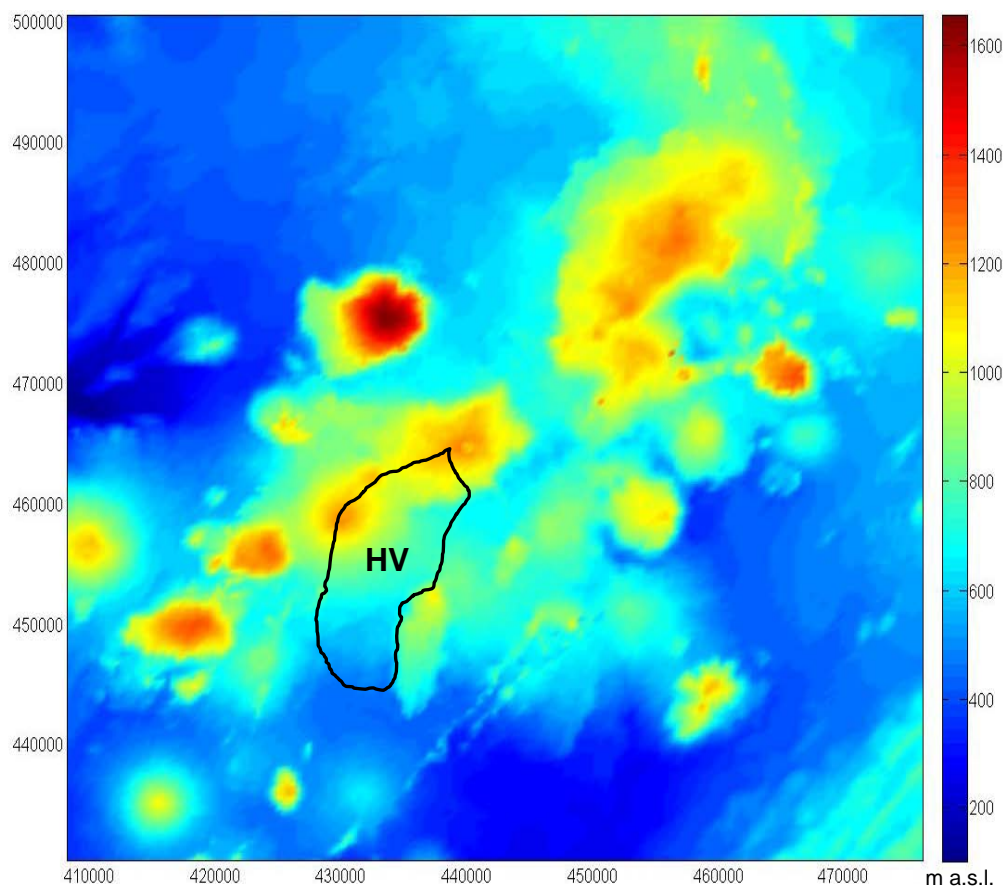


Fig. 2.1 Bed topography of Langjökull ice cap and surrounding area. This is a 100 m cubic interpolation of the original 400 m gridded data. The extent of Hagafellsjökull vestari (HV) is superimposed for reference.

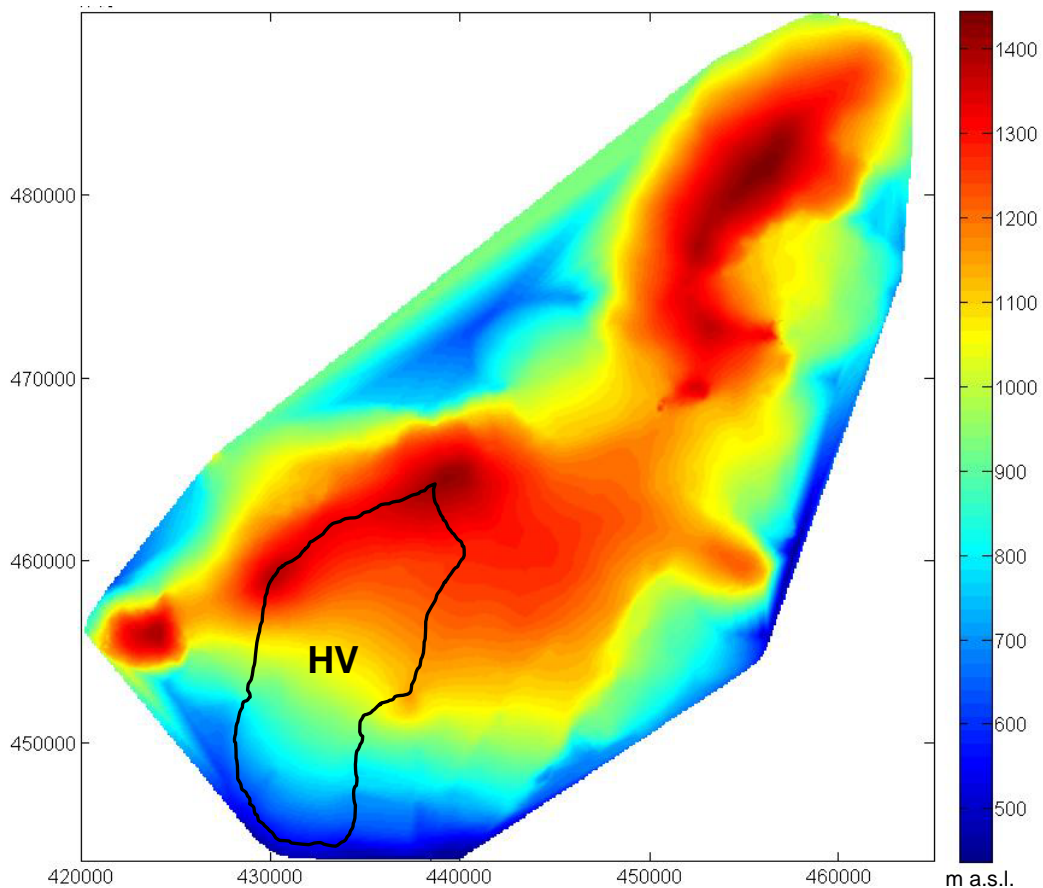


Fig. 2.2 1997 surface topography of Langjökull ice cap at 100 m spatial resolution. The extent of Hagafellsjökull vestari (HV) is superimposed for reference. The raw data for this DEM was based upon dGPS skidoo track runs over the ice cap and provided by the University of Iceland. There are some irregularities at the boundaries of the DEM that it is believed by the author relate to initial processing and interpolation of the dGPS data (note in particular the northern boundary), however, this does not affect the area of interest for this study.

The summer 2007 surface was already processed into a DEM (Figure 2.3). The high, 4 m spatial resolution afforded by the LiDAR data was, however, reduced to 100 m for uniformity with the other DEMs and to enable easier extraction of the flowline. As can be seen in Figure 2.3 there is only partial cover of the Langjökull ice cap. This was due to limited GPS satellite coverage during collection. However, near contiguous coverage was achieved for the Hagafellsjökull vestari glacier and, as will be shown later, a flowline could be extracted for the majority of the glacier from this dataset.

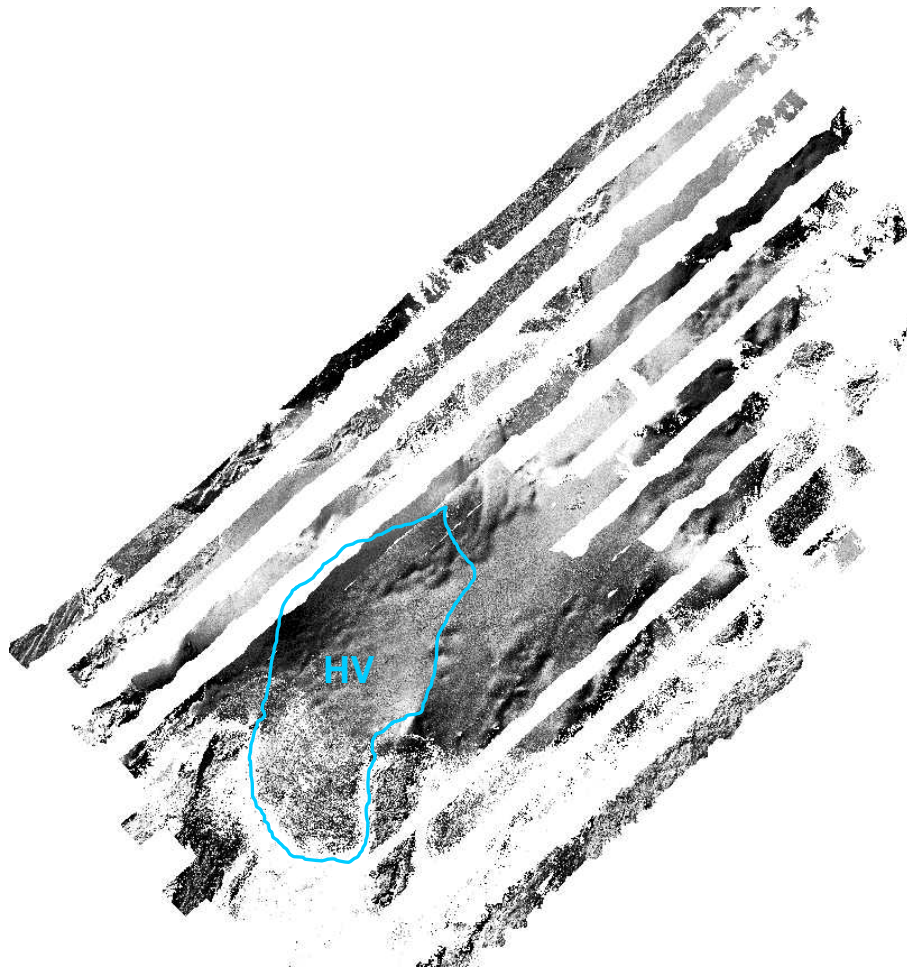


Fig. 2.3 Hill shaded image showing coverage of the LiDAR 2007 data for Langjökull ice cap. The extent of Hagafellsjökull vestari (HV) is superimposed for reference. (Source: SPRI, no date)

2.2 Determination of the glacier flowline

Determining the flowline of Hagafellsjökull vestari through analysis of the DEMs was deemed unnecessary given that the University of Iceland group had already done the required work and provided an image detailing where they calculated it to be (Figure 1.3). However, for this study, a simplification of their flowline was used which consisted of two straight lines as shown in Figure 2.4b.

2.3 Extracting profiles along the flowline

In order to extract the elevation profiles from the DEMs along this newly determined flowline, the imaging package ImageJ was used. This enabled easy extraction of both elevations from the 1997 surface and bed topography DEMs as they could be 'stacked' to ensure the flowline followed the exact same path on both. Stacking was not an option with the 2007 DEM as it was not found to be possible to stack images of differing dimensions. Instead, bedrock features identifiable on both the bed topography and 2007 LiDAR DEMs were used to locate

points along the flowline. ImageJ was again used to extract the actual profile between these points.

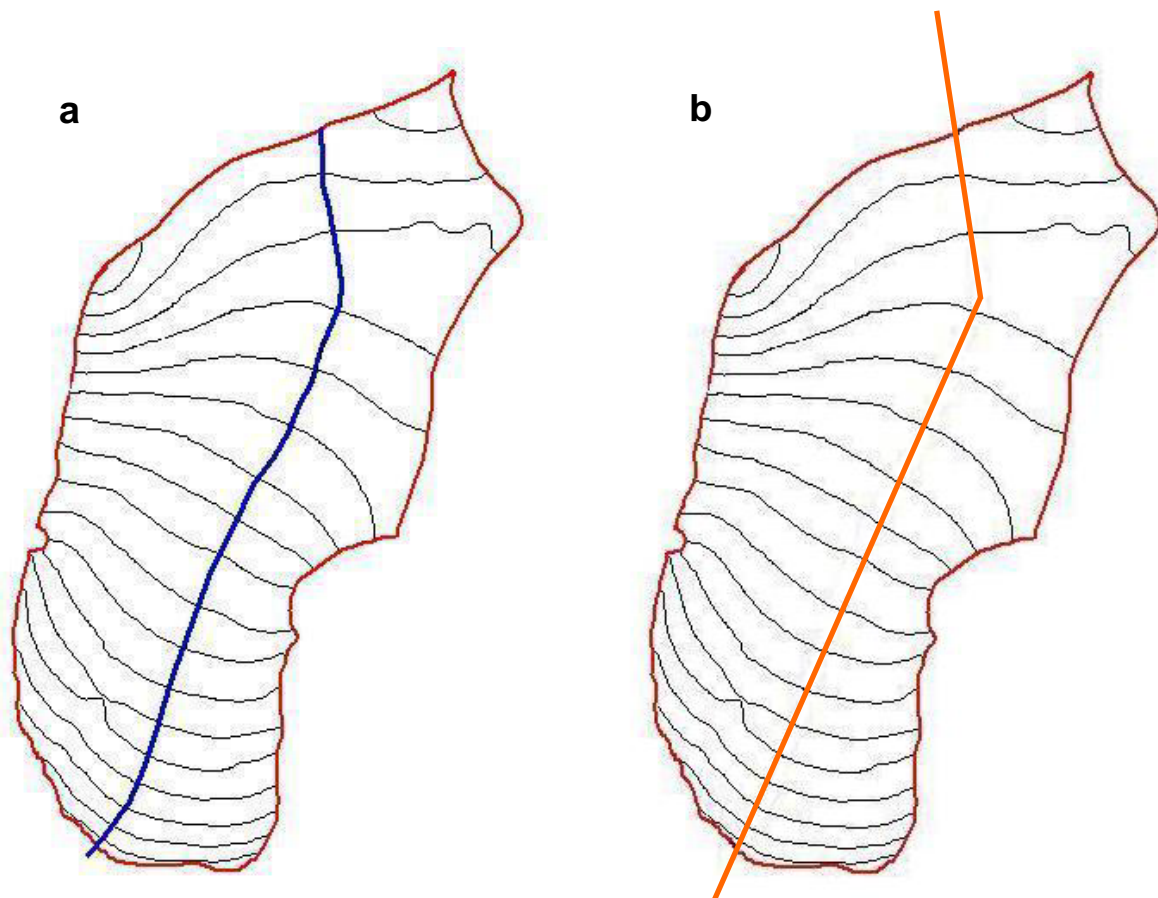


Fig. 2.4 Comparison of the Hagafellsjökull vestari flowline as determined by the University of Iceland team (a) and the author's simplified approximation (b). Contours indicate 1997 ice surface.

It should be noted that in addition to extending the profiles beyond the glacier front (to allow for glacier growth in the model) the profiles also extended beyond the Hagafellsjökull vestari watershed (as implied in Figure 2.4b). This was done due to the limitations at the boundaries of the flowline in the ice flow model in which the initial point on the flowline must be assumed to have zero ice. The flowline was extended far enough (~3.5 km) back from the watershed (as delineated by the bed topography) to ensure that any irregularities caused due to this limitation would not influence the profile along the actual glacier when the model was run. No data from this initial section of the flowline was used in the study and it purely acted as a buffer from the boundary condition. As such, all distances in this study related to the flowline are referencing the watershed grid point, with this point being 0 m, points down the flowline being positive distances, and points in the buffer zone being negative distances.

Due to the nature of the LiDAR data, the extraction of a continuous and unbroken profile of the 2007 surface was not possible. Areas where there had been no return or noise in the

LiDAR signal had to be removed. This was done through visual inspection of the data. As this profile was to be used as a means by which to calibrate the ice model rather than as a starting point from which to run the model, the author deemed it unnecessary to fill the gaps through interpolation. Instead, when analysing the performance of the model through the calculation of the root mean squared error (RMSE) between a modelled profile and the 2007 LiDAR profile, only those points on the profile for which 2007 LiDAR data is available will be considered.

When all three profiles had been extracted it was discovered that there was a systematic error in the elevation values for the 2007 LiDAR data. As can be seen in Figure 2.5, the 2007 LiDAR profile is considerably more elevated than that from the 1997 skidoo dGPS profile.

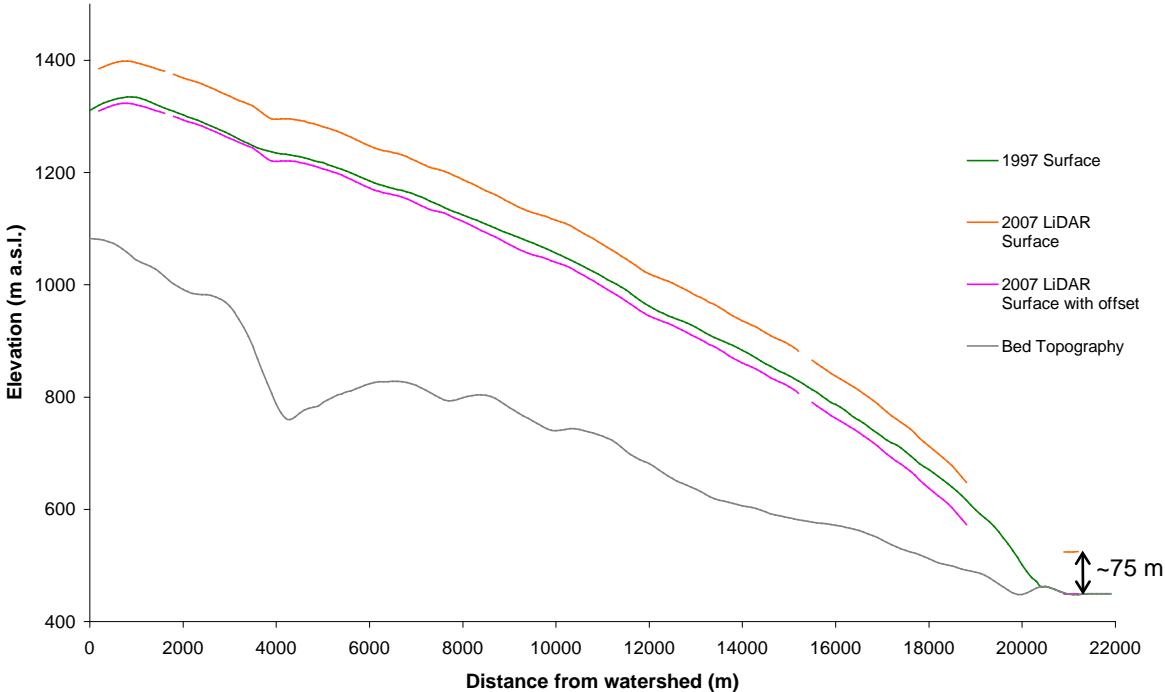


Fig. 2.5 Profiles along the flowline for the 1997 surface and bed topography provided by the University of Iceland, and the 2007 surface provided by the SPRI. In addition, the 2007 surface after the necessary correction had been performed is also shown.

As the transect extended beyond the glacier front and into an ice-free area it was possible to check for systematic error in the profiles. Although the return signal in the LiDAR data had been significantly disrupted by noise in this area, there were 4 consecutive grid points covering a distance of 300 m that could be used. On the assumption that the elevation of the bedrock in front of the glacier has not radically changed between 1997 and 2007 there is an error of almost exactly 75 m in one of the data sets (as indicated in Figure 2.5). Given that the University of Iceland data has been used in a number of published studies, this author deemed it to be more reliable than the LiDAR data which is still to be properly filtered and

checked. Because of this, and on the understanding that the relative error within the LiDAR data is insignificant, this author offset the LiDAR elevation by 75 m along the whole profile. This matched the ice free areas of this profile with that of the bed topography and also gave a more believable profile relative to the 1997 surface.

2.4 Determination of glacier width

The three-dimensional geometry of the glacier is parameterised in the ice flow model by assuming a parabolic cross-section. Given this, a reference glacier width and height must be attributed to each grid point along the transect. The reference height is accounted for by the difference between the 1997 surface and the bed topography. However, in order to provide reference widths it is necessary to somehow measure it at each grid point on the transect and with over 250 grid points this is no small undertaking. As such the author made the decision to measure the width at key points along the transect (such as maxima and minima) and to interpolate between them. This process is complicated by the fact that the model assumes symmetry about the vertical plane through the flowline at each grid point. As can be seen in Figure 2.4 the flowline itself does not even run along the centreline of the glacier immediately leading to issues when replicating the actual glacier geometry in the model. Over the course of the study a number of different reference widths were tried and tested, constantly trying to represent the real-world glacier shape more realistically. The reference widths eventually settled upon (and used throughout the rest of this report) are illustrated in plan view in Figure 2.6.

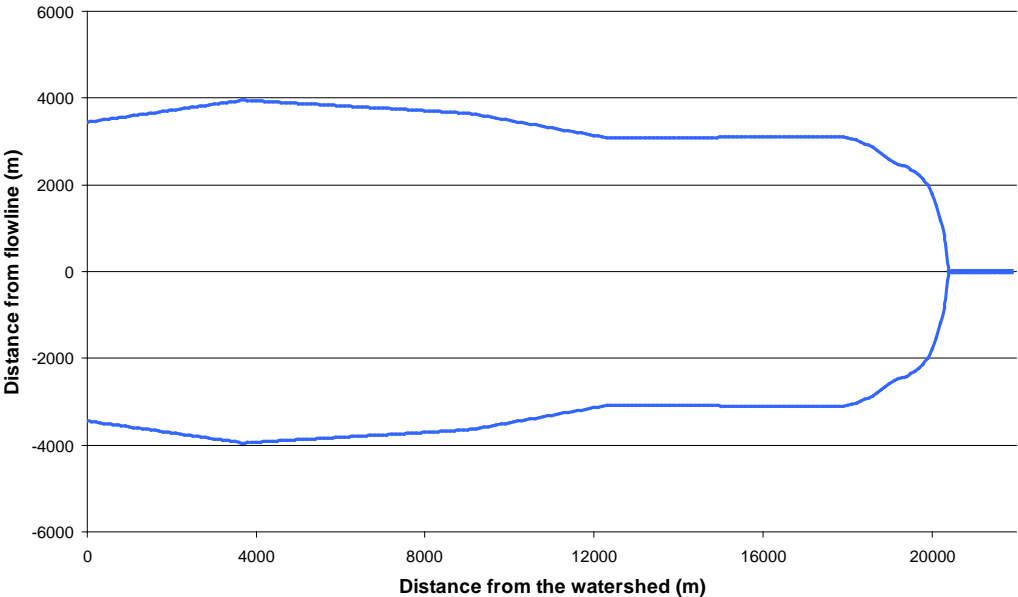


Fig. 2.6 Representation of the glacier's width at the ice surface in 1997. These widths, in conjunction with the 1997 ice thicknesses, are used by the model as reference data from which updated widths are calculated as the model run progresses and the ice thickness changes.

How this model parameterises a glacier's three-dimensional geometry is a cause for concern due to the large discrepancies from the real-world geometry that are undoubtedly introduced. However, this methodology is very similar to those employed in other flowline model studies and has to be accepted as a source of error that is inherent to it. It is a problem that is difficult to solve within a flowline model and can only really be dealt with acceptably by modelling in three-dimensions, something that is beyond the scope of this study.

It should also be noted that given the limitations of the model, it is necessary that even the ice-free points on the transect have a notional ice depth and width in the reference file (in this case the 1997 surface profile) in order that should the glacier front advance it will do so whilst maintaining a realistic three-dimensional glacier geometry.

3 THE MASS BALANCE MODEL

3.1 Choosing the mass balance model

Section 1.2 of this study discussed the advantages and disadvantages of the two most common mass balance models presently in use. An energy-balance model is not a viable option for this study due to the large data requirements needed to run such a model over the time periods used in this project, and because there are no real means with which to run such a model into the future using output from general circulation models

Given this, the clear choice of mass balance model for this study was the degree-day model. They have been shown to provide a reasonable representation of real ablation rates when used over timescales greater than days (Guðmundsson et al, 2003b). Further, there is evidence that the accuracy of the degree-day model can be improved when it is forced by temperature *not* measured in situ. Guðmundsson et al (2003a) note that this appears to be the case particularly when melting is being driven primarily by incoming solar radiation suggesting that such information tends to be “smoothed out” in temperatures over a melting glacier. As remote temperature inputs are going to be used in this study, this can only be a further positive.

3.2 The degree-day calculation

The chosen method for calculation of the glacier mass balance in this study is the degree-day model originally based upon the methodology devised in Laumann and Reeh (1993). The model determines the precipitation, snow accumulation, and melting of snow and ice as a function of altitude based on temperature and precipitation inputs. From this the total accumulation and surface ablation is calculated and the resulting net mass balance determined.

The model computations are based on monthly temperature and annual precipitation values. A statistical approach is used to determine the number of positive degree days and the fraction of precipitation that falls as snow. Temperature deviation from the monthly mean is assumed to be Gaussian in distribution with a standard deviation σ . This stochastic term is used to represent the diurnal temperature cycle in addition to random temperature fluctuations from the monthly mean. This follows the recommendation of Braithwaite (1985). Precipitation is assumed to be evenly distributed throughout time during the computation of snow accumulation.

Precipitation is assumed to fall as snow if the temperature at the altitude in question is below a certain threshold (Jóhannesson et al, 1995). The widely accepted threshold temperature for degree-day modelling on Icelandic glaciers is 1°C (Jóhannesson et al, 1995; Jóhannesson, 1997; Flowers et al 2007, 2008). Thus, the fraction f of the precipitation that falls as snow in a given month is given by

$$f = \frac{1}{\sigma\sqrt{2\pi}} \int_{-\infty}^{T_s} e^{-(T-T_m)^2/(2\sigma^2)} dT \quad (3.1)$$

where T is temperature, T_s is the rain/snow threshold temperature and T_m is the mean monthly temperature. The fraction f from (3.1) is the fraction of the period where $T < T_s$ (Jóhannesson et al, 1995).

Melting of snow and ice is determined from the number of positive degree-days (PDD). The model is able to melt snow and ice at different rates by setting different degree-day factors (i.e. the amount of melt per PDD) for the two surfaces. *PDD* for a month is given by

$$PDD = \frac{365/12}{\sigma\sqrt{2\pi}} \int_0^{\infty_s} T e^{-(T-T_m)^2/(2\sigma^2)} dT \quad (3.2)$$

It should be noted that the number of days in a month has been distributed evenly over the course of a year for simplicity.

When calculating ablation, the model will first ablate any snow by checking for that years accumulation and then (should the snow be completely removed) start ablating the ice underneath at the appropriate rate. If there is snow remaining at the end of the mass balance year, the model assumes that this is then immediately turned into ice for the purpose of the next balance year. There is no allowance for firnification in the model.

The resulting net mass balance calculated by the model relates only to the balance at the glacier surface and is taken as total accumulation over the balance year minus total ablation over the balance year.

3.3 Collation and processing of the meteorological input data

Whilst methods have been devised to recreate the annual temperature cycle from just the mean annual temperature by means of a sinusoidal function (e.g. Laumann and Reeh, 1993) this can lead to an unacceptable degree of error. At the other extreme, whilst daily temperatures could be extracted from the European Centre for Medium-Range Weather Forecasts re-analysis (ERA-40) database this would lead to a large volume of data, not be replicated in the data available for future scenarios and which would, in any case, be revised into monthly mean values for the purpose of the degree-day calculation. Monthly mean temperature values provide a reasonable representation of intra-annual trends whilst keeping data volume low. As precipitation is assumed to be evenly distributed throughout time by the model, total annual figures for this input are acceptable.

Originally, data was only sourced from the ERA-40 repository. A precedent for the use of this data in mass balance modelling has already been set (e.g. Hock et al, 2007) and it is a highly-regarded source of historical climatic information. Raw data for the grid point at 64°08'N 20°15'W (the grid point closest to Hagafellsjökull vestari, just under 50 km to the south of the glacier (Figure 3.1)) was provided by C. Rye of the SPRI (personal communication). This was then processed into the required monthly figures using a Matlab script devised by C. Rye. The monthly temperature data were reorganised into balance years that ran from the beginning of October through to the end of the following September. The monthly precipitation data was also reorganised into balance years but then summed to give annual values.

Initially, the mass balance model was calibrated against only the recorded mass balance values from 1997 to 2002, the overlap with ERA-40 reanalysis data which covers the period 1957 to 2002. In order that the full 11 years of measured mass balance data could be used in the calibration an additional source of temperature and precipitation data was sought. The Icelandic Meteorology Office (IMO) offer access to monthly readings for a number of variables at a large number of weather stations across Iceland on their old website (IMO, no date). This data was systematically searched first to find stations with records that covered the required period and then to establish which of these stations was located closest to the glacier. It was determined that the station at Stafholtsey best fitted the requirements. Given the distance between the sites (Figure 3.1) and the difference in situation and elevation (Stafholtsey being nearer the coast and at higher elevation than the inland ERA-40 grid point which is based on an elevation of 2 m) correction factors had to be devised in order to merge the Stafholtsey data with the ERA-40 data.

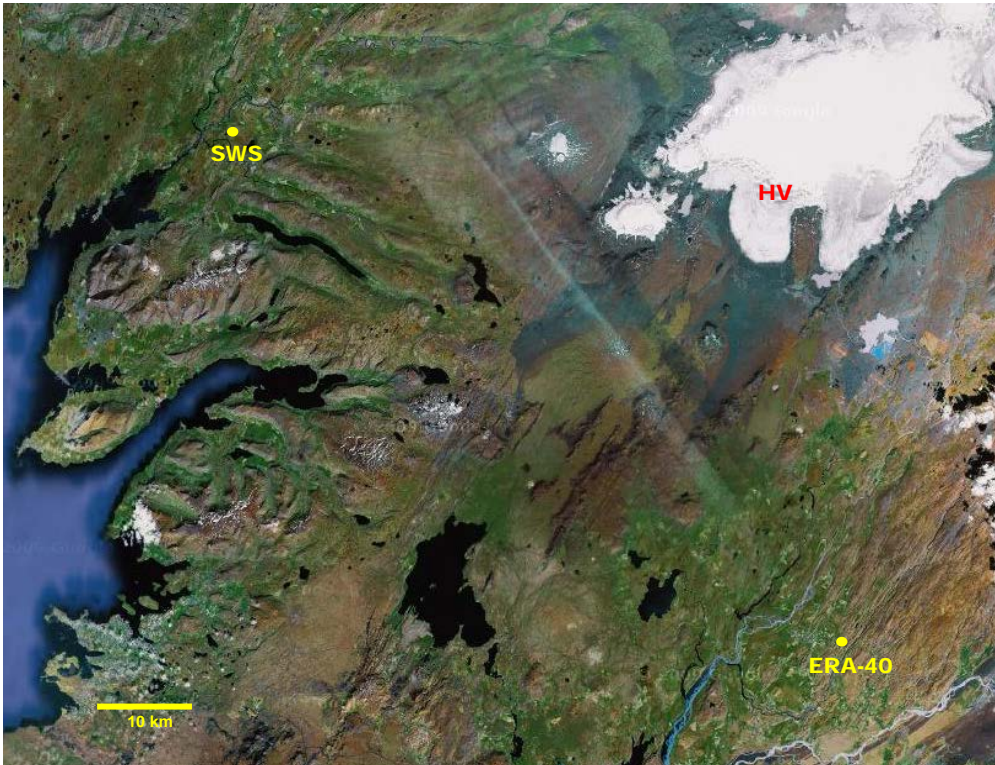


Fig. 3.1 Image displaying positions of the chosen ERA-40 data grid point (ERA-40) and the Stafholtsey weather station (SWS) relative to Hagafellsjökull vestari (HV) (Image source: Google Maps)

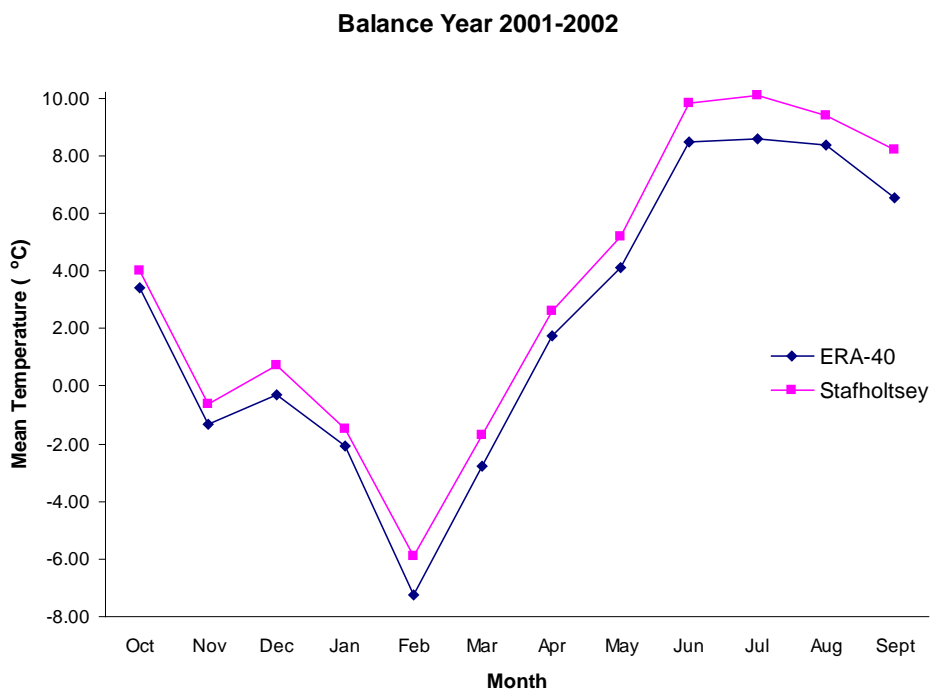


Fig. 3.2 Graph illustrating the good correlation between ERA-40 and real world Stafholtsey weather station temperature data. In order to merge the Stafholtsey data with the ERA-40 data correction factors were applied.

Analysis of the intra-annual temperature cycle for the two data sources shows good correlation (see Figure 3.2). For the period of overlap between the ERA-40 and Stafholtsey datasets, monthly temperature figures were compared and the average differences for each month calculated. The same was performed with the annual precipitation datasets. These were then used to offset the Stafholtsey data between 2002 and 2007 to make it representative of temperature and precipitation at the ERA-40 location over this period. The end result was a set of monthly temperature and annual precipitation data that ran from the balance years 1958 to 2007 but most importantly fully covering period 1997 to 2007 for which measured mass balance data is available.

3.4 The Matlab calculation

Section 3.2 outlined the basis for and fundamentals of the degree day calculation but in the Matlab code minor adjustments and additions were made from the outset and also as the study progressed.

Whilst the precipitation input is an annual figure, the fraction of precipitation as snow is calculated monthly based on the average temperature of the month in question. Given this, it can be run concurrently with the positive degree-day determination and results in the calculation in the code actually being as per (3.3) below

$$f = \sum_{m=1}^{12} \frac{1/12}{\sigma\sqrt{2\pi}} \int_{-\infty}^{T_s} e^{-(T-T_m)^2/(2\sigma^2)} dT \quad (3.3)$$

where the fraction of precipitation that falls as snow over a year is the summation of each monthly calculation divided by number of months in the year. This is only possible given that precipitation is assumed to be distributed evenly throughout the year. For completeness, and given that the model output is the net mass balance over the whole year, it should be noted that the complete *PDD* calculation is

$$PDD = \sum_{m=1}^{12} \frac{365/12}{\sigma\sqrt{2\pi}} \int_0^{\infty} T e^{-(T-T_m)^2/(2\sigma^2)} dT \quad (3.4)$$

This final, annual positive degree-day figure is then used in the calculation of ablation.

4 MASS BALANCE MODEL - CALIBRATION

4.1 Determination of model parameters

In addition to the degree-day factors, there are a range of other parameters that must be determined before the mass balance model can be used. Where possible these should be determined from analysis of actual data, rather than through educated guesswork, in order to limit parameter uncertainty. The parameters in question are the temperature lapse rate, precipitation gradient, and the stochastic term σ from Equation (3.1) and (3.2). Example values for these parameters taken from previous studies on glaciers situated in Nordic countries are shown in Table 4.1 below.

Table 4.1 Example degree-day model parameter values taken from a selection of studies based on Nordic glaciers.

Author	Year	Country	Glacier (Ice Cap)	Temp Lapse Rate (°C per m)	Ppt/Elev Gradient (1 per 100 m)	σ
Jóhannesson (1997)	1997	Iceland	Blöndujökull/Kvísíajökull (Hofsjökull)	0.0060	0.360	3.30
			Illviðrajökull (Hofsjökull)	0.0060	0.496	3.30
Jóhannesson et al (1995)	1995	Iceland	Sátujökull (Hofsjökull)	0.0053	0.550	3.32
		Norway	Nigardsbreen	0.0058	0.090	3.12
		Greenland	Qamanârssûp	0.0066	0.000	3.50
Laumann & Reeh (1993)	1993	Norway	Álfotbreen	0.0070	0.070	4.40
			Nigardsbreen	0.0075	0.080	4.40
			Hellstugubreen	0.0075	0.070	4.40

4.1.1 Determining the temperature lapse rate

Automatic weather stations (AWS) were set up on Hagafellsjökull vestari at two locations (L01 and L05 in Figure 4.1) over the summer of 2006. Given the elevation differential between these two sites (L01 at 490 m a.s.l., L05 at 1100 m a.s.l.) the author saw this as a reasonable opportunity to actually calculate the lapse rate rather than use a default, widely accepted rate or a rate used in a study on a nearby glacier or ice cap.

The raw data consisted of temperature readings every ten minutes and there was temporal overlap between the L01 and L05 datasets for a total of 154 days providing over 22,000 temperature pairs for comparison. With preliminary analysis of the data it quickly became apparent that the temperature lapse rate experienced at Hagafellsjökull vestari is highly variable.

Table 4.2 Table displaying the wide range of temperature lapse rates that were calculated using either the AWS data from sites L01 and L05 or a combination of the AWS and ERA-40 data.

Time Period	L01 Mean Temp (°C)	L05 Mean Temp (°C)	L01 - L05 Lapse Rate (°C per m)	ERA-40 Mean Temp (°C)	ERA-40 - L01 Lapse Rate (°C per m)	ERA-40 - L05 Lapse Rate (°C per m)
Jun	4.41	0.70	0.0061	7.26	0.0058	0.0060
Jul	5.26	1.87	0.0056	9.28	0.0082	0.0067
Aug	5.51	2.20	0.0054	9.75	0.0087	0.0069
Sept	5.13	1.20	0.0064	7.11	0.0041	0.0054
Mean for Jun-Sept	5.08	1.50	0.0059	8.35	0.0067	0.0062
All available data	4.33	0.56	0.0062			

In order to check for temporal variability in the lapse rate the data was initially split into months (where complete months were available - the data ran from the middle of May to the middle of October) and the lapse rate calculated. As can be seen from Table 4.2 the range in lapse rate for these four consecutive months is nearly as great as the range in the three temperature lapse rates used by Jóhannesson et al (1995) in their study of three glaciers in three different countries (see Table 4.1).

Further combinations of temperature data were used in an effort to find some parameter stability including the use of the ERA-40 mean monthly temperatures for the same period, the results of which are shown in the right hand side of Table 4.2. However, this further analysis only served to reinforce the realisation that this parameter is not stable through time. Of course the situations of the two AWS could be quite different as they are over 10 km apart, even still such great variability had not been expected by the author.

A value still had to be chosen however, and the obvious choice was to use the rate calculated over the greatest period of time and so 0.0062 °C per m will be used in the calibration of the model. There is no doubt however that this is a parameter of great uncertainty.

4.1.2 Determining the precipitation gradient

A method intimated to in Jóhannesson et al (1995) was employed to calculate the precipitation gradient and related starting elevation. The mass balance records supplied by

F. Pálsson included the winter-balance measurements and these were plotted against elevation for each of the 11 available years for sites L01 to L07 (locations as per Figure 4.1).

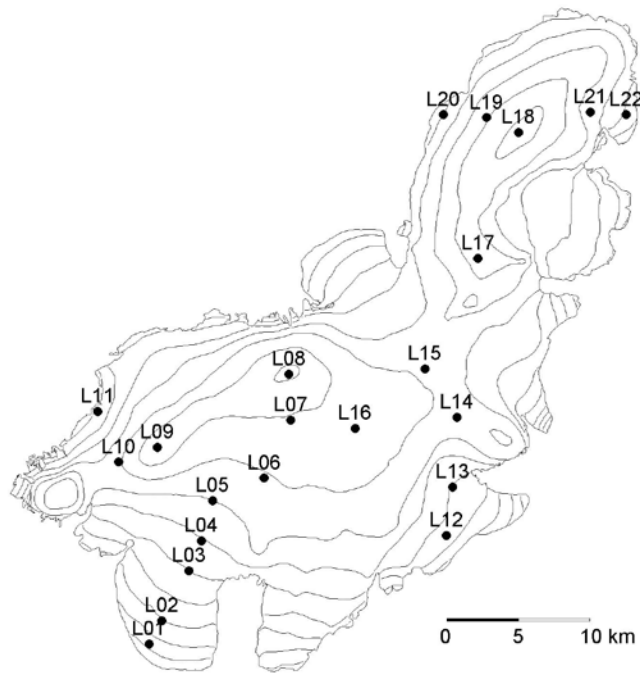


Fig. 4.1 Map detailing sites of measured mass balance on Langjökull ice cap. Mass balance data covering the balance years 1997 through to 2007 were used in the calibration of the mass balance model. Only data from sites along or nearest to the flowline were utilised (L01-07). Data from AWS set up at L01 and L05 over the summer of 2006 was also used in the calibration of the model. (Source: F. Pálsson, personal communication)

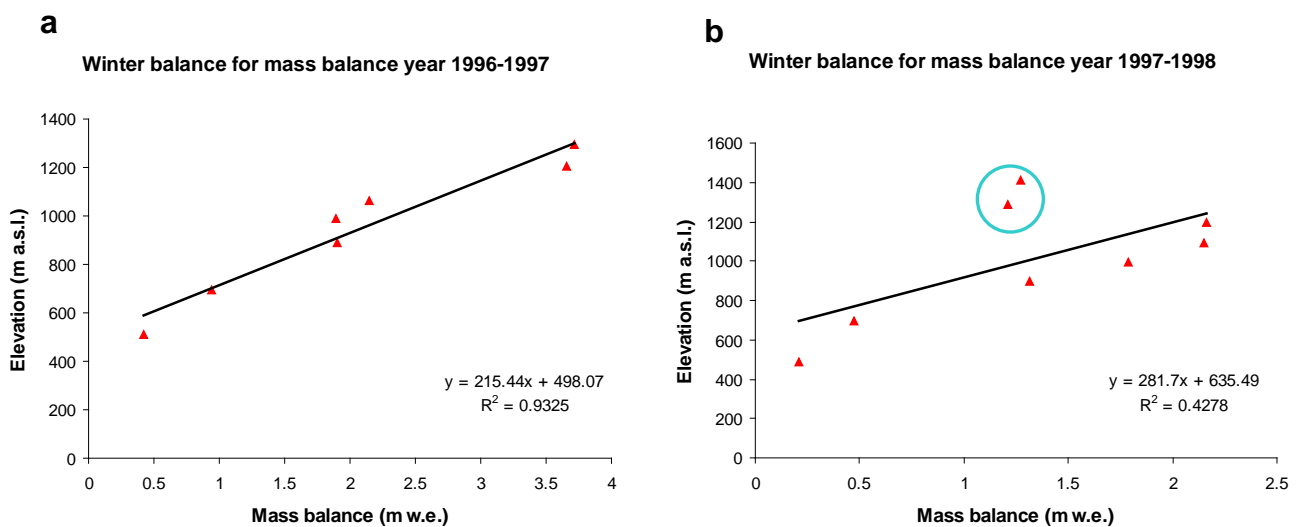


Fig. 4.2 Measured winter balance against elevation (\blacktriangle) for mass balance years 1996-1997 (a) and 1997-1998 (b) using data from sites L01 to L07. Black lines show line of best fit calculated through simple linear regression. The equation solving the line of best fit and the related coefficient of determination (R^2) are also shown for each example.

Using the assumption that no melting had occurred over each winter, it is possible to estimate the precipitation gradient by means of simple linear regression. Winter balances were plotted against elevation for all mass balance years and lines of best fit were calculated (examples from balance years 1996-1997 and 1997-1998 are shown in Figure 4.2).

A simple linear relationship fits to an acceptable degree for all balance years (with r^2 values ranging from 0.88 to 0.97) except for balance year 1997-1998 ($r^2 = 0.43$). It is clear from Figure 4.2b that the winter balance at higher elevations (L06 and L07, circled (○)) is significantly lower than would be expected. The reason for this is unknown but the author hypothesises that such a change may have been caused by a prolonged change in the prevailing wind direction causing mass drifting of snow away from these measurement locations. Information regarding prevailing wind direction at points across Iceland is available in Einarsson (1984) but the locations closest to the glacier all show significantly different patterns. Wind speed data collected by the AWS at L05 in the summer of 2006 does, however, suggest that wind speeds of up to 25 m s^{-1} are not uncommon on the glacier. Given the clear anomalous nature of this particular set of data, it was decided that it should be excluded from the calculation of the precipitation gradient.

From the remaining 10 years of data, the mean gradient and y intercept were calculated. The resulting precipitation gradient was 0.37 (1 per 100 m) which fits within the range used in studies on other Icelandic glaciers in Jóhannesson (1997). The elevation at which the precipitation gradient is enforced was taken to be the mean y intercept, 497 m a.s.l..

4.1.3 Determining σ

Laumann and Reeh (1993) state that σ should account for both temperature deviations from the long-term annual cycle and also the daily temperature cycle. However, in their paper, Laumann and Reeh (1993) were approximating the annual temperature cycle using a sinusoidal function which does not allow for random temperature fluctuations. This author believes that the use of mean monthly temperatures in this study enables much of this variation to be captured (see for example the temperature distribution over the year in Figure 3.2). Therefore, in this study σ will be used to represent only deviations due to the diurnal temperature cycle. The AWS data from 2006 was used once again as the basis for this determination.

The data for both stations was processed to give maximum and minimum temperatures for each of the 153 available days. Given the 10 min sampling rate it can be assumed that near

enough the true maximum and minimum temperatures were captured. The temperature range was calculated and the average over all days for each location was found.

Perhaps unsurprisingly, it was found that there was a small but significant difference between the mean diurnal temperature range between the two locations, with L01 = 4.443 °C and L05 = 4.16 °C. Over the full elevation range of the glacier, and assuming a linear relationship, this will result in a difference of nearly half a degree (0.43 °C). Given this, it was decided that in the mass balance model, σ will be a function of elevation according to the linear relationship

$$\sigma = -0.0005E + 4.6699 \quad (4.1)$$

where E is elevation in m a.s.l.. Whilst the resulting change may be small it could prove significant in certain circumstances and in addition the rewrite of the Matlab code was simple to perform. Whilst, as with the determination of the temperature gradient, more data would be desirable in order to establish this relationship (not only over more years but also over the winter months) this is the only real world data available with which to determine this parameter.

4.2 Establishing the degree-day factors

Much has been written about the calculation and performance of degree-day factors and a comprehensive overview of both the theory behind positive degree-day modelling and attempts to improve its performance can be found in Hock (2003). Hock (2003) also provides a list of degree-day factors taken from a wide-ranging selection of studies. Comparisons in the performance of advanced degree-day models against that of energy balance models in approximating ablation from testing actually carried out on Hagafellsjökull vestari can be found in Guðmundsson et al (2003a) Guðmundsson et al (2003b). In this study, however, a simple, well established degree-day model methodology will be used that differentiates between just two types of glacier surface, snow (DDF_s) and ice (DDF_i). Table 4.3 provides examples of degree-day factors for these two surfaces used in studies on glaciers in Nordic countries.

To establish the optimal degree-day factors, the mass balance model is run over the 11 years covered by the mass balance measurements collected by the University of Iceland and the resulting net mass balance profiles compared. The model is forced by temperature and precipitation data (details of which can be found in section (3.3)). A recap of the other parameter values is shown in Table 4.4.

Table 4.3 Example degree-day factors (for ice (DDF_i) and snow (DDF_s)) taken from studies on other glaciers in Nordic countries.

Author	Year	Country	Glacier (Ice Cap)	DDF_i (m w.e. °C ⁻¹ d ⁻¹)	DDF_s (m w.e. °C ⁻¹ d ⁻¹)
Jóhannesson (1997)	1997	Iceland	Blöndujökull/Kvísíslajökull (Hofsjökull)	0.00495	0.00450
			Illviðrajökull (Hofsjökull)	0.00756	0.00560
Jóhannesson et al (1995)	1995	Iceland	Sátujökull (Hofsjökull)	0.00770	0.00560
		Norway	Nigardsbreen	0.00640	0.00440
		Greenland	Qamanârssúp	0.00730	0.00280
Laumann & Reeh (1993)	1993	Norway	Álfotbreen	0.00600	0.00450
			Nigardsbreen	0.00550	0.00400
			Hellstugubreen	0.00550	0.00350

Table 4.4 Model parameters used during initial determination of degree-day factors for snow and ice.

Parameter	Value
Temperature lapse rate (°C per m)	0.0062
Precipitation gradient (1 per 100 m)	0.37
Starting elevation for precipitation gradient	497
σ gradient	-0.0005
σ intercept	4.6699
Snow threshold temperature (°C)	1

One of the changes made to the Matlab script was the introduction of a raft of output files which record the value of all useful parameters at all points along the flowline for every year the model is run. In this instance, the surface elevations and corresponding net mass balance values are required. In order to compare like with like, one must locate within the model output the net mass balances at the same elevations that the actual net mass balance measurements were made. As can be seen in Table 4.5 below, due to the dynamic nature of the glacier, these elevations changed every year.

Table 4.5 Elevations (m a.s.l.) of the measurement locations used in the calibration of the mass balance model and how they changed over time. (Source: F. Pálsson)

Mass Balance Year	Measurement Location						
	L01	L02	L03	L04	L05	L06	L07
1996-1997	511	693	889	992	1064	1203	1297
1997-1998	490	696	896	992	1091	1196	1290
1998-1999	505	695	899	1093	1200	1293	1293
1999-2000	490	700	898	978	1063	1165	1293
2000-2001	485	694	897	992	1055	1192	1288
2001-2002	486	692	896	992	1107	1199	1283
2002-2003	500	688	897	994	1104	1197	1287
2003-2004	514	686	896	993	1110	1201	1285
2004-2005	502	679	890	989	1108	1198	1283
2005-2006	498	676	892	992	1109	1201	1287
2006-2007	522	676	889	989	1109	1201	1288

In spite of their being over 200 grid points along the flowline, matching elevations could not always be found. Therefore, the author wrote a short piece of code ('mbcal.m') that would estimate the net mass balance for the required elevation through interpolation. This greatly speeds up the calibration process enabling very rapid processing and analysis of a model run.

With each model run, the modelled net mass balances for each of the 11 balance years were compared with the measured balances both on a year-by-year and overall basis. The statistical measures of coefficient of correlation (r^2) and root mean squared error (RMSE) were calculated to help assess the validity of the model output, but the main source of information as to the goodness-of-fit was provided by graphing the measured balances against the modelled balances. By analysing the distribution of data points it was possible to infer as to whether one, or both, of the degree-day factors was too large or too small. The basic rules adopted by the author in the calibration are illustrated in Figure 4.3 below.

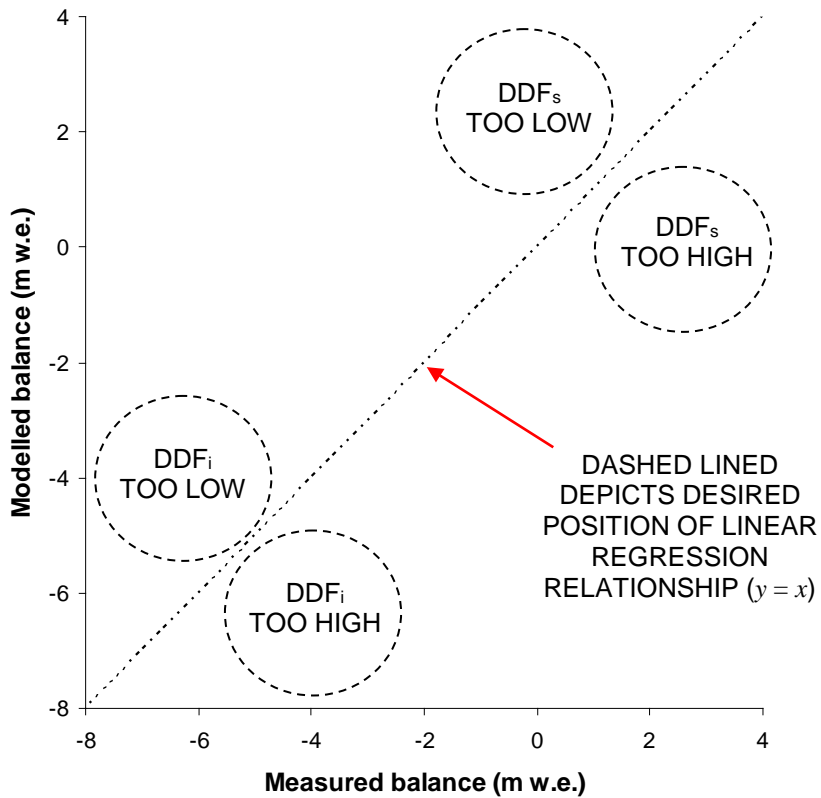


Fig. 4.3 Basic rules that were followed in the calibration of the mass balance model. The degree-day factors were amended for the next model run based on the distribution of data points from the preceding run. The ultimate goal being to have all points plotted on the dashed, central line.

4.2.1 Initial calibration

Starting with degree-day factors for snow and ice used for Illviðrajökull glacier in Jóhannesson (1997), the degree-day factors that best represented the measured mass balance were then gradually refined over many model runs. The degree-day factors that gave the best-fit to the measured mass balance records when used in conjunction with the other parameter values in Table 4.4 were $DDF_s = 0.0101 \text{ m w.e. } ^\circ\text{C}^{-1} \text{ d}^{-1}$ and $DDF_i = 0.00873 \text{ m w.e. } ^\circ\text{C}^{-1} \text{ d}^{-1}$. The resulting measured-against-modelled net mass balance graph is shown in Figure 4.4.

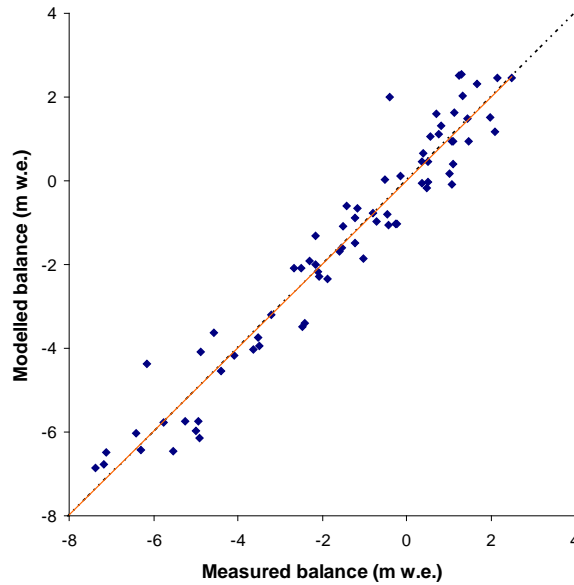


Fig. 4.4 Measured and modelled net mass balance for the balance years 1996-1997 to 2006-2007 with $DDF_s = 0.0101 \text{ m w.e. } ^\circ\text{C}^{-1} \text{ d}^{-1}$ and $DDF_i = 0.00873 \text{ m w.e. } ^\circ\text{C}^{-1} \text{ d}^{-1}$. Orange line shows calculated linear regression relationship.

Using this set of parameters the model displays good correlation with $r^2 = 0.95$ and reasonably low scatter with $RMSE = 0.69 \text{ m w.e.}$ which compares favourably with similar papers (such as Jóhannesson et al (1995)). However, whilst there are cases in which the degree-day factors for snow and ice are very similar (e.g. the Jóhannesson (1997) study of Blöndujökull/Kvísíajökull glacier (see Table 4.3)) this author was unable to find another study in which the factor for snow exceeded that for ice. Indeed, such a situation is highly unlikely as the reasoning behind the use of two degree-day factors is that ice melts faster than snow given its lower albedo (Hock, 2005). Paterson (1994) gives dry snow an albedo range of 0.80-0.97 whilst clean ice falls between 0.34-0.51. Taking this into account, it seems highly unlikely that the degree-day factors calculated above are correct. If this is the case, one of the parameters in Table 4.4 must be incorrect and, given the uncertainty surrounding its calculation (see section 4.1.1), there is good reason to suspect that the temperature lapse rate is the problematic one.

4.2.2 'Reverse engineering' the temperature lapse rate

It was reasoned that in order to lower DDF_s and increase DDF_i the temperature lapse rate would have to be reduced thus lowering the accumulation in the upper reaches of the glacier to a greater degree than in the lower areas. However, rather than arbitrarily pick a new, lower temperature lapse rate, it was decided that it could be a worthwhile exercise to 'reverse engineer' the lapse rate using the degree-day factors from other studies. It seemed sensible

to concentrate on studies that centred on glaciers from Iceland. The results are outlined briefly below.

4.2.2.1 Jóhannesson (1997), Blöndujökull / Kvíslajökull glacier, Iceland

$$DDF_s = 0.00450 \text{ (m w.e. } ^\circ\text{C}^{-1} \text{ d}^{-1}\text{)} \quad DDF_i = 0.00495 \text{ (m w.e. } ^\circ\text{C}^{-1} \text{ d}^{-1}\text{)}$$

Using these degree-day factors the author was unable to achieve a reasonable match with the measured balance data no matter what temperature lapse rate was used. As the degree-day factors in Flowers et al (2008) are similar to these values, it was deemed unnecessary to try these as well.

4.2.2.2 Jóhannesson (1997), Illviðrajökull glacier, Iceland

$$DDF_s = 0.00560 \text{ (m w.e. } ^\circ\text{C}^{-1} \text{ d}^{-1}\text{)} \quad DDF_i = 0.00756 \text{ (m w.e. } ^\circ\text{C}^{-1} \text{ d}^{-1}\text{)}$$

The following match was obtained using a lapse rate of $0.0046 \text{ } ^\circ\text{C m}^{-1}$ (Figure 4.5).

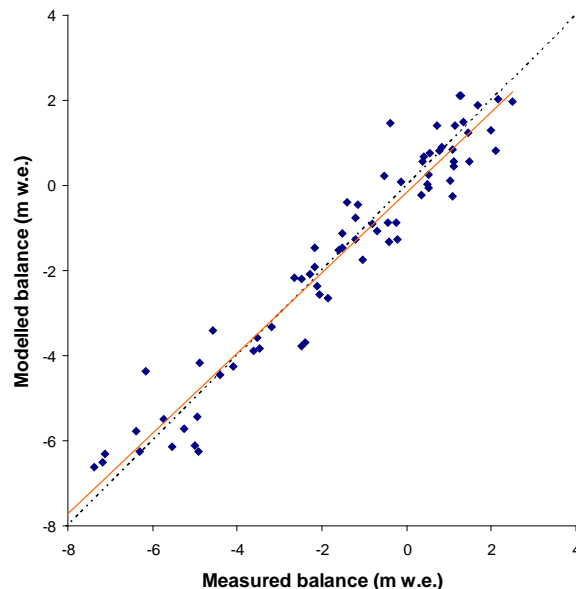


Fig. 4.5 Measured and modelled net mass balance for the balance years 1996-1997 to 2006-2007 with temperature lapse rate at $0.0046 \text{ } ^\circ\text{C m}^{-1}$ and degree day factors taken from a study of Illviðrajökull glacier (Jóhannesson, 1997). Orange line shows calculated linear regression relationship.

Whilst the data is well correlated ($r^2 = 0.94$) and error is virtually the same as in the initial calibration (RMSE = 0.69 m w.e.), Figure 4.5 shows how the model is over-estimating net mass balance at lower elevations and under-estimating at higher elevations, unlike the initial

calibration which was reasonable over the full range (Figure 4.4). Of even greater concern is the level to which the temperature lapse rate had to be lowered to in order to achieve this result. $0.0046 \text{ }^\circ\text{C m}^{-1}$ is considerably lower than that used in any other studies that this author is aware of. For completeness, the same process was carried out using factors taken from the study of Sátujökull glacier in Jóhannesson et al (1995) but the factors were very similar as, unsurprisingly, was the result (best fit with lapse rate of $0.0047 \text{ }^\circ\text{C m}^{-1}$).

This author considers these temperature lapse rates to be too low and the modelled balances not accurate enough for any of the above combinations of lapse rate and degree-day factors to be used and so a new solution was sought.

4.2.3 Arbitrary values of temperature lapse rate

Given the issues encountered in determining an acceptable temperature lapse rate, the unenviable decision was made to not refer to the AWS data at all but instead use a lapse rate from a previous study. It was realised that in fact no value could be truly representative of the real world lapse rate given how it was proved in the determination of σ (section 4.1.3) that the lapse rate could not be a constant (as the diurnal temperature range varied with elevation). Given this, a compromise was made and it was decided that the average lapse rate from the studies of the three Icelandic glaciers in Jóhannesson et al (1995) and Jóhannesson (1997) would be tried.

4.2.3.1 Average of studies on glaciers from neighbouring Hofsjökull ice cap

The average of these three rates (0.0060; 0.0060; 0.0053) is $0.00577 \text{ }^\circ\text{C m}^{-1}$. After calibration, the resulting degree-day factors were $\text{DDF}_s = 0.008458 \text{ m w.e. }^\circ\text{C}^{-1} \text{ d}^{-1}$ and $\text{DDF}_i = 0.008443 \text{ m w.e. }^\circ\text{C}^{-1} \text{ d}^{-1}$. Once again, $\text{DDF}_s > \text{DDF}_i$ and so this was not deemed acceptable.

4.2.3.2 Lowest value from studies on glaciers from neighbouring Hofsjökull ice cap

Realising that the lapse rate had to be lowered still further, the decision was made to use the lowest of all the rates, $0.0053 \text{ }^\circ\text{C m}^{-1}$. After calibration, the resulting degree-day factors were $\text{DDF}_s = 0.00694 \text{ m w.e. }^\circ\text{C}^{-1} \text{ d}^{-1}$ and $\text{DDF}_i = 0.00822 \text{ m w.e. }^\circ\text{C}^{-1} \text{ d}^{-1}$. This finally resulted in what this author believes to be acceptable degree-day factors with a temperature lapse rate that is not unrealistically low.

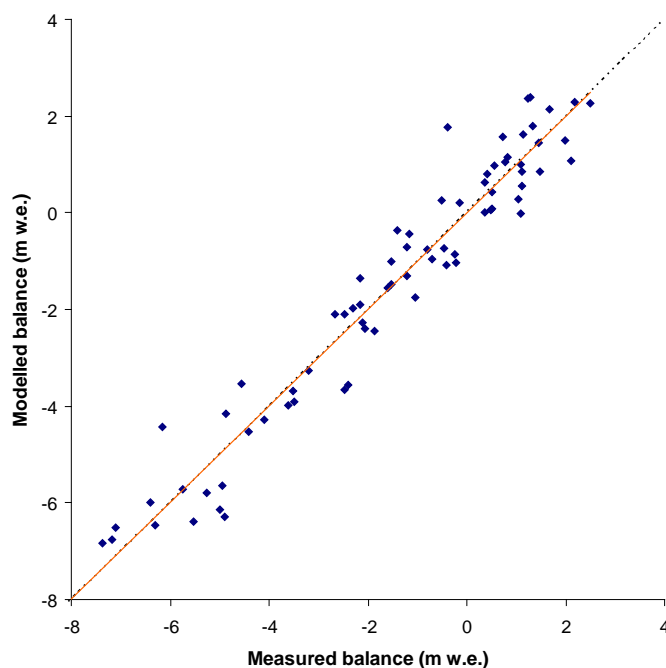


Fig. 4.6 Measured and modelled net mass balance for the balance years 1996-1997 to 2006-2007 with $DDF_s = 0.00694 \text{ m w.e. } ^\circ\text{C}^{-1} \text{ d}^{-1}$, $DDF_i = 0.00822 \text{ m w.e. } ^\circ\text{C}^{-1} \text{ d}^{-1}$ and temperature lapse rate of $0.0053 \text{ } ^\circ\text{C m}^{-1}$. Orange line shows calculated linear regression relationship.

The coefficient of correlation is as high as the initial calibration ($r^2 = 0.95$), error has improved slightly (RMSE = 0.68 m w.e.) and the linear regression approximates $y = x$ near perfectly ($y = 0.9981x - 0.0011$).

Nonetheless, these degree-day factors are considerably higher than those used by Flowers et al (2007) in their modelling of Langjökull ice cap ($DDF_s = 0.0046 \text{ m w.e. } ^\circ\text{C}^{-1} \text{ d}^{-1}$ and $DDF_i = 0.0058 \text{ m w.e. } ^\circ\text{C}^{-1} \text{ d}^{-1}$). However, their climatic data used for calibration was sourced from Hveravellir weather station which is situated in a sheltered location between Langjökull and Hofsjökull ice caps and doubt has been cast on the validity of using data from this station in mass balance modelling (Jóhannesson, 1997). In fact, Flowers et al (2007) do note that their values are lower than point values obtained in a more recent, unpublished study of Langjökull by Guðmundsson. Also, for the first time, these newly derived degree-day factors both fall within the ranges specified in Guðmundsson et al (2003b) (ranges given are $0.0040\text{--}0.0079 \text{ m w.e. } ^\circ\text{C}^{-1} \text{ d}^{-1}$ for snow and $0.0049\text{--}0.011 \text{ m w.e. } ^\circ\text{C}^{-1} \text{ d}^{-1}$ for ice/firn) adding weight to their credibility.

The use of the newly found degree-day factors was finally settled when it was found that the mean value of the ratio DDF_s/DDF_i for 13 pairs of degree-day factors for outlet glaciers on

Langjökull and Vatnajökull was 0.8 (Guðmundsson et al (2003b) *in* Flowers et al (2007)). The ratio of the newly found degree-day factors was an acceptably close 0.84.

4.3 The finalised mass balance model parameter values

Table 4.6 details the mass balance model parameter values that will be used as default values in the remainder of the study.

Table 4.6 Finalised mass balance model parameter values.

Parameter	Value
DDF _s (m w.e. °C ⁻¹ d ⁻¹)	0.00694
DDF _i (m w.e. °C ⁻¹ d ⁻¹)	0.00822
Temperature lapse rate (°C per m)	0.0053
Precipitation gradient (1 per 100 m)	0.37
Starting elevation for precipitation gradient	497
σ gradient	-0.0005
σ intercept	4.6699
Snow threshold temperature (°C)	1

This calibration process has highlighted one of the fundamental problems underlying degree-day modelling. Given so many parameters one is able to match measured mass balance histories using a number of different combinations. As in this case, one can only sanity check the parameter values they do choose to use in addition to utilising as long and as detailed a measured mass balance history as possible with which to calibrate the model.

5 MASS BALANCE MODEL – SENSITIVITY ANALYSIS

5.1 Sensitivity analysis

Simple sensitivity analysis was carried out on the mass balance model to give a greater understanding of the relative influence of each of the parameters. Table 5.1 details the values of the parameters after both increasing and decreasing them by 10 and 20 percent.

Table 5.1 Parameter values used in sensitivity analysis.

Change (%)	Temperature Lapse Rate (°C per m)	Ppt Gradient (1 per 100 m)	Snow Threshold (°C)	σ Gradient
+ 20	0.00636	0.444	1.2	-0.00060
+ 10	0.00583	0.407	1.1	-0.00055
0 (Default)	0.00530	0.370	1.0	-0.00050
- 10	0.00477	0.333	0.9	-0.00045
- 20	0.00424	0.296	0.8	-0.00040

In each test, one parameter value would be changed from those set out in Table 4.6 (from now on the 'Default' values) and then the model would be run for the mass balance year 1996-1997. The model output was then assessed.

5.1.1 Sensitivity to temperature lapse rate

It was realised during the calibration of the mass balance model that small changes in the temperature lapse rate could lead to large changes to the mass balance output. However, using the data from the output files it was possible to assess in greater detail as to which elements of the degree-day model were the most sensitive. The percentage change in both positive degree-days with elevation and snowfall as a fraction of precipitation with elevation was calculated and the results are shown in Figure. 5.1.

As would be expected, changes in temperature lapse rate have greater effect with increasing elevation on the percentage change in number of positive degree-days (Figure 5.1a). This can be accounted for by the fact that the temperatures due to the new lapse rates will diverge from the default with increasing elevation. What is less obvious is why the change from the default does not increase with a constant rate and why a decrease in lapse rate has a greater effect than an equivalent increase for a given elevation.

Initially it was thought the curved nature of the plots in Figure 5.1a could be caused by σ , which in the model is a function of elevation (as per section 4.1.3). However, this was investigated and found not to be the case. When sigma was fixed at 4.443 (the value calculated at 490 m a.s.l.) the graph of temperature lapse rate reduced by 20 % was more curved, with a percentage change from default nearing 60 % at ~1,300 m a.s.l.. When σ is a function of elevation it is actually working to straighten the curves. It was then remembered that the calculation of positive degree-days is essentially integration over part of a normal distribution and that the changes observed may be explained by the shape of this distribution. The average temperature for the month of October in 1996 (1.68 °C) was used to investigate if this was the case.

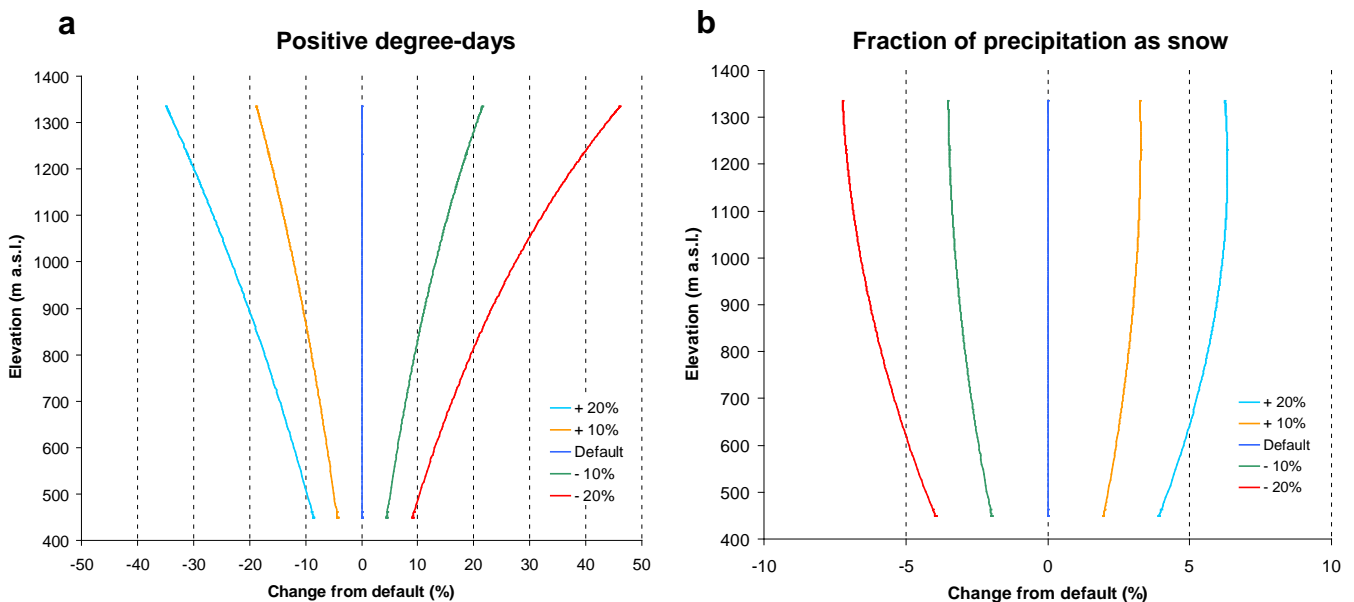


Fig. 5.1 Percentage change from the default values over elevation for both positive degree-days and the fraction of precipitation that falls as snow given a percentage change in the temperature lapse rate.

The probability density function was calculated and plotted for the maximum and minimum ice surface elevations in the 1997 surface profile for three different temperature lapse rates (default, +20% and -20%) and is shown in Figure 5.2a.

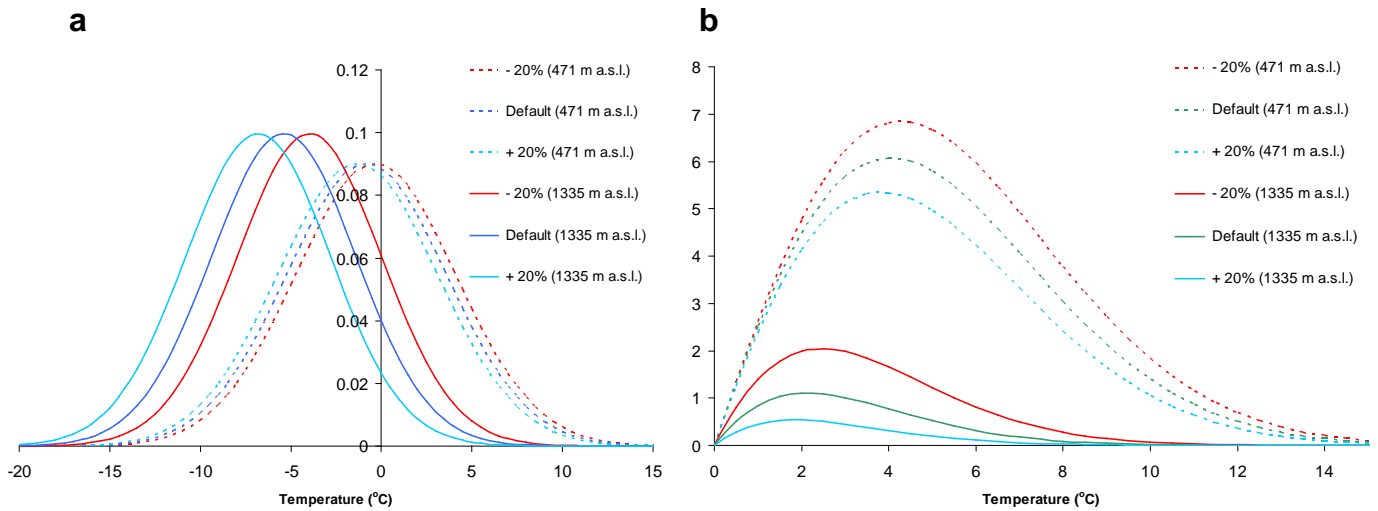


Fig. 5.2 (a) Probability density functions for temperature for elevations of 471 m a.s.l. (broken lines) and 1335 m a.s.l. (continuous lines) given mean monthly temperature at 2 m a.s.l. of 1.68 °C, temperature lapse rate of 0.0053 °C per m) and $\pm 20\%$, and σ as a function of elevation (as per section 4.1.3). (b) Positive degree-days represented graphically from probability density functions in (a). Integration between 0°C and ∞ °C will give number of positive degree-days for this month (October 1996).

From Figure 5.2a it is clear to see how the change in temperature due to the lapse rate offsets the distribution, both due to elevation and also the effect of changing the lapse rate itself. Additionally, it can be seen how the change in σ changes the shape of the distribution. However, it is in Figure 5.2b that an explanation for the shape of the curves in Figure 5.1a can be found. The plots in Fig 5.2b are graphical representations of the number of positive degree-days for the month of October in 1996 for the same two elevations and multiple lapse rates. What is important is the difference in area under the curves for each lapse rate at the different elevations. At 471 m a.s.l. the relative differences in area under the curve are much smaller than at 1335 m a.s.l. and the percentage increase in area from a lapse rate of -20% is greater than the percentage decrease in area from a lapse rate of +20%. All of the variation in Figure 5.1a can therefore be explained by the fact that the model assumes a Gaussian distribution for temperature.

From Figure 5.1b it should first be noted that the impact of changing temperature lapse rate on fraction of precipitation that falls as snow is far smaller than on number of positive degree-days. However, as with positive degree-days, it has a greater sensitivity to a decrease in lapse rate than an increase. Once again the curved nature of the plots in Figure 5.1b can be

attributed to the temperature probability density function (Figure 5.3). In this case, the fraction of precipitation that falls as snow is calculated directly from this function with the area under the graph to the left of the dashed black line (at 1°C – the snow threshold temperature) being the value.

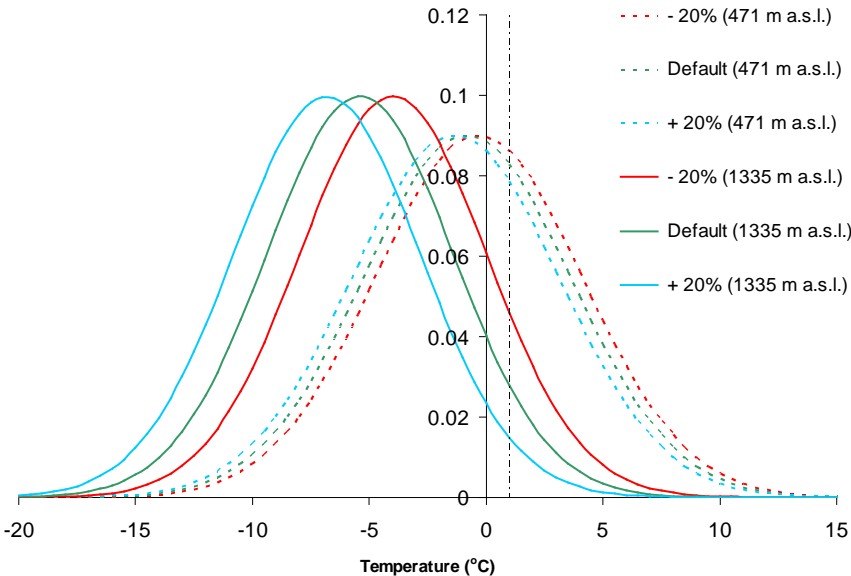


Fig. 5.3 Probability density functions for temperature for elevations of 471 m a.s.l. (broken lines) and 1335 m a.s.l. (continuous lines) given mean monthly temperature at 2 m a.s.l. of 1.68 °C, temperature lapse rate of 0.0053 °C per m) and ±20%, and σ as a function of elevation (as per section 4.1.3). Black dashed line denotes snow threshold temperature (1°C) and fraction of area under a curve to the left of this line is the fraction of precipitation that will fall as snow.

When cold enough, the difference in this value between the default temperature lapse rate and an alternative lapse rate will be zero as *all* precipitation will fall as snow in both cases. An indication of this is seen in Figure 5.1b with temperature lapse rate at +20% where the percentage difference is closing at the upper elevations.

Looking at the sensitivity of net mass balance overall to changes in temperature lapse rate one is able to confirm that a decrease in lapse rate will cause a greater loss in mass balance than an equivalent increase would cause gain (Figure 5.4). However, this differential appears dependent upon elevation.

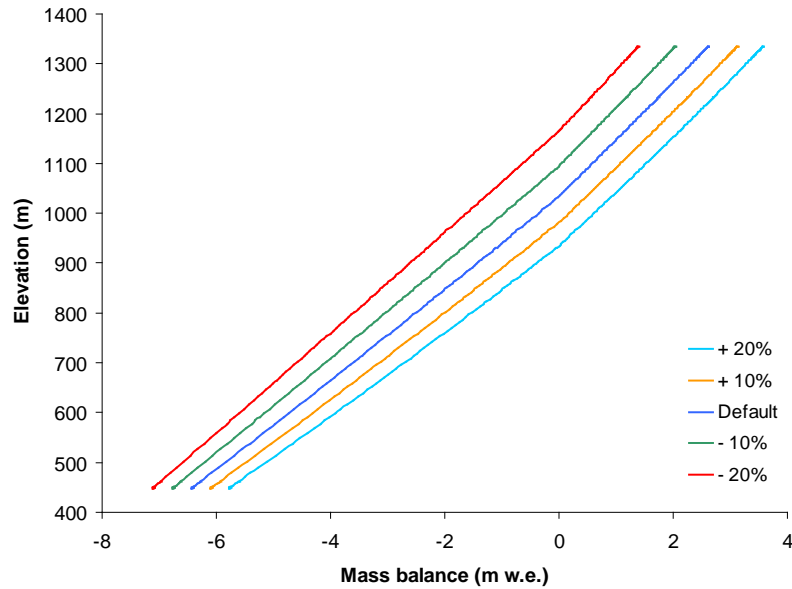


Fig. 5.4 Net mass balance gradients for mass balance year 1996-1997 modelled with different temperature lapse rates.

5.1.2 Sensitivity to the precipitation gradient

The effect of changing the precipitation gradient on net mass balance is far less subtle. Increasing the gradient will lead to a greater precipitation with increasing elevation. This is clearly shown in Figure 5.5 in which all gradients diverge as elevation increases. It should be noted that the gradients diverge from 497 m a.s.l. as this is the elevation from which the gradient is initiated (as per methodology in Jóhannesson et al (1997)).

Within the elevation range specified here, the effect on net mass balance for a given percentage change in precipitation gradient is significantly smaller than the equivalent change in temperature lapse rate.

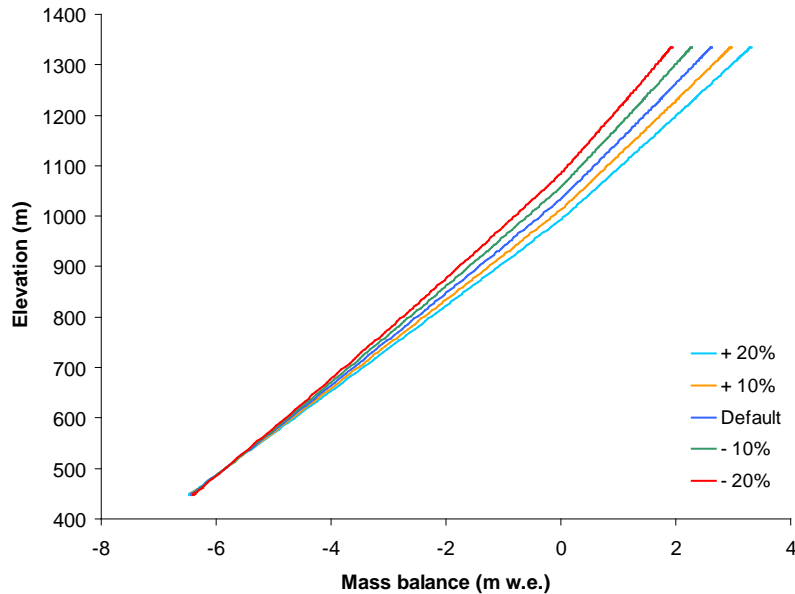


Fig. 5.5 Net mass balance gradients for mass balance year 1996-1997 modelled with different precipitation gradient rates.

5.1.3 Sensitivity to snow threshold temperature

The changes in mass balance gradient due to the changes in snow threshold temperature were so small as to not make them possible to resolve in a graph such as Figure 5.4 or Figure 5.5. However, when rerun with considerably larger changes (threshold temp -1°C and 3°C) it was apparent that the effect of a change was more acute the higher the elevation.

5.1.4 Sensitivity to σ gradient

As per the threshold temperature, the changes to the gradient for σ had an almost imperceptible effect on the net mass balance values. However, increasing the gradient has the effect of tightening the normal distribution as elevation increases by reducing the size of the standard deviation of the normal distribution (as seen in Figure 5.2a). This has the effect of lowering the rate of ablation and increasing the fraction of precipitation that falls as snow thus increasing overall net mass balance values.

5.2 Conclusions from sensitivity analysis

It has become clear that the degree-day model is highly sensitive to the temperature lapse rate. This is understandable given that temperature drives both the calculation of the number of positive degree-days and the fraction of precipitation that falls as snow. However, it has also become clear that the relationship between mass balance and temperature lapse rate is not straightforward. This reinforces this author's belief that the degree-day mass balance

model could be greatly improved if the parameterisation of temperature lapse rate was in some way made more representative of real world conditions. However, to devise such a parameter would likely require temperature data from the site of interest which is unlikely to have been collected. It also increases the dissatisfaction of having to arbitrarily choose a temperature lapse rate for this study.

The precipitation gradient is shown to have a sizeable degree of influence on the degree-day model. However, unlike the temperature lapse rate, its relationship to mass balance is a comparatively simple one.

6 THE DYNAMIC GLACIER MODEL

6.1 Basic equations

This dynamic glacier model is based on the original work of Huybrechts et al (1989) and Greuell (1992). It is a one-dimensional (central flowline) model, with x as the variable in the flow direction. The three-dimensional geometry of the glacier is parameterised assuming a parabolic cross-section and changes in ice thickness and ice velocity are calculated at grid points along the flowline. The model was originally written into Matlab code by A.J. Payne of the University of Bristol. The following is a brief outline of the mechanics of the model.

The model is based on the ice continuity equation

$$\frac{\delta H}{\delta t} = b - \frac{\delta q}{\delta x} - \frac{q}{w} \frac{\delta w}{\delta x} \quad (6.1)$$

where $\delta H/\delta t$ is the change in ice thickness, b is the specific mass balance, $\delta q/\delta x$ is the glacier flow divergence, and w is glacier spreading with valley width. It is assumed that the ice density is constant throughout the glacier. In this study the specific mass balance is calculated by a degree-day model (discussed in sections 3 to 5).

The flux of ice, q , through a point is determined from the application of Glen's flow law

$$q = \frac{2A}{n+2} H^2 \tau^n \quad (6.2)$$

where H is ice thickness, A is the flow law parameter, n is the flow law exponent, and τ is the gravitational driving stress, given by the basal shear stress,

$$\tau = -\rho g H \frac{\delta s}{\delta x} \quad (6.3)$$

where $\delta s/\delta x$ is the ice surface slope, ρ is the ice density (taken as 910 kg m^{-3}), and g is the acceleration due to gravity (9.81 m s^{-2}). The value of q describes the flux of ice due to internal deformation only. According to Huybrechts et al (1989), however, "since there is with respect to (vertical) mean velocity not so much difference between deformation (concentrated near

the base) and basal sliding, any basal sliding may be assumed to be reflected in the value of the flow parameter". This assumes that by adjusting the value of the flow law parameter A in the model, one is able to model the bulk flux of ice due to internal deformation *and* basal sliding with the just the input from (6.2).

The substitution of (6.3) into (6.2) enables one to calculate the diffusivities of flow, D , shown below

$$q = \frac{2A}{n+2} H^2 \tau^3 = -\frac{2A(\rho g)^3}{n+2} H^5 \left(\frac{\delta s}{\delta x} \right)^3 = -D \frac{\delta s}{\delta x} \quad (6.4)$$

The final element of the model is the calculation of the valley cross-sectional profile. Unlike the work of Schlosser (1997) and Zuo and Oerlemans (1997) in which the cross-sectional profile of the glacier is represented by a trapezoidal shape, this model assumes that the valley profile is a parabola with width at the ice surface, w , being

$$w = w_0 \left(\frac{H}{H_0} \right)^{1/2} \quad (6.5)$$

where w_0 is the reference width, and H_0 is the reference thickness. Hence, the valley width at a point depends on the ice thickness, H . Details regarding the determination of the reference width and ice thickness for this study are provided in section 2.

Substituting (6.4) into (6.1) results in the final equation used in the model, where

$$\frac{\delta H}{\delta t} = b + \frac{\delta}{\delta x} D \frac{\delta s}{\delta x} - \frac{q}{w} \frac{\delta w}{\delta x} \quad (6.6)$$

This is applied to each point along the flowline for each time step in a model run.

6.2 The Matlab calculation

The parameters in the ice flow model with widely accepted default values are detailed in Table 6.1 below. The parameters that can be altered include the main 'tuning' parameter A

(the flow law coefficient), the distance between points on the transect δx , and the time step δt .

Table 6.1 Default parameters used in the ice flow model.

Parameter	Value
Glen's flow law exponent	3
Density of ice (kg m^{-3})	910
Gravity (m s^{-2})	9.81

Initial testing of the model had produced unusual artefacts in the resulting glacier surface profiles. These artefacts consisted of 'steps' in the profile that would oscillate as the run progressed (Figure 6.1).

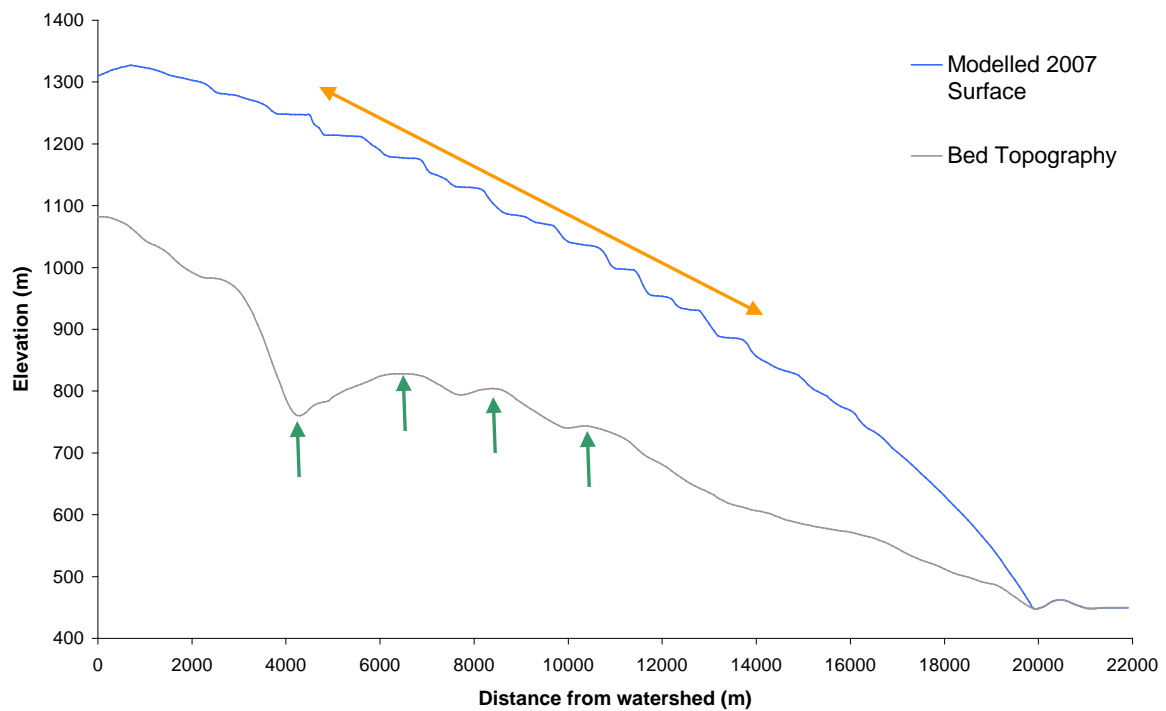


Fig 6.1 Ice surface profile plot illustrating the 'step' artefacts (along the section indicated by orange arrow) being generated by the ice flow model. Green arrows indicate both the initial bed over-deepening and subsequent hummocky terrain. This profile is the result of a 10 year run (balance years 1997-1998 to 2006-2007) with $A = 6.8e-15 \text{ s}^{-1} (\text{kP})^{-3}$ and δt 1 year.

Various tests were run to try to ascertain the reason behind this irregularity. Initially it was thought that the steps were initiated by the large over-deepening in the bed topography at 4 km from the watershed (indicated in Figure 6.1) and that this then propagated down the flowline as the glacier advanced and was sustained by the continuing 'hummocky' bed topography over the proceeding 5 km. To test this, new input files for artificial slopes and wedges of ice were created and the mass balance model was changed to provide specific mass balances of zero along the whole length of the new transect. This enabled an analysis of the performance of the ice flow model unencumbered by the influence of uneven topography and changing mass balance input. However, even in this situation artefacts would materialise. This confirmed that it was not the influence of the topography that (directly at least) caused the stepping. A test was also performed on a rectangular block of ice resting on a completely flat surface. As this deformed stepping initially occurred but, as the ice flattened over time the stepping dissipated. Further tests indicated that the stepping was more pronounced as A was increased (thus increasing the 'softness' of the ice and enabling faster deformation). Having generated new input files for reference widths and heights with larger distances between points along the transect, further runs indicated that increasing δx would also reduce the prevalence of stepping; however, this would also, of course, reduce the model's spatial resolution.

The attention of the author was drawn back to the fact that the ice model was solving differential equations and that accuracy in their solution could be improved by reducing δt . The time step for all runs up until this point had been 1 year and when rewriting the Matlab code to integrate the degree-day model, this had been hardcoded. However, once this problem had been overcome with a further rewrite, the model was rerun halving δt each time. The resulting profiles can be seen in Figure 6.2.

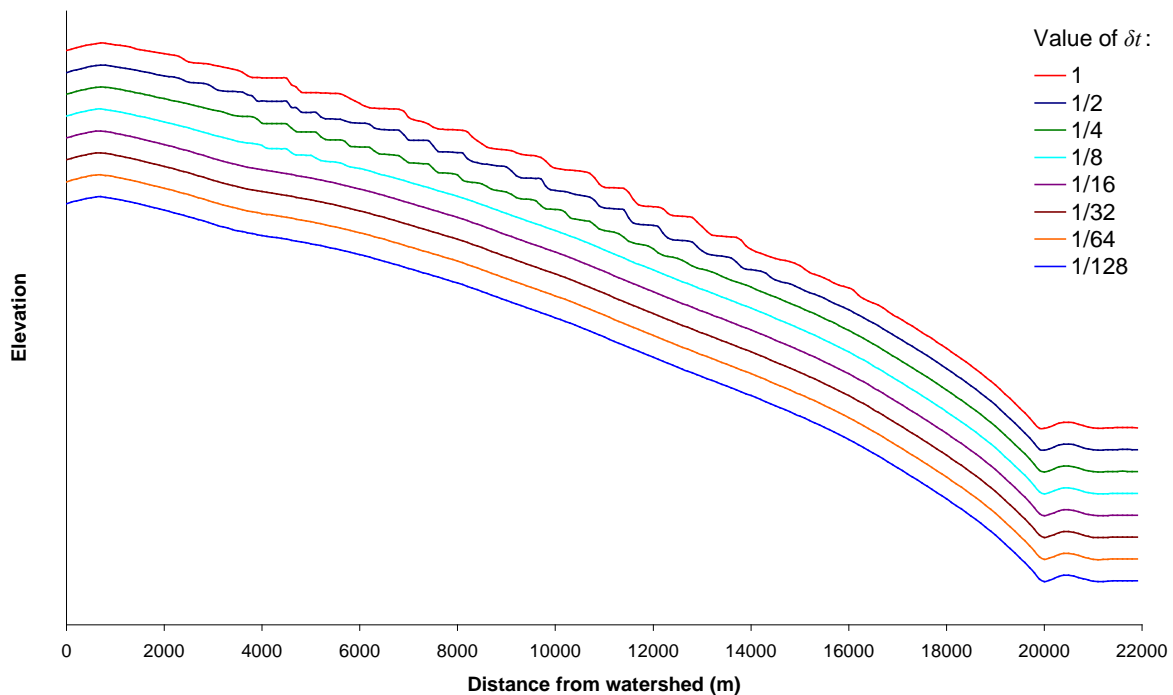


Fig 6.2 Ice surface profile plots illustrating the reduction in 'step' artefacts being generated by the ice flow model as δt is reduced (fractions indicate fractions of a year). Profiles are offset for easier viewing. All profiles are a result of a 10 year run (balance years 1997-1998 to 2006-2007) with $A = 6.8e-15 \text{ s}^{-1} (\text{kP})^{-3}$ and $\delta x = 100 \text{ m}$.

Figure 6.2 clearly demonstrates that step artefacts can be effectively eliminated if δt is reduced far enough. The only limiting factor on reducing δt in this case was the possible detrimental effect on computer processing time. In amending the Matlab code to enable the reduction of δt it had already been realised that the bulk of the processing time in a model run was dedicated to the mass balance calculations. As such, the rewrite was devised such that the mass balance model was only initiated when t was an integer. Without this, reducing δt by half doubles the length of time taken for a model run which is not an acceptable situation. However, even with this new script, it was realised that there would still have to be a trade-off between the size of δt and the additional processing time required. To establish a good compromise, the timed model runs were made (Table 6.2).

Surprisingly, reducing δt initially reduces the time taken to run the model (this was checked a number of times). The reason for this is unclear but the unexpected benefit is a welcome one. Degradation in the model runtime is not apparent until δt is 1/128 or smaller. Whilst the increases in runtime over this range are still small, with the stepping issue seemingly absent from $\delta t = 1/16$ it would be unnecessary to go this far, especially given the large number of model runs that were likely required in the calibration of the model. It was decided that the

best compromise was at $\delta t = 1/64$ as this was the smallest δt with no apparent degradation in processing time.

Table 6.2 Time taken to complete 10 year run (balance years 1997-1998 to 2006-2007) given changing values of δt . Other parameters constant at $A = 6.8e-15 \text{ s}^{-1} (\text{kP})^{-3}$ and $\delta x = 100 \text{ m}$.

δt (yr)	Time taken for 10 yr model run (s)
1	58.97
1/2	57.56
1/4	57.54
1/8	57.60
1/16	57.66
1/32	57.63
1/64	57.90
1/128	58.74
1/256	59.34
1/512	60.75
1/1024	63.84

6.3 The default ice flow model parameters

With the initial problems regarding the ice flow model overcome and the default parameters identified (Table 6.3) the calibration of the ice flow model could start using the flow law coefficient A as the tuning parameter.

Table 6.3 Default parameters to be used in the calibration of the ice flow model and throughout the rest of the study.

Parameter	Value
Glen's flow law exponent	3
Density of ice (kg m^{-3})	910
Gravity (m s^{-2})	9.81
δx (m)	100
δt (yr)	1/64

7 THE DYNAMIC GLACIER MODEL - CALIBRATION

7.1 Glen's flow law coefficient, A

Calibration of dynamic glacier flowline models is performed through the adjustment of Glen's flow law coefficient, A . The use of the term 'law' is misleading given that this constitutive relationship between the amount and rate of deformation given an applied stress is not a universal law but rather is dependent on a range of factors such as the loading conditions, confining pressure, state of stress, etc (Paterson, 1994). Paterson (1994) provides a detailed explanation of the influence that factors specific to ice can have on its deformation, but for the purposes of this study it is necessary only to know that increasing A will soften the ice allowing for increased deformation and, effectively, faster glacier flow. As a starting point for initial values of A in this calibration one can refer to the values of A in Paterson (1994) that have been recommended for ice at different temperatures (Table 7.1).

Table 7.1 Recommended values of flow parameter A at different temperatures and $n = 3$. (Source: Paterson, 1994)

Temperature (°C)	A ($\text{s}^{-1} (\text{kPa})^{-3}$)
0	6.8×10^{-15}
-2	2.4
-5	1.6
-10	4.9×10^{-16}
-15	2.9
-20	1.7
-25	9.4×10^{-17}
-30	5.1
-35	2.7
-40	1.4
-45	7.3×10^{-18}
-50	3.6

Whilst ideally one would determine the temperature of the glacier ice and the corresponding value of A to be used in the model, the ice within a glacier is heterogeneous not only in terms of temperature but also with regard to pressure, crystal size and orientation, presence of water, presence of impurities, and density all of which can effect the manner and rate at which ice deforms. In addition, one must remember that in this ice flow model the deformation term is actually trying to represent motion due to basal sliding, deformation at the bed, and any sliding of the bed substrate itself as well as the deformation of the actual glacier ice. Therefore, the reality is that a value of A is chosen that best enables the model to match a

known glacier behaviour such as historical glacier front positions (e.g. Stroeve et al (1989); Zuo and Oerlemans (1997)) and/or where possible, a measured glacier surface profile (e.g. Schlosser (1997); Oerlemans (1997)).

7.2 Calibration methodology

In the case of this study the model will be run for the balance years 1996-1997 to 2006-2007 with the initial surface profile being that determined from the 1997 surface DEM and the now calibrated mass balance model being forced by the meteorological input file (details about which are in section 3.3). After the 11 year run, the resulting surface profile will then be compared to the 2007 surface profile as it was determined from the LiDAR DEM. The aim of the calibration will be to reduce the root mean squared error (RMSE) as far as possible whilst at the same time accurately representing the shape of the profile. Ideally, the size and sign (+/-) of error between the modelled and measured 2007 profiles should also be randomly distributed along the length of the profile, resulting in the sum of all errors being zero.

In order to make the calibration process as efficient as possible, the model was developed to enable a 'calibration mode'. In this mode the graphical user interface (GUI) is adapted from the normal model to: enable a clearer view of the changing modelled surface profile; display the 2007 measured surface profile to allow the quick, visual comparison of modelled against measured profiles; display the calculated RMSE as the model is run negating the need for further calculations (Figure 7.1). Other details on this calibration GUI as shown in Figure 7.1 will be explained in the following sections.

7.3 Initial investigations with A

As a starting point, the flow coefficient for ice at melting point ($6.8 \times 10^{-15} \text{ s}^{-1} (\text{kPa})^{-3}$) was used. This was chosen on the basis that the glacier ice is believed to be temperate throughout (Eyre et al, 2005) and that the flow parameter is also likely to be accounting for basal sliding and/or bed deformation. These additional basal processes are highly likely to be of significance for Hagafellsjökull vestari glacier as it is believed to be resting on deformable sediments, as implied by the subglacial bed forms identified by Hart (1995) in the foreland of the glacier and the analysis of the till layer exposed after glacier retreat from the 1980 surge by Fuller and Murray (2002).

This run however, did not provide a reasonable fit of the measured profile. It can be seen in the comparison plot (Figure 7.2a) that there is a very large, positive discrepancy for the middle 14 km of the profile and then at the snout the model profile had retreated too rapidly. The RMSE for this run was 11.22 m.

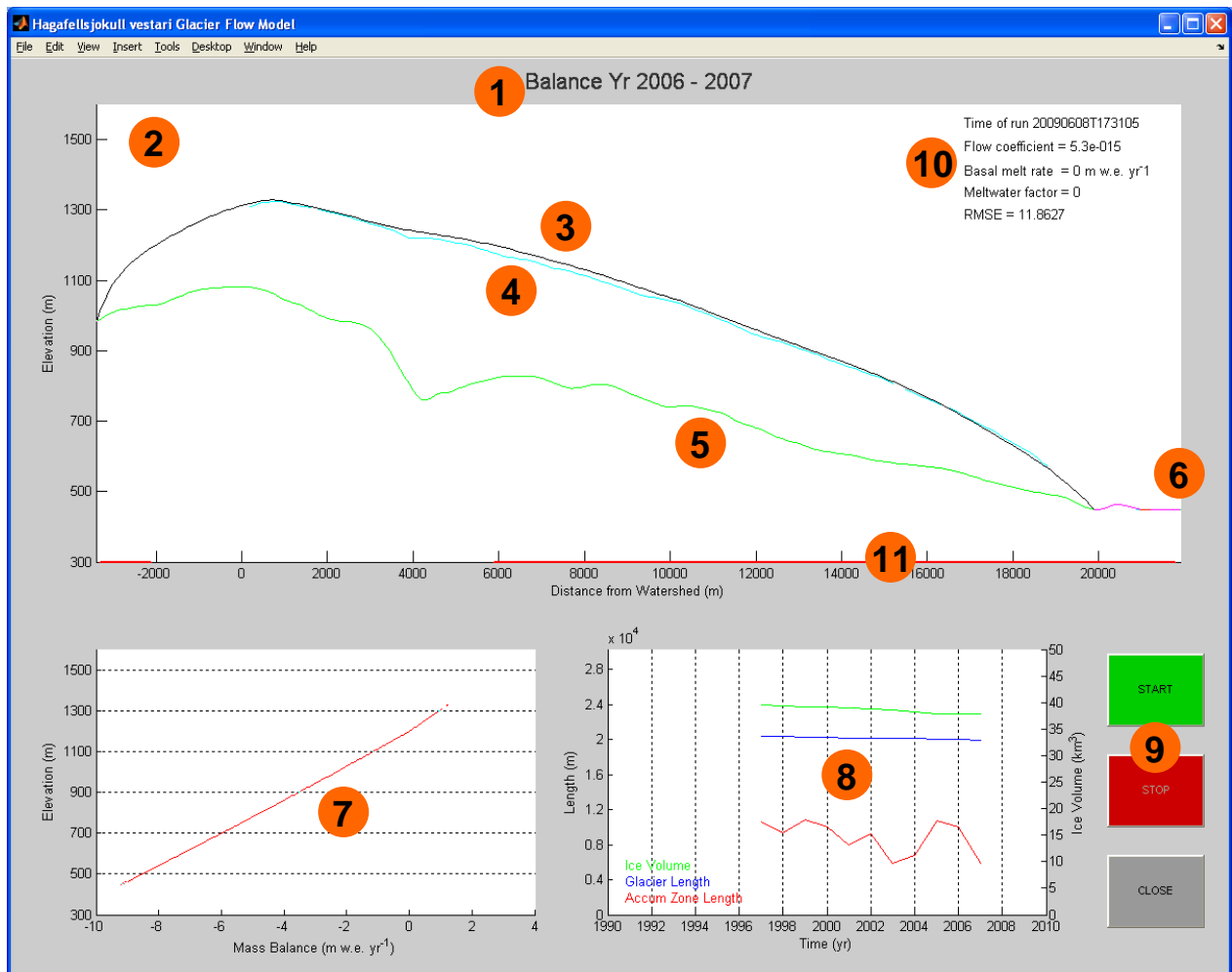


Fig. 7.1 Screenshot of the ice model calibration graphical user interface. (1) The balance year of the data that the surface profile window (2) and mass balance gradient window (7) are displaying. Within the surface profile window is also found the current modelled surface profile (black line (3)); the 2007 measured profile (blue line (4)); the bed topography (green line (5)); the section of the profile that is ice free (pink line (6)); information pertaining to both chosen parameter values for this particular run (Flow coefficient, Basal melt rate, Meltwater factor) and the time the run was initiated but also the RMSE of the current profile against the 2007 profile; and the region of the profile that has a snow free surface after the mass balance model is run (red line along x axis (11)). (8) is the glacier metrics window and displays calculated ice volume (green), glacier length (blue) and the size of the glacier accumulation zone (red) for each year of the model run. (9) buttons to start and stop the model run and to close the GUI window.

The obvious adjustment to make for the next run was to encourage ice flow by increasing A . Figures 7.2b and 7.2c display the resulting profile from runs with $A = 10.0 \times 10^{-15} \text{ s}^{-1} (\text{kPa})^{-3}$ respectively $A = 20.0 \times 10^{-15} \text{ s}^{-1} (\text{kPa})^{-3}$. The first of these does improve the position at the snout but at the expense of a less accurately modelled first couple of kilometres. The problematic middle section from the initial run remains similarly problematic in this run and this is reflected in the similarly poor RMSE of 11.52 m.

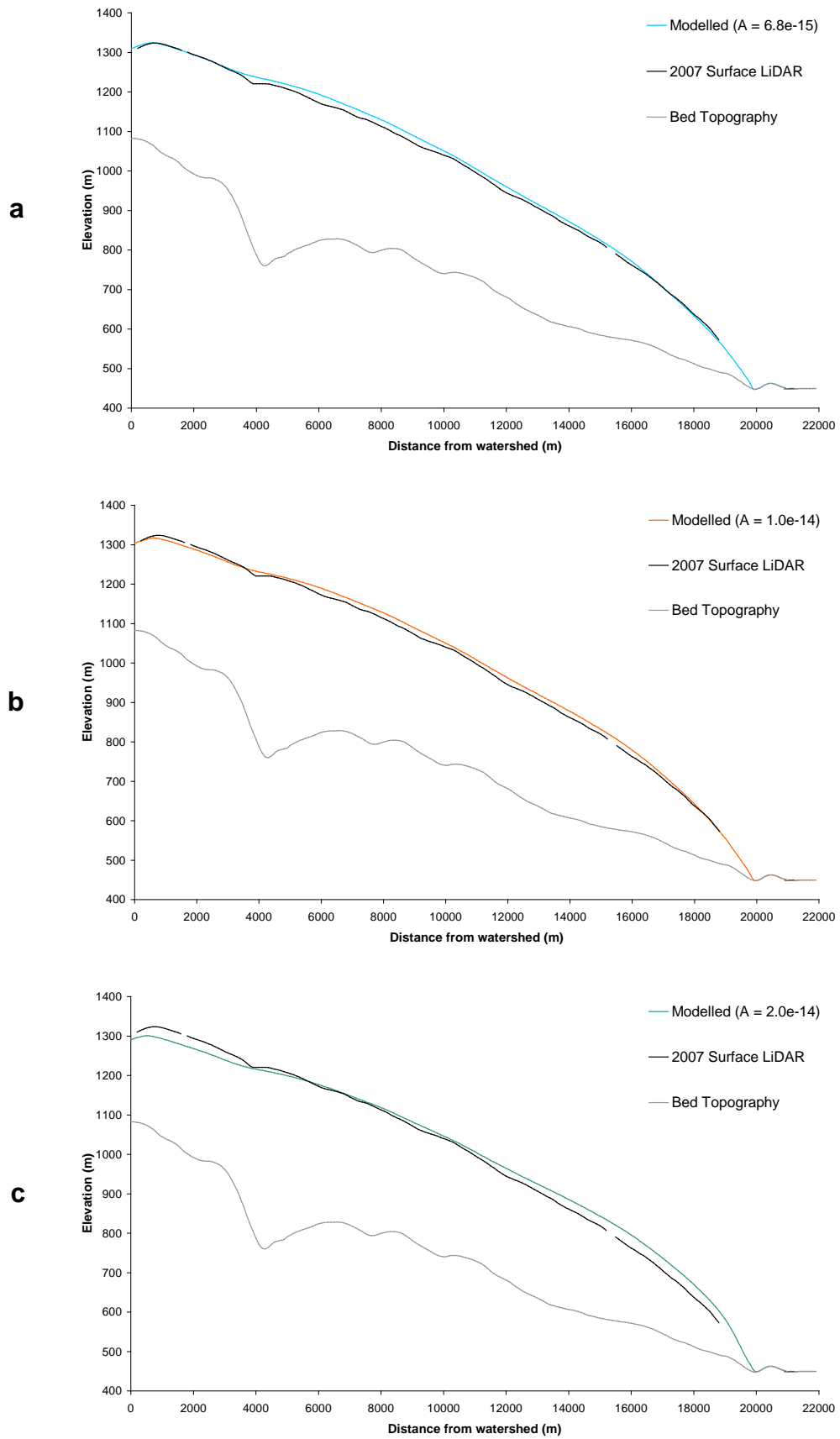


Fig. 7.2 Plotted modelled 2007 surface profiles when $A = 6.8 \times 10^{-15} \text{ s}^{-1} (\text{kPa})^{-3}$ (a); $A = 10.0 \times 10^{-15} \text{ s}^{-1} (\text{kPa})^{-3}$ (b); $A = 20.0 \times 10^{-15} \text{ s}^{-1} (\text{kPa})^{-3}$ (c). None of these runs approached an acceptable fit and had RMSE values of 11.22 m, 11.56 m and 19.75 m respectively.

In a final effort to resolve the positive bias in the mid section, A was doubled in the third run. This had the desired effect of accelerating the ice down slope but the profile was the least representative yet (Figure 7.2c) and the RMSE was close to double at 19.75 m.

With further runs it was clear that it would not be possible to represent the measured 2007 profile with a uniform flow law coefficient along the length of the transect. A new method would have to be devised.

7.4 Sectioning the transect

It was reasoned that in order to reduced the positive bias in the mid-section of the glacier without reducing the surface at the higher elevations too greatly, different values of A would be used in different sections of the transect. Rather than simply move the positive bias further down slope, it was expected that the increased ablation at lower elevations would remove this additional mass.

To make this possible the Matlab code was amended leading to a number of new variables that could be changed. These included the points along the transect that bounded the different sections and the additional values of A that acted within these sections. It was decided that the transect should be split into three sections: an 'upland' section, being the first 3-4 km of the transect; a 'mid-section' that contained the large bed irregularities between 4 and 12 km; and a 'lowland' section that was the remainder. These were designated as sections A, B and C respectively. There was tacit reasoning behind the sectioning of the transect in that it could be representational of the possible influence of increased subglacial hydrology with decreasing elevation if A was increased in each subsequent section.

However, it was quickly apparent that the introduction of so many new adjustable variables does not make the calibration process easier but rather makes the whole process a series of guesses with a change in one variable leading to undesired affects all along the profile. The most successful of the many attempts are shown in Figure 7.3. Figure 7.3a is shown because despite all of the combinations attempted this was the one that gave the lowest RMSE at 10.20 m, a modest improvement on what was achieved previously with uniform A . However, this improvement was purely due to the better fit in section A. Sections B and C were still positively biased.

In Figure 7.3b, the aim of the sectioning of the transect has been achieved. Increasing the coefficient as distance from the watershed increases has lowered the modelled profile in

section B without over-lowering section A. However, the profile in C is now tens of metres too high. The high coefficient has led to a transfer of mass downslope, however, the increase in ablation at the lower elevations has not been great enough to remove this mass thus causing a positive bias and leading to an RMSE of 13.55 m for the model run.

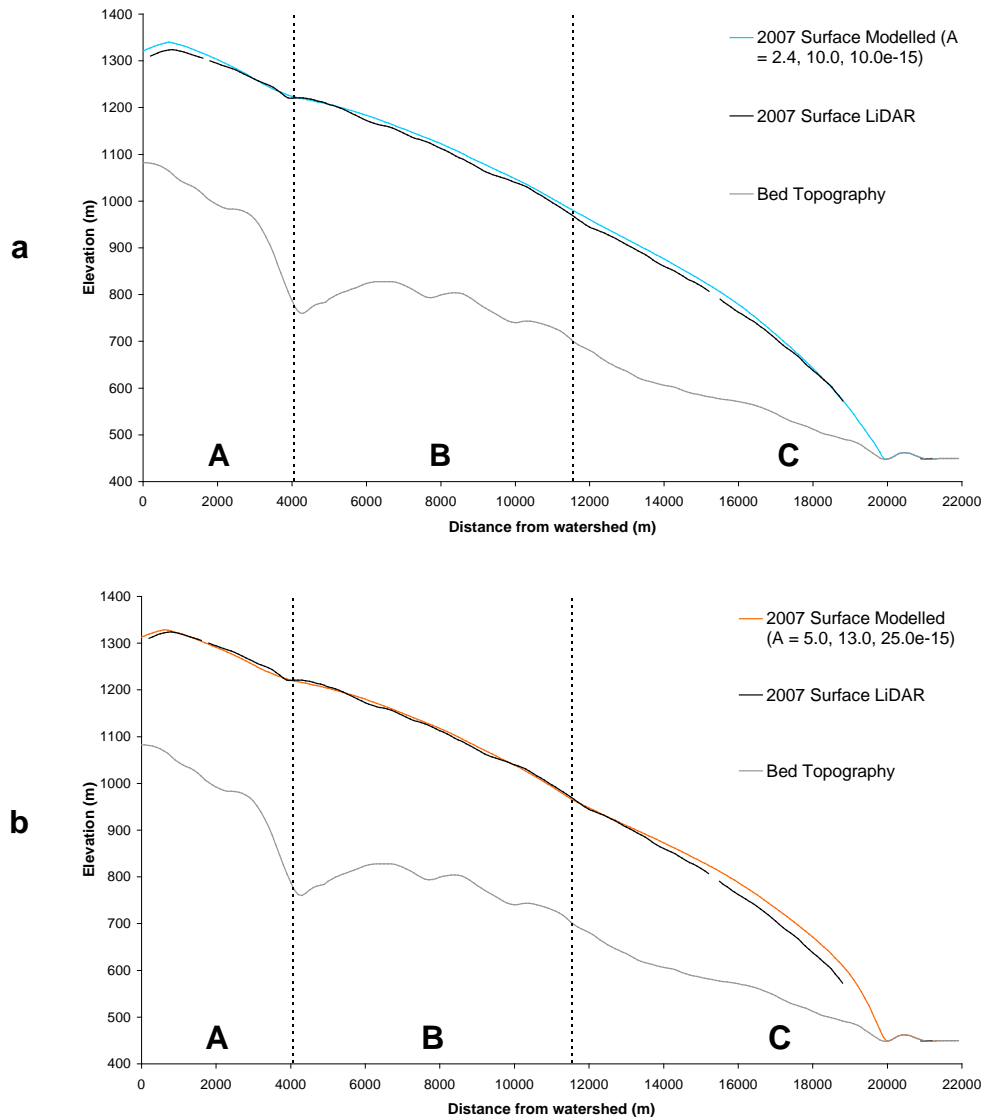


Fig. 7.3 Plotted modelled 2007 surface profiles with sectioned transect. In (a) the values of the flow law coefficient are $A = 2.4 \times 10^{-15}$, 10.0×10^{-15} , $10.0 \times 10^{-15} \text{ s}^{-1} (\text{kPa})^{-3}$ and the $\text{RMSE} = 10.20 \text{ m}$. In (b) the coefficients are $A = 5.0 \times 10^{-15}$, 13.0×10^{-15} , $25.0 \times 10^{-15} \text{ s}^{-1} (\text{kPa})^{-3}$ and $\text{RMSE} = 13.55$.

In addition to the continued problems related to trying to achieve an acceptable match along the full length of the transect, there were more fundamental issues with regard to the sectioning of the transect. Firstly, should one actually be able to achieve a decent match to the measured 2007 profile, it will have been done with scant regard for the processes that are actually acting on the glacier. In addition, should the shape of the glacier change (in

particular if it should retreat) the size of the sections will not change with it. Therefore a more dynamic approach to this problem was sought.

7.5 Linking ice flow to water flux

Using the mass balance model it is possible to evaluate which points on the transect will be free of snow come the end of the balance year. This author realised that this could be used as a proxy to infer where supraglacial drainage on the glacier surface would occur as at these points meltwater would be able to flow unencumbered by a snow layer. In addition, during their fieldwork on the glacier, Eyre et al (2005) noted that there was the “widespread presence of moulins” and that this “implies that meltwater can reach the glacier bed freely”. The rate of motion of a glacier is known to be sensitively dependent on the pressure and distribution of water at the bed (Benn and Evans, 1998) although the exact mechanics are still a topic of much debate (e.g. Barthomlomaus et al (2008); Bingham et al (2008)). Indeed, some processes such as basal sliding require the presence of liquid water to occur at all. Based on these points, this author formulated a new method for changing the flow law coefficient (and hence the effective speed of ice flow) that is dependent upon the flux of water at that point on the glacier.

Within the mass balance model code the new variable ‘bareice’ tracks the points on the glacier where that year’s snowfall is completely ablated. Where this is the case bareice = 1. Subsequently, for each point on the transect

$$A = \begin{cases} A_0 \lambda (a + r) & \text{where bareice} = 1 \\ A_0 & \text{where bareice} \neq 1 \end{cases} \quad (7.1)$$

where A_0 is a reference flow law coefficient, λ is a newly devised water lubrication factor, a is ablation in m w.e. and r is the precipitation that falls as rain in m. Therefore, where the surface of the glacier is bare ice, the flow coefficient will be a function of the sum of ablation and rain. This model is based on the assumptions that surface water will immediately reach the bed and that glacier flow increases with increasing water flux at the bed.

Clearly this is a huge simplification of the actual impact that water has on a glacier and it makes some big assumptions as well as avoiding some fundamental issues (what about the liquid water that is generated at points where there is still a snow layer?), but overall the concept is plausible to an extent. In addition, the model adapts to changing conditions and

only introduces one new variable (the water lubrication factor, λ). One further change made to the model was the inclusion of a visual indicator in the calibration GUI to show where along the transect this accelerated flow is being applied ((11) in Figure 7.1).

From watching the calibration GUI during the model runs it was clear that the section of the glacier that had bare ice for a given balance year was quite variable during the 11 year period used for calibration with the initiation point (effectively the equilibrium line altitude) ranging from between 5.5 km and 11 km from the watershed. This demonstrates how the model is able to adapt to the changing input from the mass balance model but also that the part of the transect that is being targeted by the model is the majority of the problematic mid-section. Figure 7.4 shows the results of two of the model runs.

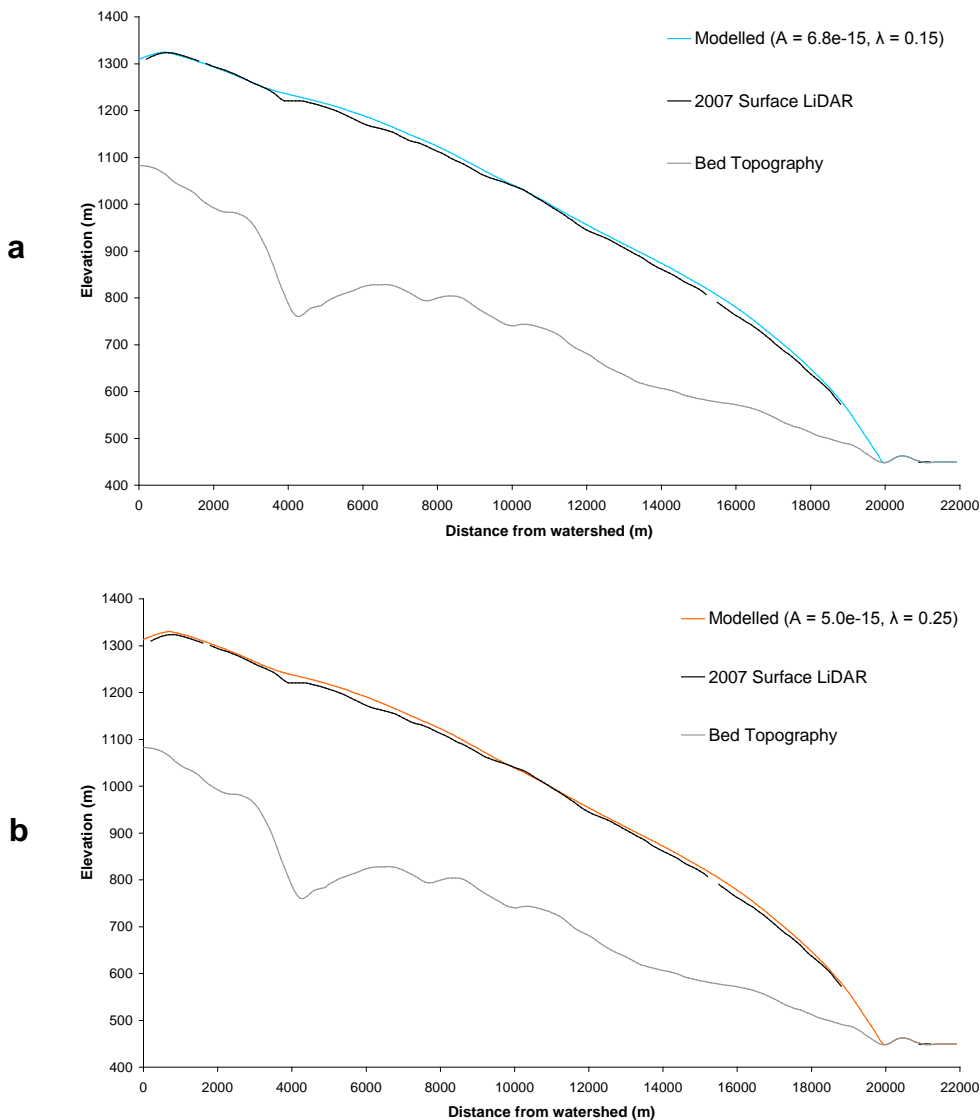


Fig. 7.4 Plotted modelled 2007 surface profiles produced with new water flux model. In (a) $\lambda = 0.15$ and $A_0 = 6.8 \times 10^{-15} \text{ s}^{-1} (\text{kPa})^{-3}$ resulting in a RMSE = 9.71 m. In (b) $\lambda = 0.25$ and $A_0 = 5.0 \times 10^{-15} \text{ s}^{-1} (\text{kPa})^{-3}$ resulting in a RMSE = 9.44 m.

This new methodology however, provides limited success when compared to the measured profile. Whilst it has provided the best representation of the shape of the profile over the entire length (Figure 7.4b) of all the model runs so far, the reduction in error is very modest with RMSE = 9.44 m for this run. It appeared to be the case that no matter how A was altered, the average elevation of the modelled profile would always be too high. For example, in the most representative model run so far (Figure 7.b) the sum of errors for the 184 points along the profile that are available for comparison is +1535.8 m. Referring back to section 7.2, a good fit requires the sum of errors being equal to zero.

In order to get an idea of how the net mass balance is distributed along the profile over the course of the calibration period, the ice flow model was disabled and the script rerun. The differences between the resulting profile and the measured 1997 profile will be an estimate of the cumulative net mass balance. Whilst not perfect (ignoring as it does the glacier's areal distribution with elevation and also how output from previous years will influence the net balance of future years among other factors), this gives an indication of the balance of the glacier as a whole over this period.

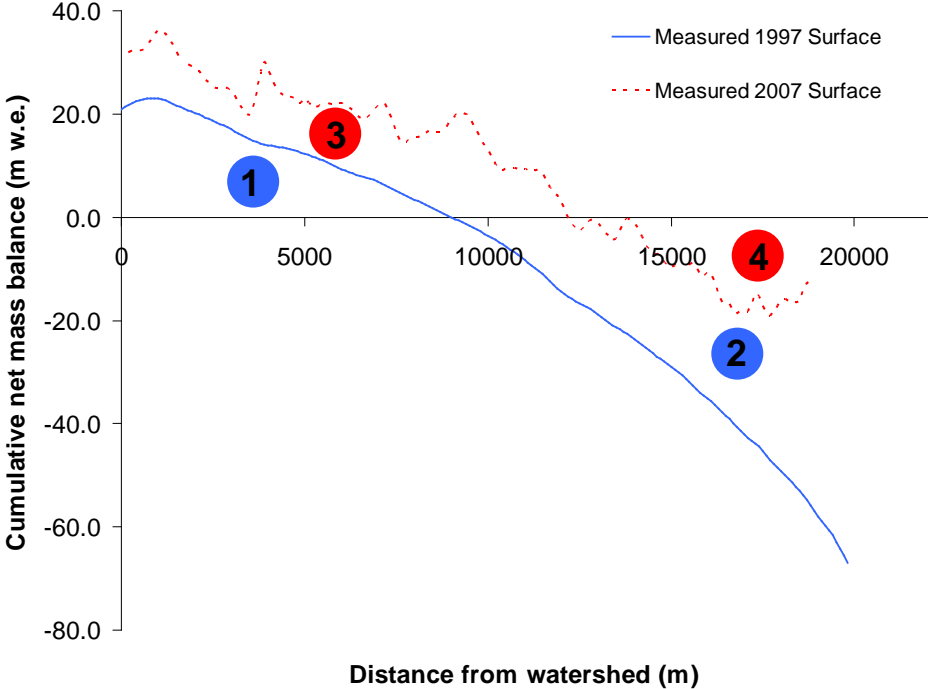


Fig. 7.5 Approximation of the cumulative net mass balance for the glacier over the balance years 1996-1997 to 2006-2007 (blue line). Additionally plotted is the difference between the cumulative net mass balance profile and the 2007 measured profile (red dotted line). In this model run the ice flow model was disabled and the only input was the net mass balance for each point as calculated by the mass balance model.

Should the glacier be in balance over the time period one would expect the areas under the graph of (1) and (2) in Figure 7.5 to be the same however, there is clearly a deficit. This is not surprising given that Langjökull ice cap as a whole is believed to have been in negative balance for the period 1990-2000 (Björnsson et al, 2006) and there is no indication in the climate records that the temperature has cooled or precipitation greatly increased since then. This negative balance is also required for the glacier to shrink to the 2007 profile.

The second plot (red dotted line) shows the differences between the modelled profile and the 2007 surface. If the model is to be able to remove enough mass from the glacier to enable it to match the 2007 surface profile this author would expect the sum of the areas under the graph for (3) and (4) in Figure 7.5 to equal zero. Clearly there is instead a large positive balance. Even allowing for the inaccuracies inherent in methodology employed to determine this, it appears clear that the ice flow model will simply not be able to match the 2007 measured profile until there is a greater mass loss from the glacier than the mass balance model calculations permit.

The calibrated mass balance model has been shown to match the measured mass balances to a very high standard (see section 4.2.3.2) and as such, this author does not believe that the mass balance model is at fault. Rather, the supposition put forward by the author is that the mass balance measurements have not been capturing the full mass loss from the glacier. The summer balances were derived from the measurement of changes in the snow core density during the summer in the accumulation area and from readings at stakes and wires drilled into the ice in the ablation area. These measurements were made in the autumn of each year. The winter balance was estimated by drilling ice cores through the winter layer in the spring (F. Pálsson, personal communication). These are well established methods and together provide an accurate measure of the net mass balance at a point on the *surface* of a glacier. However, mass loss from the *base* of the glacier is not accounted for in any way. It is proposed that there is a degree of ablation at the base of the glacier that the model is currently not accounting for.

7.6 Geothermal heating – the missing link?

Glacier ice is an excellent thermal insulator and heat generated at the bed is primarily used to warm the basal ice or, if the ice is at the pressure-melting point, enhance the rate of basal melting (van der Veen et al, 2007). Viscous heat dissipation (frictional heating from deforming or sliding ice) at the base of a glacier is known to produce subglacial melt but it is

of the order of mm yr^{-1} and therefore not to the degree necessitated by the apparent discrepancy observable in Figure 7.5.

Another source of energy is from geothermal heat originating within the Earth. It is common practice in glacier models that include geothermal heat flux in their calculations to assume a flux value that is based on continental-scale studies like Sclater et al (1980), on a particular lithology (e.g. Huybrechts, 1996; Huybrechts and T'siobbel, 1995), or a value calculated for an area nearby assumed to be of similar geothermal characteristics (e.g. Flowers et al, 1997). These assumptions are made because the magnitude of geothermal heating under bodies of ice is poorly constrained, not least because of the inaccessibility of the glacier bed (van der Veen, 2007). As with estimates for viscous dissipation, melt caused by geothermal heating is thought to be of the order of mm yr^{-1} , however there have been studies to suggest that there is high spatial variability and that melt rates can be orders of magnitude greater. An example of this is Fahnestock et al (2001) in which basal melt in a region of Greenland that was previously believed to be frozen to the bed (Huybrechts, 1996) was actually found to be up to 0.2 m yr^{-1} . Understandably, given the heat flux required for such melting, Fahnestock et al (2001) speculated that the source of the heat was volcanic.

The Langjökull ice cap is known to sit within the volcanic zone that covers much of central Iceland (Figure 1.2). Paying particular attention to Langjökull (Figure 7.6) one can see that north and south Langjökull overlie central volcanoes and the southern volcano underlies the majority of Hagafellsjökull vestari.

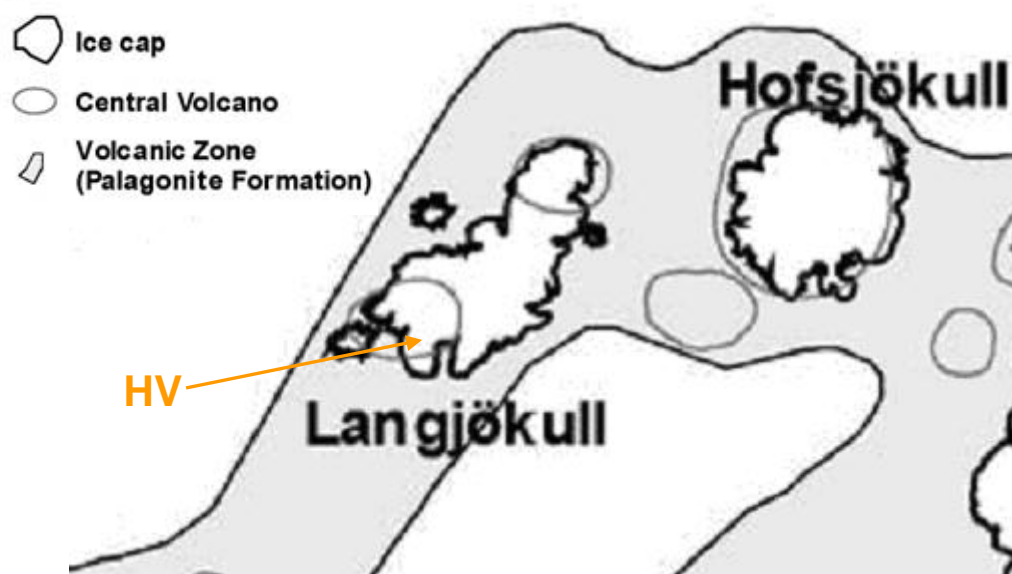


Fig. 7.6 Map detailing the situation of ice caps Langjökull and Hofsjökull relative to the volcanic zone and the central volcanoes within it. Of particular note is the central volcano under the southern part of Langjökull which Hagafellsjökull vestari (HV) overlies. (Source: adapted from Björnsson, 2002)

However, a review of the literature would suggest that neither of the volcanoes under Langjökull are active (Björnsson, 2002), nor is it believed that there are any other active geothermal areas under the ice cap (Flowers et al, 2007). On this basis Flowers et al (2007; 2008) use a uniform and constant value for geothermal heat flux in their modelling of Langjökull. Whilst they admit that the variation in background geothermal flux is unknown they do not consider it a significant source of melt. They then go further saying that “given the porous nature of the geologic substrate under Langjökull and western Vatnajökull, it has been estimated that groundwater flow is sufficient to transport most of the background geothermal energy away from the base of the ice cap (personal communication, Ó. Flóvenz, 2001)” (Flowers et al, 2007) effectively saying that they believe the geothermal heat flux they do apply in their models could even be an overestimate. With the flux value that Flowers et al (2007) use (150 mW m^{-2}) one can estimate that the basal melt rate in their model was $\sim 7 \text{ mm yr}^{-1}$ (based on the findings of Dahl-Jensen et al, 2003).

This is three orders of magnitude smaller than that estimated melt rate caused by the Grímsvötn caldera located beneath Vatnajökull ($\sim 8 \text{ m}_{\text{ice}} \text{ yr}^{-1}$, Bourgeois et al (2000)). Estimates of the caldera’s heat flux vary (50 W m^{-2} (Bourgeois et al, 2000) to 280 W m^{-2} (Jarosch and Guðmundsson, 2007) but it is responsible for increased basal melt across an area of 60 km^2 . Whilst not suggesting that there is caldera beneath Langjökull that has somehow gone unnoticed, this author believes that there is at least a possibility that the geothermal heat flux beneath Hagafellsjökull vestari is actually somewhere between the extremes given in Flowers et al (2007) and Jarosch and Guðmundsson (2007).

It so happens that such a middle ground is known to exist already in Iceland. Transient to long-lived small depressions can be found on the surface of Mýrdalsjökull ice cap (Figure 7.7) and they are believed to develop above long-lived geothermal heat sources (Björnsson, 2003). As per Jarosch and Guðmundsson (2007) the heat sources responsible are at the lower end of the scale in terms of magnitude and spatial extent (diameters are of the same order of magnitude as the ice thickness) but are also the “most common type of ice surface depression in Iceland”. In some cases the basal melt will accumulate forming small subglacial lakes that then drain in minor jökulhlaups, in others the meltwater drains continuously (Björnsson, 2002).

If similar geothermal heat sources were to exist beneath Hagafellsjökull vestari it is possible that they could produce basal melting at a rate that is necessary to account for the current discrepancy in ice mass between the modelled and measured 2007 glacier profiles.

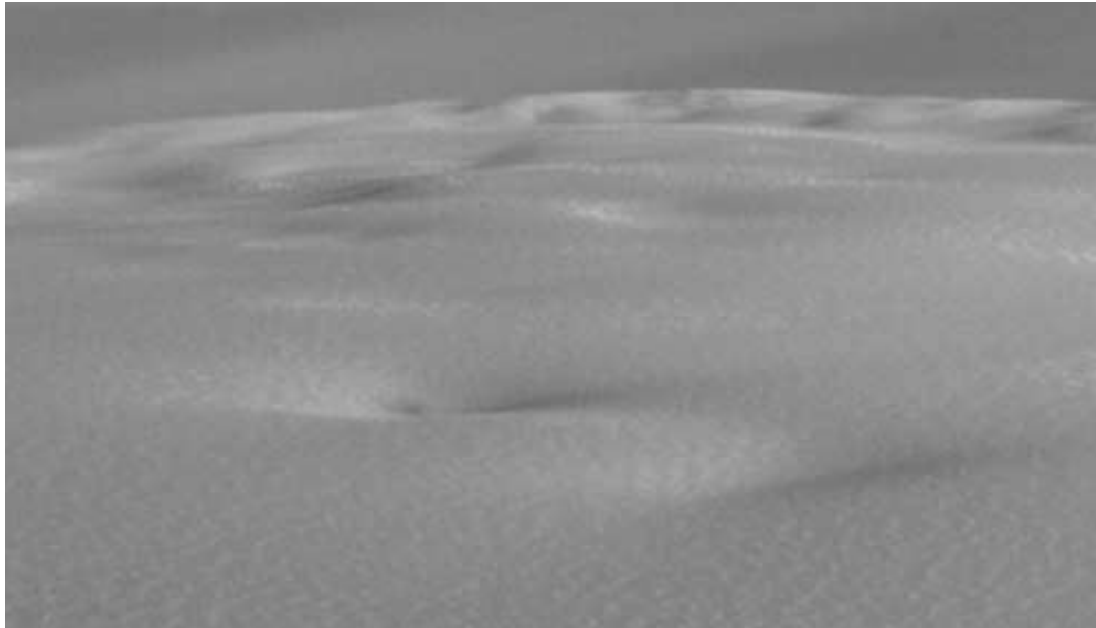


Fig. 7.7 Transient to long-lived small depressions on Mýrdalsjökull ice cap which are result of long-lived, low magnitude geothermal heat sources. Their diameter is of the same magnitude as the ice thickness and according to Jarosch and Guðmundsson (2007) they are the “most common type of ice surface depression in Iceland”. (Source: Jarosch and Guðmundsson, 2007)

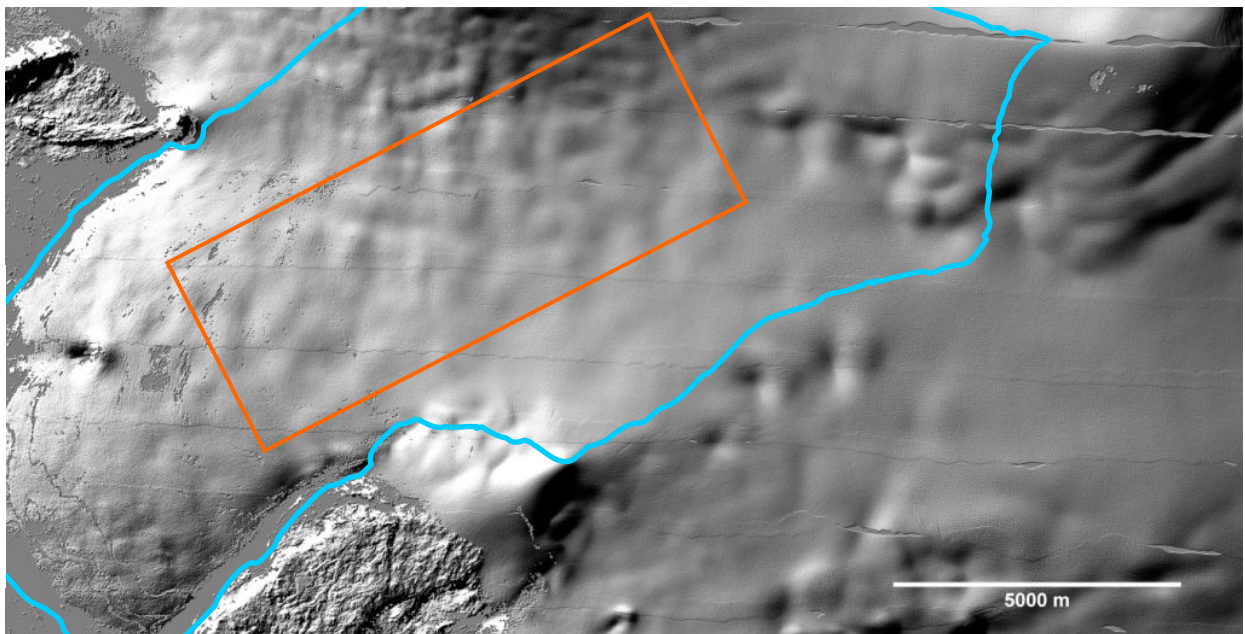


Fig. 7.8 Extract from 2007 surface DEM LiDAR that has then been hill-shaded. The image would suggest that there is a high degree of ‘pitting’ on much of the glacier surface (particularly within orange box). 1997 margin of Hagafellsjökull vestari outlined for reference (blue).

The original, 4 metre spatial resolution LiDAR DEM provides an opportunity to analyse the glacier surface to a degree not afforded by other data sources. With a ranging accuracy of ~0.15 m the LiDAR instrument enables the resolution of subtle surface undulations and certainly would resolve the features in Figure 7.7. Figure 7.8 is an extract from the original LiDAR DEM after the application of a hill-shading function. In it can clearly be seen that there is a degree of 'pitting' on a large part of the glacier surface. Further investigation showed that the undulations were of the order of 3-8 m deep and in many cases cut into the slope of the glacier rather than being caused by protrusions from it. The depth of the dips is considerably smaller than the average on Mýrdalsjökull (20-50 m (Björnsson, 2002)) but the widths of the features are within the expected bounds. However, the actual shape of the features is not absolutely clear from the image and attempts to determine it by analysis of multiple profiles was inconclusive. It is fair to say though that the glacier surface does not appear to have clearly defined, circular depressions that would definitely indicate the presence of geothermal heat sources as found on Mýrdalsjökull. However, this author postulates that the movement of the glacier ice downslope could be scrambling the form of the features making them less regular than those on Mýrdalsjökull. In any case, the cause of the features that are visible on the surface is not known but this author believes that the influence of spatially distributed, low-magnitude heat sources is one possibility.

It was decided that, whilst evidence was inconclusive, the addition of a basal melt term was a reasonable one. Whilst the low-magnitude heat sources on Mýrdalsjökull are spatially distributed, it was decided that for simplicity (and because the positioning of point sources of geothermal heat along the profile would necessarily be guesswork) a uniform basal melt rate would be applied to the model. However, this meltwater would be contributing to the water flux (Equation 7.1) and hence influence the flow law coefficient. The new variable would be termed 'basalmelt' in the model and would be of the form m w.e. yr^{-1} .

After initial investigations, it was clear that the addition of this term could greatly improve the performance of the model. However, with three 'tuning' parameters now in use, calibration needed to be more structured. Using results from the initial investigations, likely ranges for each parameter were determined and a methodical calibration was carried out. In all, 118 model runs were performed before the best combination of A , λ (the water 'lubrication' factor) and basal melt rate was determined (full results shown in Appendix). The resulting profile is shown in Figure 7.9.

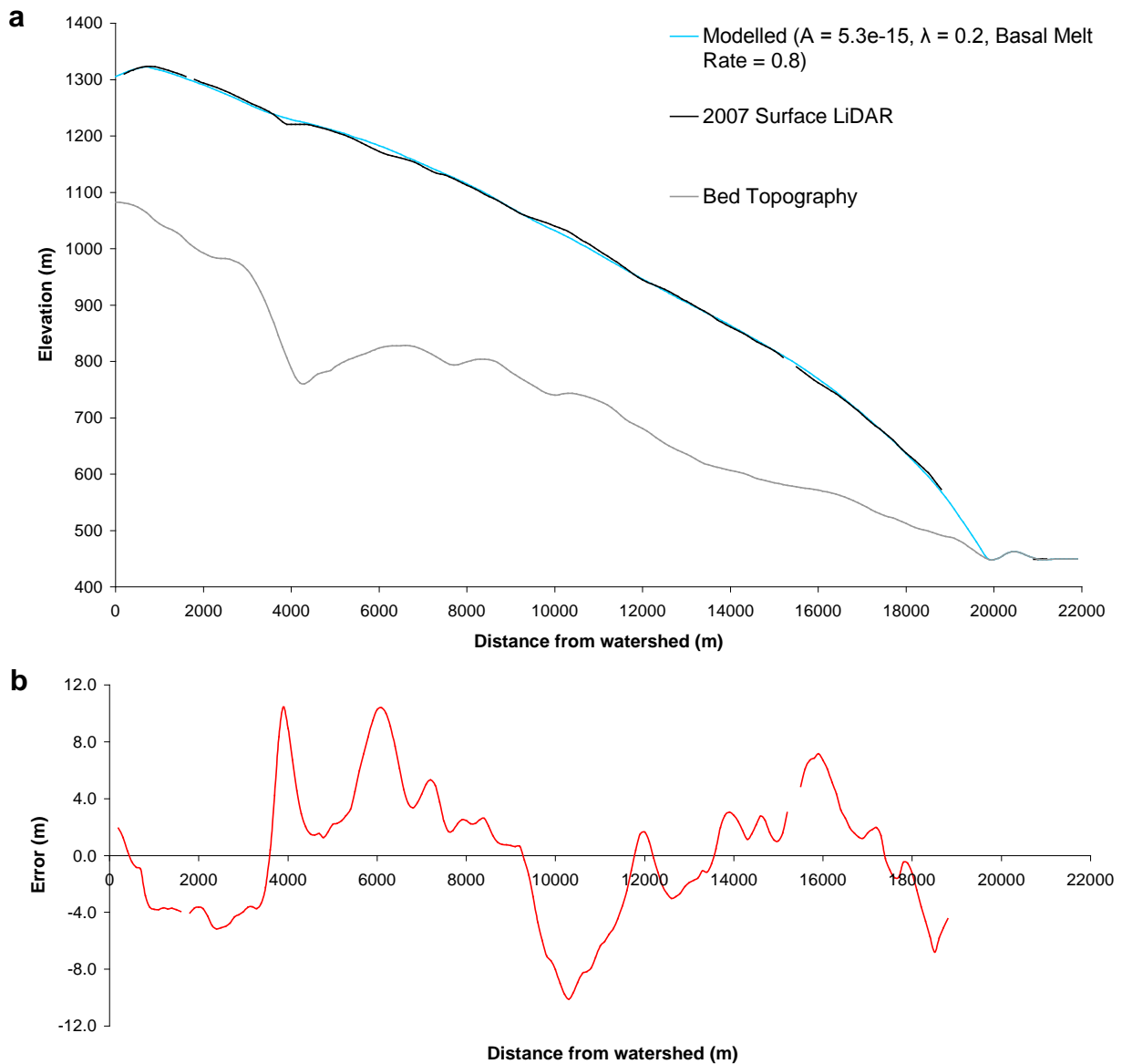


Fig. 7.9 (a) Plotted modelled 2007 surface profile produced with finalised model. $A_0 = 5.3 \times 10^{-15} \text{ s}^{-1} (\text{kPa})^{-3}$, $\lambda = 0.2$ and basal melt rate = $0.8 \text{ m w.e. yr}^{-1}$. Resulting RMSE = 4.41 m. (b) Plot of model error along the profile. There is no indication of major bias in the profile with positive and negative errors occurring along its full length. The sum of errors for all 184 available pairs is only +11.4 m.

In comparison to all other earlier efforts, this modelled profile is more representative of the measured profile in all respects. The general shape of the modelled surface is good with no particular bias in error towards one section of the profile (as can be seen in Figure 7.9b). In addition the RMSE is just 4.41 m, a reduction of over 60% from the best of the model runs in which a uniform flow law coefficient was used to tune the model. Finally, the sum of errors for the full length of the glacier was just +11.4 m further demonstrating the lack of error bias.

The actual values of the parameters used in the ice flow model were $A_0 = 5.3 \times 10^{-15} \text{ s}^{-1} (\text{kPa})^{-3}$, $\lambda = 0.2$ and basal melt rate = $0.8 \text{ m w.e. yr}^{-1}$ (Table 7.2). From comparison with suggested values from Paterson (1994) (Table 7.1) the value of A_0 would suggest an ice temperature of between -2 and 0°C which is certainly within expectations for a temperate glacier such as Hagafellsjökull vestari. The required basal melt rate, however, is some hundred times higher than this author believes to have been calculated in Flowers et al (2007) for Langjökull ice cap as a whole but it is also an order of magnitude smaller than melting estimated for Grímsvötn caldera beneath Vatnajökull. This places it firmly in the middle-ground and suggests to this author, at least, that the existence of active geothermal areas under Hagafellsjökull vestari is a distinct possibility.

Table 7.2 Finalised ice flow model parameters. These parameters will remain unchanged for the modelling of glacier behaviour to future climates.

Parameter	Value
Glen's flow law coefficient, $A_0 \text{ (s}^{-1} (\text{kPa})^{-3})$	5.3×10^{-15}
Water lubrication factor, λ	0.2
Basal melt rate (m w.e. yr ⁻¹)	0.8
Glen's flow law exponent	3
Density of ice (kg m ⁻³)	910
Gravity (m s ⁻²)	9.81

Using this finalised model, it is now possible to investigate the behaviour of the glacier in response to future climate scenarios.

8 THE RESPONSE OF HAGAFELLSJÖKULL VESTARI GLACIER TO FUTURE CLIMATE CHANGE SCENARIOS

8.1 Climate change scenarios

There are a few ways in which the climatic forcing for models run into the future can be determined. It can be done through what is essentially sensitivity analysis in which temperature and precipitation are changed at constant rates over time (e.g. Jóhannesson, 1997), or temperature and precipitation inputs can be based on the results from global circulation models (GCMs) that have predicted climatic variables based on a given scenario (e.g. Ren and Karoly, 2008). The latter is the method chosen in this study.

“Future greenhouse gas emissions are the product of complex dynamic systems determined by driving forces such as demographic development, socio-economic development, and technological change. Their future evolution is highly uncertain” (IPCC, 2000). Given this, the Intergovernmental Panel on Climate Change (IPCC) devised a set of scenarios for how the future might unfold, creating a tool with which to analyse how driving forces may influence future emission outcomes. These scenarios have provided a uniform framework on which the many competing teams developing GCMs can base their model runs. Each scenario is given a designation and a useful graphic providing a qualitative description of each scenario is shown below (Figure 8.1).

Scenario	Population	Economy	Environment	Equity	Technology	Globalisation	Climate
A1FI							
A1B							
A1T							
B1							
A2							
B2							

Fig. 8.1 Graphic providing a qualitative description of the IPCC emission scenarios (Source: adapted from IPCC (2001))

The IPCC also maintain a Data Distribution Centre (<http://www.ipcc-data.org/index.html>) that makes available online limited sets of output data from a large number of GCMs and for a number of the scenarios shown in Figure 8.1. It was from this repository that data for future climate scenarios was sourced for this study. Which scenarios and GCM were chosen was determined by the availability of the data in terms of proximity to the glacier and length of time into the future over which the GCM had been run. As a result, this study uses output from the 'ECHAM5' GCM (developed by the Max Planck Institute for Meteorology) with data for scenarios A1B, A2 and B1. In addition to these scenarios, mean values for temperature and precipitation were also calculated for the periods 1961-1990 and 1978-2007 using the ERA-40 reanalysis and Stafholtsey weather station data that has already been collected and processed (section 3.3). These 30-year averages would enable the modelling of the behaviour of Hagafellsjökull vestari glacier given the situation of no future climate changes.

8.2 Processing and interpolating scenario data

Monthly mean temperature and precipitation data were available for the time period up until 2099, however, the time was covered with just 3 values (twenty year averages for 2011-2030, 2046-2065 and 2080-2099). The data was of the form 'change from the 1961-1990 average', with temperature change in °C and precipitation change in m month⁻¹. The grid point for which the ERA-40 reanalysis data was calculated (64°08'N 20°15'W) was in between grid points for the GCM data (62°28'N 20°37'W and 64°20'N 20°37'W) so initially two sets of GCM data were acquired and the necessary interpolation was performed.

It was then necessary to convert the time series from the three twenty-year averages into a continuous time series from which yearly values could then be extracted. Initially this was attempted with the curve fitting algorithms in Matlab; however, it was soon clear that with so few points on which to base the curves and with fairly irregular patterns in the data, this was not a viable method. Instead, a simple linear relationship between successive points was established and the yearly values between them calculated (e.g. Figure 8.2) (N.B. in order to enable model runs of 100 years into the future, the final linear relationship was actually extended through to 2109). These monthly time series were rearranged into balance years to match the format of the climate input data used in the model's calibration and then the precipitation changes were summed to give the annual change from the 1961-1990 average for each balance year. The actual temperature and precipitation values were then calculated by adding the relevant 1961-1990 average from the ERA-40 reanalysis data. As measured data was already available for the period up until 2007, data for each scenario would only be

used forward of this time and so the new data series were overwritten up to this point. The full time series are provided in the Appendices.

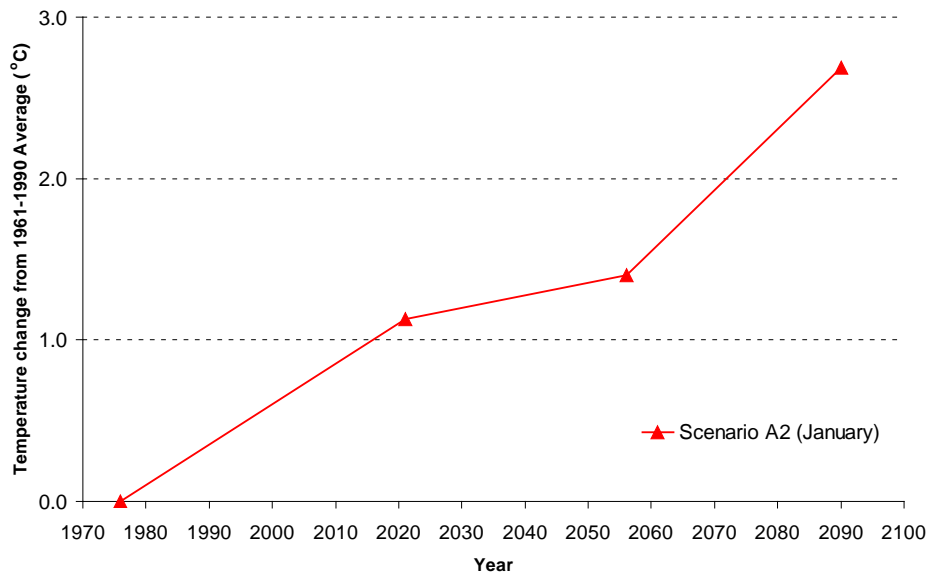


Fig. 8.2 Temperature change from the 1961-1990 average over time for the month of January given climate change scenario A2. Triangles (▲) denote points of known data. The only reasonable method for interpolation between these points was through the calculation of simple linear relationships between successive points (red lines). This process was performed for all months for temperature data; the combined annual change for precipitation data; and for each climate scenario.

8.3 Trends in the scenario data

Figure 8.3 shows the trends in the scenario data. Unsurprisingly, all three scenarios lead to increasing temperature with B1 presenting a linear relationship with time and A1B a virtually linear relationship with time. As a point of note, the rate of increase displayed by A1B approximates the climate scenario used in the Climate Change and Energy Production project (Jóhannesson, 1997). The graph for A2 is the most variable with warming approximating that of B1 for the first ~50 years before rapidly increasing thereafter. As can be seen in Figure 8.1, this is the only scenario out of the three in which world population continues to grow and the rapid temperature increase may be a consequence of it. After 125 years, scenario A2 will have resulted in an almost trebling of the average annual 1961-1990 temperature (1.68°C to 4.69 °C). It should be noted that the temperature graph does not capture any seasonal trends in the data, however, as the model input will be monthly rather than mean yearly data any such trends will be captured by the degree-day model.

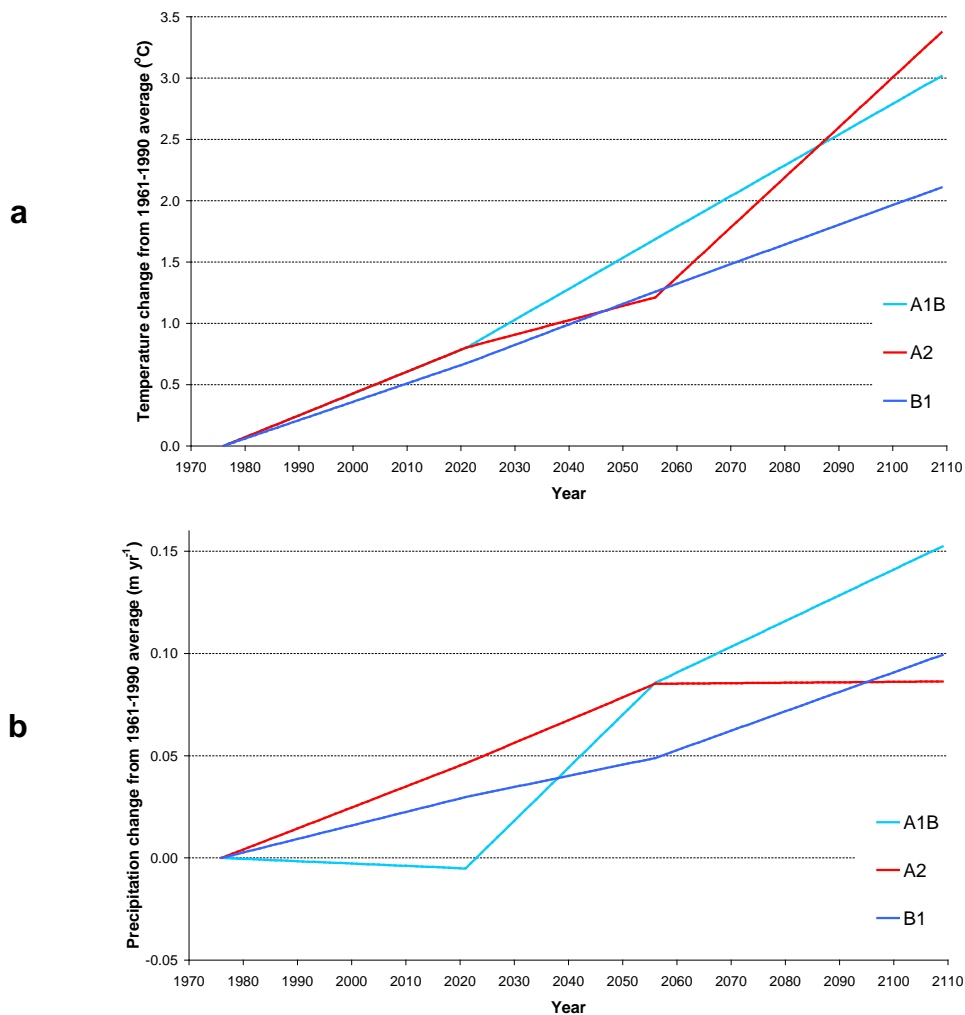


Fig. 8.3 Annual temperature change (a) and annual precipitation change (b) from the 1961-1990 average against time for each of the IPCC climate change scenarios. Underlying data was calculated by the ECHAM5 global circulation model.

Compared to the changes in temperature, the changes in precipitation are relatively modest for all scenarios. The greatest change after 100 years is the increase seen as a result of scenario A1B in which precipitation has increased by ~10% from the annual average for 1961-1990 (1.31 m yr⁻¹ to 1.45 m yr⁻¹).

8.4 Results and interpretation

For each scenario the model was run for the period 1997 to 2109. The start year was chosen to allow the model to initiate with the measured glacier geometry used in the calibration. It is worthy of note that Jóhannesson (1997) believed that as of 1990 Icelandic glaciers were relatively close to a steady-state condition after periods of advance and retreat since 1850. Björnsson et al (1996) also believe that Langjökull's specific net mass balance for the period

1981-2000 is close to zero. As advised in section 8.2, the first 11 years of each model run are the same as the known temperature and precipitation record was used for this period.

Analysis will initially concentrate on the glacier length and volume. The glacier length is measured from the glacier basin's watershed and the model calculates the volume of the glacier based on the assumption of a parabolic cross-section at each point on the transect from the watershed to the glacier front. Figure 8.4 shows the percentage change in glacier length and volume over the course of the model run relative to the 2007 values (remembering that the output up until 2007 is the same for all runs).

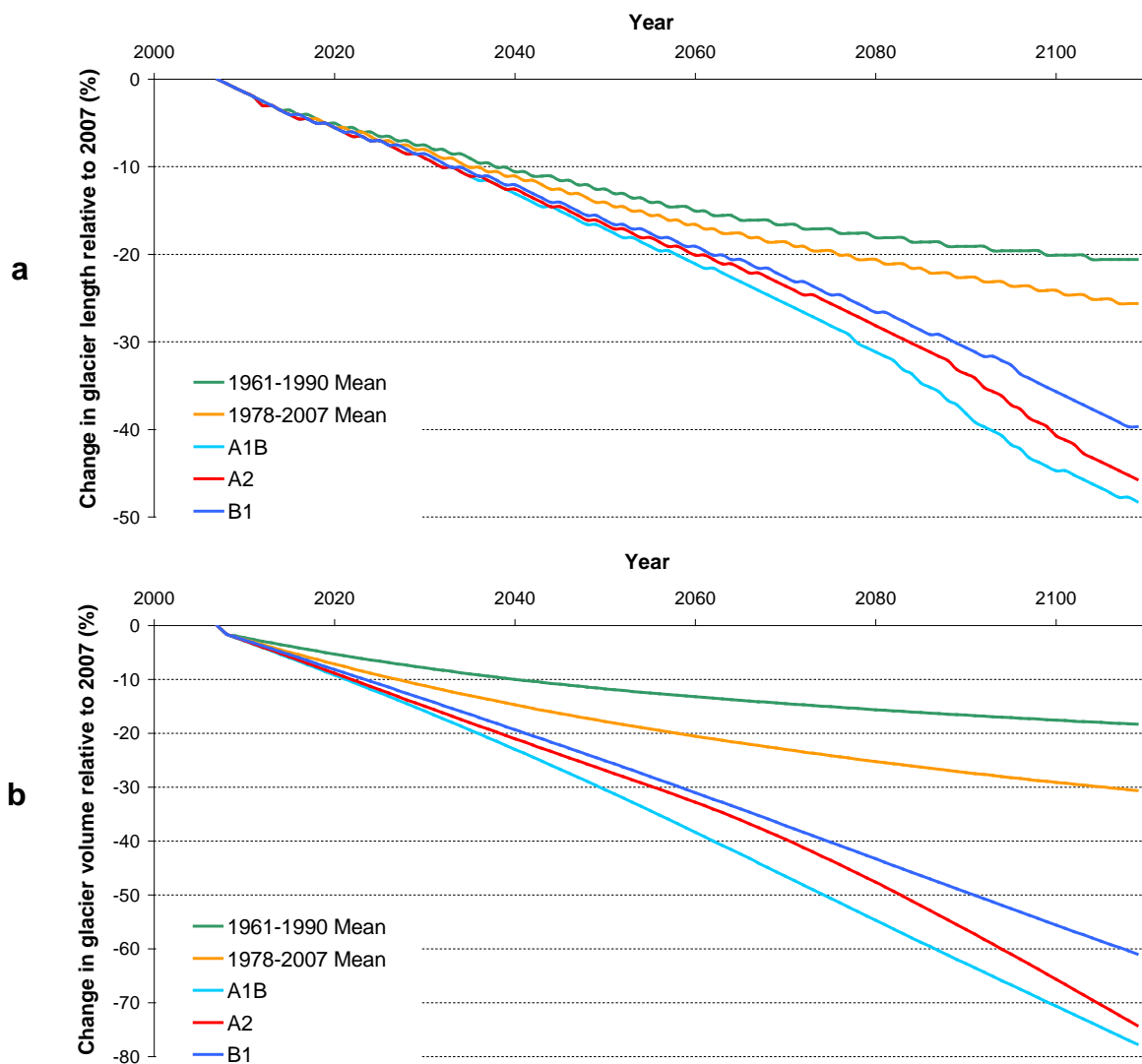


Fig. 8.4 Change in the length (a) and volume (b) of Hagafellsjökull vestari glacier over time relative to length and volume as at 2007. Graphs are given for each of the IPCC climate scenarios and also the 1961-1990 and 1978-2007 30-year averages. (N.B. 'steps' in (a) are due to the models 100 m resolution of glacier length).

The results of the model runs are, in the main, as one would expect given the temperature trends apparent in Figure 8.3a. As known from the sensitivity analysis (section 5), temperature is the primary driver in the mass balance model and given the only modest increases in precipitation (Figure 8.3b) it is not surprising that there are large losses both in terms of glacier length and volume. Under scenarios A1B and A2 the glacier loses over 45% of its length and ~75% of its mass in just over a century. Losses from scenario B1 are only slightly less pronounced with a reduction in length of 40% and a volume loss of just over 60%. The shape of the curves in Figure 8.4a and 8.4b mirror the shape of their respective temperature change curves in Figure 8.3a, further reinforcing the dominance that temperature exerts on the state of a glacier’s mass balance.

The response of the glacier to the 1961-1990 and 1978-2007 30-year averages is interesting. They indicate that it was highly unlikely that the glacier was in near steady-state at the start of the model run. In addition, from the convex shape of their curves in Figure 8.4a and 8.4b one can estimate that the dynamic response time of Hagafellsjökull vestari glacier is in the order of 150 years.

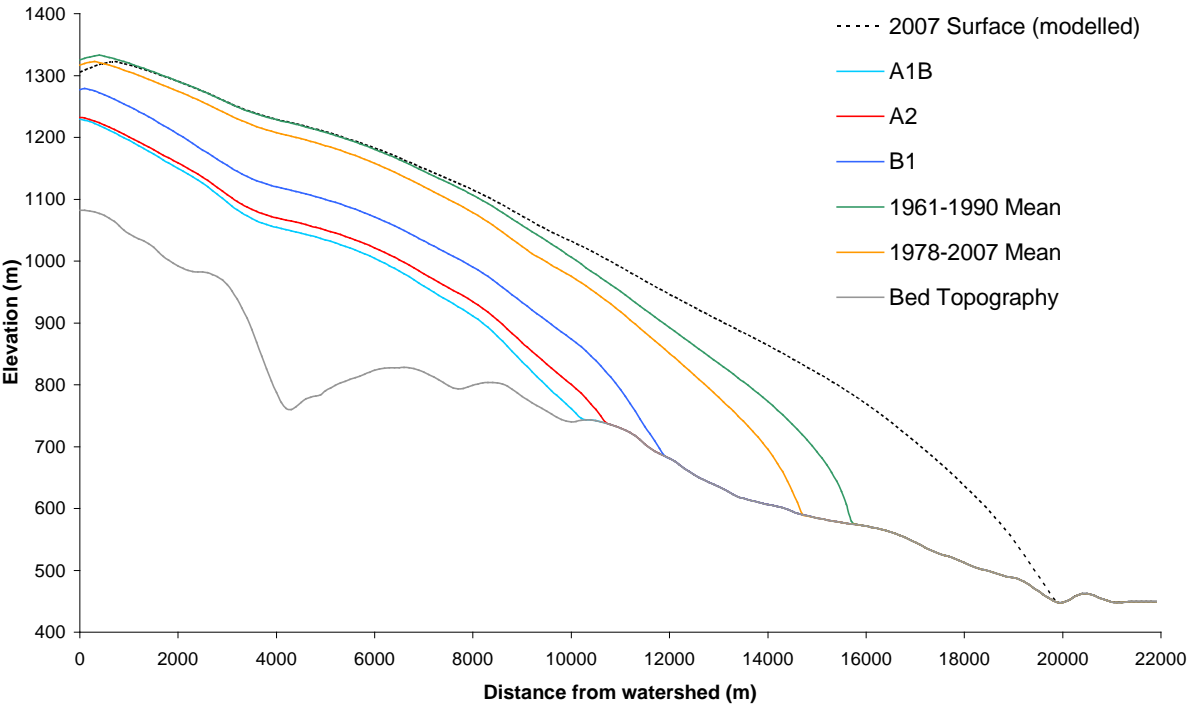


Fig. 8.5 Comparison of glacier surface profiles as at the end of their respective model runs (year 2109). The modelled 2007 surface profile (black dashed line) is included for reference.

Figure 8.5 clearly shows the impact that the warming scenarios have on the glacier profile. The IPCC scenarios will all result in significant lowering of the profile along the whole of the transect. In contrast, the 30-year averages appear to lose the bulk of their mass from the glacier snout. I believe that this supports the notion suggested above, that by the end of the model run the glacier is approaching a steady-state with respect to these two climates and is unlikely to suffer much further loss should the climate remain stable.

A major limitation with the model developed in this study is that when it is run over long time frames (as it has in these cases) it has no ability to predict the occurrence of (or model the behaviour resulting from) surges. During the calibration of the flow model it was known that no surges had occurred over those particular 11 years. However, with two surges in the last 40 years the likelihood of at least that many occurring over the next century is very high. Increased ablation post-surge could have a dramatic effect on the rate of mass loss, speeding up the process significantly. Given this, the results of the model runs can be considered as an upper-bound for each scenario, with actual likely mass loss being significantly larger.

In comparison to the modelling of the whole of Langjökull ice cap by Björnsson et al (2006) the results of this model appear plausible. Only one climate scenario was applied to their model but it is similar yet again (see section 8.3) to scenario A1B in this study. If it can be assumed that in Björnsson et al (2006) percentage volume loss for Langjökull ice cap as a whole closely approximates percentage volume loss for just Hagafellsjökull vestari glacier on its own, then the predicted loss due to scenario A1B in this study appears to be a near perfect match.

The main findings from the future climate model runs in this study are that: Hagafellsjökull vestari is not currently in equilibrium with the recent climate; the dynamic response time of the glacier is greater than 100 years and this author would approximate it to be ~150 years based around rates of volume loss from the 30-year average model runs; minimum volume loss from the glacier over the next century is likely to be ~20% in comparison to the 2007 volume; actual volume loss over the next century is likely to be 60-80% but could be even greater should the glacier surge frequently; the profile of the glacier is going to change dramatically should any of the five situations modelled actually occur.

9 CONCLUSIONS

The integration of the degree-day model into the original model script and the myriad other changes and adaptations made during the study have all been a great success. The model is now easier to use; can adapt to changing inputs; has a script that is logical and easy to follow; and now produces a range of output data that allows one to analyse every variable calculated by the degree-day and ice flow models. This last point in particular has enabled the inclusion in this report of in-depth analysis of the performance of both models.

Objectives relating to the generation of reference data have all been completed successfully. The use of the 2007 LiDAR DEM as a means of calibrating the ice flow model turned out to be of greater benefit than might initially have been expected when analysis of the high resolution DEM offered possible reasons for unexpected glacier behaviour during the calibration of the ice flow model. Additionally, having to combine data from Stafholtsey weather station with the ERA-40 reanalysis data removed the doubt that the author had had over the accuracy of such a data source. The ERA-40 reanalysis proved to be very well matched with regards to annual cycles and general magnitude of temperature and precipitation, in comparison to data from the nearby weather station (Figure 3.2).

The calibration of the degree-day mass balance model was at once both successful yet concerning. Whilst this author is confident that the final parameter values chosen (Table 4.6) provide a very accurate representation of the mass balance history of the glacier for the 11 years over which the calibration was run, he is not confident that the parameter values themselves are actually representative of the physical processes they were trying to reproduce. A case in point being the fact that the degree-day model was 'successfully' calibrated twice with the only reason for the first 'success' being rejected due to the unlikelihood of snow melting at a greater rate than ice. Whilst in this case a simple sanity check of the parameter values allowed the author to dismiss the result, with so many parameters poorly constrained, it is not overly cynical to suggest that the calibration could have resulted in a whole range of plausible parameter combinations. Only through more studies such as those carried out by Guðmundsson et al (2003a; 2003b), in which the output from degree-day models is compared directly to actual measurements recorded on a glacier surface, can parameters be better constrained. This would lead to a greater degree of faith in the output from such models.

A final point on degree-day models is made with regard to whether they are suitable for use in studies modelling future climate change at all. Guðmundsson et al (2003a) believe that the good performance achieved with degree-day models in past studies is in part due to the timing of certain independent trends within the energy balance cancelling the effects of each other during the ablation season. They propose that a changing climate could alter the relative timing of these trends, something that a degree-day model would not be able to account for. Presently, however, there is no alternative available and so the use of such a model in this study was unavoidable.

Calibration of the dynamic glacier model has led this author to believe that the assumptions others have made with regard to the level of geothermal heat flux under Langjökull ice cap can be called into question. As shown by the graph in Figure 7.5, total mass loss from the glacier since 1997, as implied by the measured mass balances, is simply not large enough to account for the mass loss implied by elevation along the 2007 measured profile. Believing that the measured mass balances are accurately recording the mass loss from the surface of the glacier, the logical conclusion, to this author at least, is that there must be mass loss at the glacier's base. Whilst fully aware that the adapted model is in no way attempting to actually model the physical processes behind geothermal heating, the inclusion of a uniform basal melt rate as a factor in the model enabled a much improved representation of the measured 2007 surface profile. Added to this, the fact that the LiDAR DEM appears to show unusual surface features that are not too far removed from those observed on the surface of the geothermally active Mýrdalsjökull ice cap, this author believes that the possibility of at least low magnitude geothermal activity below Hagafellsjökull vestari can at least be entertained. Whilst the annual melt rate of 0.8 m w.e. yr⁻¹ suggested from the model is high, recent research (Fahnestock et al, 2001) suggesting that melting of 0.2 m w.e. yr⁻¹ could be occurring under a section of the Greenland ice sheet previously thought to be frozen to the bed (Huybrechts, 1996) gives the author reason for optimism, especially given that the glacier in *this* study overlies a known volcanic zone (Figure 7.6). Whilst it might be expected that an additional mass loss of around 0.8 m w.e. yr⁻¹ across the whole of the glacier would be picked up by the monitoring of surface streams fed by it, it is actually believed that a significant part of the meltwater from Langjökull ice cap drains directly into a groundwater aquifer (Sigurðsson, 1990 *in* Guðmundsson et al, 2003a).

Given all the points made above, this author strongly believes that subglacial melting caused by geothermal heating does play a far larger role in the behaviour of Hagafellsjökull vestari glacier than others currently give it credit for.

The results from the future climate scenario runs are in line with those reported for a study modelling change for the whole of Langjökull ice cap (Björnsson et al, 2006). In the worst case scenario, the glacier will lose nearly 80% of its total volume in the next 100 years. Even in the least aggressive IPCC warming scenario, the glacier is predicted to lose over 60%.

Results from using 30-year climate averages show that the glacier is not in balance with the recent climate. Using average temperature and precipitation values for the period 1961-1990 will result in a volume loss of just under 20%; for averages for the period 1978-2007 the loss rises to just over 30%. It would appear, however, that after 100 years the glacier will be starting to approach equilibrium with the respective climates. This is in sharp contrast to all three warming scenarios in which the rate of volume loss is actually increasing with time.

This model makes no attempt to model the occurrence of, or behaviour resulting from, surges. Should a surge occur, the accelerated movement of ice downslope to lower elevations would result in increased subsequent ablation. As a result, this author proposes that the results from the future climate model runs are in fact the lower boundary of probable mass loss. A model run was also performed with the 1978-2007 30-year averages as the climatic forcing but this time starting with a bare bedrock surface. Without the extra elevation afforded by the 1997 ice thickness, the model demonstrated how the glacier would not be able to establish itself. As such, this author proposes that even with no further climate warming, a succession of glacier surges in the next century could lead to Hagafellsjökull vestari being pushed from a state of relative balance with climate to a state of high negative-balance and a period of terminal volume loss resulting in the complete disappearance of the glacier altogether.

LIST OF REFERENCES

- Anslow, F.S., Hostetler, S., Bidlake, W.R., and Clarke, P.U. (2008) Distributed energy balance modeling of South Cascade Glacier, Washington and assessment of model uncertainty. *J. Geophys. Res. Earth Surf.*, 113(F2), F02019.
- Arnold, N., Willis, I.C., Richards, K.S., and Lawson, W.J. (1996) A distributed surface energy balance model of a small valley glacier. I. Development and testing for the Haut Glacier D'Arolla, Valais, Switzerland. *J. Glaciol.*, 42, 77-89.
- Bamber, J.L. and Payne, A.J. (2004) Introduction and background. In Bamber, J.L. and Payne, A.J. (eds.) *Mass Balance of the Cryosphere: Observations and modelling of contemporary and future changes*. Cambridge, Cambridge Univ. Press, 1-10.
- Bartholomaeus, T.C., Anderson, R.S., and Anderson, S.P. (2008) Response of glacier basal motion to transient water storage. *Nature Geosci.*, 1(1), 33-37.
- Benn, D.I., Evans, D.J.A. (1988) *Glaciers and Glaciation*. Arnold, London.
- Bingham, R.G., Hubbard, A.L., Nienow, P.W., and Sharp, M.J. (2008) An investigation into the mechanisms controlling seasonal speedup events at a High Arctic glacier. *J. Geophys. Res. Earth Sci.*, 113(F2), F02006.
- Björnsson, H. (2002) Subglacial lakes and jökulhlaups in Iceland. *Glob. Plan. Change*, 35, 255-271.
- Björnsson, H., Pálsson, F, Sigurðsson, O., and Flowers, G.E. (2003) Surges of glaciers in Iceland. *Ann. Glaciol.*, 36, 82-90.
- Björnsson, H., Aðalgeirsdóttir, G., Guðmundsson, S., Jóhannesson, T., Sigurðsson, O., and Pálsson, F. (2006) Climate change response of three Vatnajökull, Höfsjökull and Langjökull ice caps, Iceland [online]. *European Conference on Impacts of Climate Change on Renewable Energy Sources*. Available from www.raunvis.hi.is/~sg/Gudmundsson_et_al.pdf [Accessed on: 25 May 2009].

Bøggild, C.E., Reeh, N., and Oerter, H. (1994) Modelling ablation and mass-balance sensitivity to climate change of Storstrømmen, Northeast Greenland. *Glob. Plan. Change.*, 9, 79-90.

Bourgeois, O., Dauteuil, O., van Vliet-Lanoë, B. (2002) Geothermal control on flow patterns in the last glacial maximum ice sheet of Iceland. *Earth Surf. Procs. Landforms*, 25, 59-76.

Braithwaite, R.J. (1981) On glacier energy balance, ablation, and air temperature. *J. Glaciol.*, 27(97), 381-391.

Braithwaite, R.J. (1985) Calculation of degree-days for glacier-climate research. *Z. Gletscherkd. Glazialgeol.*, 20, 1984, 1-8.

Braithwaite, R.J. (1995) Positive degree-day factors for ablation on the Greenland ice sheet studies by energy-balance modelling. *J. Glaciol.*, 41(137), 153-160.

Braithwaite, R.J., and Raper, S.C.B. (2007) Glaciological conditions in seven contrasting regions estimated with the degree-day model. *Ann. Glaciol.*, 46, 297-302.

Cazenave, A., Lombard, A. and Llovel, W. (2008) Present day sea level rise: A synthesis. *Oceanography*, 340(11), 761-770.

Dahl-Jensen, D., Gundestrup, N., Gogineni, S. P., and Miller, H. (2003) Basal melt at NorthGRIP modeled from borehole, ice-core and radioecho sounder observations. *Ann. Glaciol.*, 37, 207– 212.

Dyurgerov, M. (2002) Glacier Mass Balance and Regime: Data of Measurements and Analysis. *University of Colorado, Institute of Arctic and Alpine Research, Occasional Paper* 55, 268p.

Einarsson, M.A. (1984) Climate of Iceland, in van Loon, H. (ed.) *World survey of climatology: 15: Climates of the oceans*. Elsevier, Amsterdam. 673-697.

Eyre, N.S., Payne, A.J., Baldwin, D.J., and Björnsson, H. (2005) The use of salt injection and conductivity monitoring to infer near-margin hydrological conditions on Vestari-Hagafellsjökull, Iceland. *Ann. Glaciol.*, 40, 83-88.

Fahnestock, M., Abdalati, W., Joughin, I., Brozena, J., and Gogineni, P. (2001) High geothermal heat flow, basal melt, and the origin of rapid ice flow in central Greenland. *Science*, 294, 2338-2342.

Flowers, G.E., Björnsson, H., Geirsdóttir, Á., Miller, G.H, and Clarke, G.K.C. (2007) Glacier fluctuation and inferred climatology of Langjökull ice cap through the Little Ice Age. *Quat. Sci. Rev.*, 26, 2337-2353.

Flowers, G.E., Björnsson, H., Geirsdóttir, Á., Miller, G.H, Black, J., and Clarke, G.K.C. (2008) Holocene climate conditions and glacier variation in central Iceland from physical modelling and empirical evidence. *Quat. Sci. Rev.*, 27, 797-813.

Fuller, S. and Murray, T. (2002) Sedimentological investigations in the forefield of an Icelandic surge-type glacier: implications for the surge mechanism. *Quat. Sci. Rev.*, 21(12-13), 1503-1520.

Greuell, W. (1992) Hintereisferner, Austria – Mass balance reconstruction and numerical modelling of the historical length variations. *J. Glaciol.*, 38(129), 233-244.

Guðmundsson, S., Björnsson, H., Pálsson, F., and Haraldsson, H.H. (2003a) Comparison of physical and regression models of summer ablation on ice caps in Iceland. *Raunvísindastofnun Háskólans*. RH-15-2003. Available from <http://www.raunvis.hi.is/~sg/emodels.pdf> [Accessed on: 24 May 2009].

Guðmundsson, S., Björnsson, H., Pálsson, F., and Haraldsson, H.H. (2003b) Physical energy balance and degree-day models of summer ablation on Langjökull ice cap, SW-Iceland. *Raunvísindastofnun Háskólans*. RH-20-2003. Available from <http://www.raunvis.hi.is/~sg/lmodels.pdf> [Accessed on: 24 May 2009].

Hart, J.K. (1995) Recent drumlins, flutes and lineations at Vestari-Hagafellsjökull , Iceland. *J. Glaciol.*, 41(139), 596-606.

Hock, R. (2003) Temperature index melt modelling in mountain areas. *J. Hydrol.*, 282, 104-115.

Hock, R., Radic, V., and De Woul, M. (2007) Climate sensitivity of Storglaciären, Sweden: an intercomparison of mass-balance models using ERA-40 re-analysis and regional climate model data. *Ann. Glaciol.*, 46, 342-348.

Hoinkes, H.C. (1968) Glacier variation and the weather. *J. Glaciol.*, 7(49), 3-19.

Hubbard, A. (2006) The validation and sensitivity of a model of the Icelandic ice sheet. *Quat. Sci. Rev.*, 25, 2297-2313.

Hughes, P.D. and Braithwaite, R.J. (2008) Application of a degree-day model to reconstruct Pleistocene glacial climates. *Quat. Res.*, 69, 110-116.

Huybrechts, P. (1996) Basal temperature conditions of the Greenland ice sheet during the glacial cycles, *Ann. Glaciol.*, 23, 226-236.

Huybrechts, P.H., de Nooze, P., and Declair, H. (1989) Numerical modelling of Glacier d'Argentiere and its historic front variations. In Oerlemans, J. (ed.) *Glacier fluctuations and climate change*. Dordrecht, etc., Kluwer Academic Publishers, 373-390.

Huybrechts, P.H. and T'siobbel, S. (1996) Thermomechanical modelling of Northern Hemisphere ice sheets with a two-level mass-balance parameterization. *Ann. Glaciol.*, 21, 111-116.

Huybrechts, P.H. and de Wolde, J. (1999) The dynamic response of the Greenland and Antarctic ice sheets to multiple-century climatic warming. *J. Climate*, 12(8), 2169-2188.

IMO (no date) Icelandic Climatic Data [online]. Available from http://andvari.vedur.is/vedurfar/yfirlit/vedurfarsgogn_en.html [Accessed on: 05 May 2009].

IPCC (2000) IPCC Special Report: Emission Scenarios. Summary for policy makers [online] Intergovernmental Panel on Climate Change. Available from: <http://www.ipcc.ch/pdf/special-reports/spm/sres-en.pdf> [Accessed: 15 May 2009].

IPCC (2001) Climate Change 2001: Mitigation Report of the IPCC [online] Intergovernmental Panel on Climate Change. Available from: http://www.grida.no/climate/ipcc_tar/ [Accessed on: 15 May 2009]

IPCC (2007) Climate Change 2007 Synthesis Report [online] Intergovernmental Panel on Climate Change. Available from <http://www.ipcc.ch/ipccreports/ar4-syr.htm> [Accessed on: 15 May 2009].

Jarosch, A. H. and Guðmundsson, M. T. (2007) Numerical studies of ice flow over subglacial geothermal heat sources at Grímsvötn, Iceland, using Full Stokes equations. *J. Geophys. Res.*, 112, F02008,

Jóhannesson, T. (1997) The response of two Icelandic glaciers to climate warming computed with a degree-day glacier mass-balance model coupled to a dynamic glacier model. *J. Glaciol.*, 43(143), 321-327.

Jóhannesson, T., Sigurdsson, O., Laumann, T., and Kennet, M. (1995) Degree-day glacier mass-balance modelling with applications to glaciers in Iceland, Norway and Greenland. *J. Glaciol.*, 41(138), 345-358.

Knight, P.G. (1999) *Glaciers*. Cheltenham, Stanley Thornes (Publishers).

Kulkarni, A.V., Rathore, B.P., and Alex, S. (2004) Monitoring of glacial mass balance in the Baspa basin using accumulation area ratio method. *Current Science*, 86(1), 185-190.

Laumann, T. and Reeh, N. (1993) Sensitivity to climate change of the mass balance of glaciers in southern Norway. *J. Glaciol.*, 39(133), 656-665.

Letreguilly, A. (1988) Relation between the mass balance of western Canadian mountain glaciers and meteorological data. *J. Glaciol.*, 34(116), 11-18.

Meier, M.F. (1965) Glaciers and climate. In Wright, H.E. and D.G. Frey (eds.), *The Quaternary of the United States*, Princeton University Press, Princeton, New Jersey, 795-805.

Meier, M.F., Dyurgerov, M.B., Rick, U.K., O'Neel, S., Pfeffer, W.T., Anderson, R.S., Anderson, S.P. and Glazovsky, A.F. (2007) Glaciers dominate eustatic sea-level rise in the 21st century. *Science*, 317, 1064-1067.

Oerlemans, J. (1994) Quantifying global warming from the retreat of glaciers. *Science*, 264(5156), 243-245.

Oerlemans, J. (1997) A flow-line model for Nigardsbreen, Norway: projection of future glacier length based on dynamic calibration with the historic record. *Ann. Glaciol.*, 24, 382-389.

Oerlemans, J. (1989) On the response of valley glaciers to climatic change. In Oerlemans, J., (ed.) *Glacier fluctuations and climate change*. Dordrecht, etc., Kluwer Academic Publishers, 353-371.

Oerlemans, J. (2005) Extracting a climate signal from 169 glacier records. *Science*, 308(5722), 675-677.

Paterson, W.S.B. (1994) *The Physics of Glaciers* (third edition). Oxford, Pergamon Press.

Rasmussen, L.A., and Conway, H. (2001) Estimating South Cascade Glacier (Washington, U.S.A.) mass balance from a distant radiosonde and comparison with Blue Glacier. *J. Glaciol.*, 47(159), 579-588

Reeh, N. (1991) Parameterization of melt rate and surface temperature on the Greenland ice sheet. *Polarforschung.*, 59(3), 113-128.

Ren, D. and Karoly, D.J. (2008) Predicting the response of seven Asian glaciers to future climate scenarios using a simple linear glacier model. *J. Geophys. Res. - Atmos.*, 113(D5), D05103.

Schlosser, E. (1997) Numerical simulation of fluctuations of Hintereisferner, Otztal Alps, since AD 1850. *Ann. Glaciol.*, 24, 199-202.

Sclater, J.G., Jaupart, C., and Galson, D. (1980) The heat flow through oceanic and continental crust and the heat loss of the Earth. *Rev. Geophys. Space Phys.*, 18, 269-311.

Sigurðsson, Freysteinn (1990) Groundwater from glacial areas in Iceland. *Jökull*, 40, 119-146.

Sigurðsson, O. and Williams, R.S. (2008) Geographic names of Iceland's glaciers: Historic and modern. *U.S. Geological Survey Professional Paper 1746*, 225 p. Available from: <http://pubs.usgs.gov/pp/1746/> [Accessed 10 May 2009]

SPRI (unpublished) Geometry and Mass Balance Changes of Langjökull, Iceland [online] Scott Polar Research Institute, Cambridge. Available from: <http://www.spri.cam.ac.uk/research/projects/langjokullmassbalance/> [Accessed 29 May 2009]

Stroeven, A., van de Wal, R.S.W., and Oerlemans, J. (1989) Historic front variations of the Rhone Glacier: simulation with an ice flow model. In Oerlemans, J., (ed.) *Glacier fluctuations and climate change*. Dordrecht, etc., Kluwer Academic Publishers, 391-406.

Tangborn, W.V. (1980) Two models for estimating climate-glacier relationships in the North Cascades, Washington, U.S.A.. *J. Glaciol.*, 25(91), 3-22.

Tangborn, W.V. (1984) Prediction of glacier derived runoff for hydroelectric development. *Geogr. Ann.*, 66A(3), 257-265.

van der Veen, C.J. (2002) Polar ice sheets and global sea level: how well can we predict the future? *Glob. Plan. Chnge.*, 32, 165-194.

van der Veen, C.J., Leftwich, T., von Frese, R., Csatho, B.M., Li, J. (2007) Subglacial topography and geothermal heat flux: Potential interactions with drainage of the Greenland ice sheet. *Geophys. Res. Let.*, 34, L12501.

Zuo, Z., and Oerlemans, J. (1997) Numerical modelling of the historic front variations and the future behaviour of the Pasterze glacier, Austria. *Ann. Glaciol.*, 24, 234-241.

APPENDIX 1

Appendix 1.1 The Matlab script

- 1.1.1 Adaptations to the original Matlab script
- 1.1.2 Basic instructions for running the finished model

Appendix 1.2 Printout of the final Matlab script

Appendix 1.3 Data from reference input file detailing bed topography elevation and the 2007 surface profile in addition to the 1997 reference widths and thicknesses along the profile

Appendix 1.4 Data from the input files relating to the different climate scenarios

- 1.4.1 ERA-40 reanalysis / Stafholtsey weather station data
- 1.4.2 1961-1990 30-year average data (after 2007)
- 1.4.3 1978-2008 30-year average data (after 2007)
- 1.4.4 IPCC Scenario A1B (based on ECHAM5 GCM output) (after 2007)
- 1.4.5 IPCC Scenario A2 (based on ECHAM5 GCM output) (after 2007)
- 1.4.6 IPCC Scenario B2 (based on ECHAM5 GCM output) (after 2007)

Appendix 1.4 CD

- 1.4.1 readme.txt
- 1.4.2 Folder containing files required to replicate the model runs performed in this study (Matlab scripts and input files)
- 1.4.3 Folder containing other Matlab code and associated file written to assist in data processing whilst calibrating mass balance model

Appendix 1.1

1.1.1 Adaptations to the original Matlab script

Over the course of the study the Matlab code provided by N.S. Arnold was completely overhauled. By the time the 'iceflo.m' script was finalised and used to perform the climate change scenario runs, it had been through more than 150 iterations and the only part of the original code still included and unaltered related to the initialisation of the graphical user interface at the start of a run.

The original script was over 1000 lines in length. Working through the code line by line this author was able to reduce it to 450 lines having removed all obsolete code and any other code unnecessary to achieve the aims of this project. As the project progressed the script grew to the 670 lines that it is now, after original code was adapted and new code added in. It should be noted that if any changes were made to the script that could inadvertently impact the output from previous runs, these earlier runs would be re-performed with the new script to ensure consistency.

Whilst all of the changes and improvements made to the script would be too numerous to list, some examples are given below:

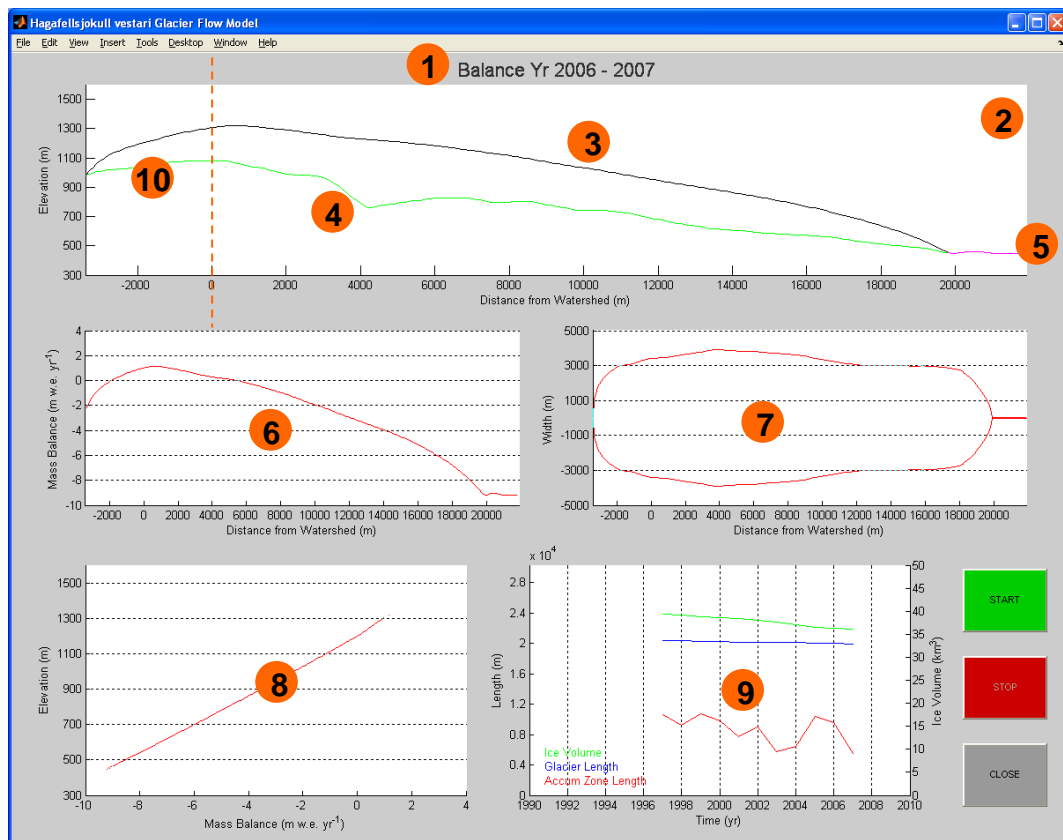
- completely reorganised and annotated the code to make it easier to follow and far easier to navigate
- reduced the number of required input files
- integrated the degree-day calculation into the script
- overhauled the graphical user interface (GUI) to make it clearer, more relevant and able to adapt to changing ranges of input data
- introduced the option of a 'Calibration GUI' (Figure 7.1) that gives preference in the GUI window to data applicable to the calibration of the ice flow model (e.g. larger profile window, information regarding the current RMSE when compared to the 2007 surface profile, the parameter values that are currently in use, etc.)
- the ice flow model is now capable of parameterising the water flux at the glacier bed (and the subsequent effect on its behaviour) through the introduction of the water lubrication factor and the capability to calculate water flux at each point on the transect
- the model is also now capable of parameterising the impact of basal melt both in terms of its affect on ablation rates, and on the glacier's dynamic behaviour through its contribution to the water flux

- essential to the analysis of both the performance of the model and the outcome of the model runs, the script has been rewritten to produce time-stamped, time-series output files for virtually all variables calculated in the model; in addition it generates a time-stamped folder in the workspace to save them in. If the model run is interrupted, it has been designed so that output files with data up until that point will still be generated.
- additionally there is the introduction of a 'logfile' that details the values of all parameters set by the user for that particular run
- it was discovered that the model requires a 'spin-up' of one time-step cycle in order to accurately calculate the glacier's volume. This has now been hardcoded into the model and with the default time-step of 1/64th of a year, this does not lead to any significant impact on model runs.

1.1.2 Basic instructions for running the finished model

The Matlab files 'iceflo.m', 'pddcalc.m', and 'pptfrac.m' in addition to the folder 'Input Files' must be in the 'Current Directory' in Matlab before the run is initiated.

To run the model in its default state, type 'iceflo' in the Command Window and hit enter. This will bring up the GUI. Hit 'START' to begin the run. The run can be interrupted at any time by pressing 'STOP', however, that particular run cannot then be restarted. The default model GUI is shown below.



The different features of the GUI are (1) the balance year of the most recently calculated time step (information in all other windows will relate to this time); (2) the glacier profile window within which is the modelled profile (black (3)), the bed topography (pink (4)), and any ice free areas (pink (5)); (6) the net mass balance as a function of distance from the watershed; (7) a plan view of the glacier surface extent; (8) net mass balance as a function of elevation; (9) ice volume (green), glacier length (blue) and the total length of the accumulation zone (red) as a function of time (N.B. these values are only with respect to the glacier forward of the watershed and do not include data from the 'buffer zone' indicated by (10) and dashed orange line).

To alter any parameters, one must open the 'iceflo.m' file and navigate to the parameter setup area (from line 110) shown below.

```

110 %----- PARAMETER SET UP ----- %
111
112 %----- READ IN CLIMATE DATA AND REFERENCE DATA
113
114 calibrating = 0; % If calibrating against 2007 LiDAR data say '1'. This will
115 % draw 2007 profile and provide data useful for calibration
116
117 show1997 = 0; % If '1' then will display 1997 reference surface
118
119 outputfiles = 1; % Determines whether output files will be generated by this
120 % run. If equals '1' then files will be generated
121
122 initial_ice = 1; % Initial ice cover. If '1' then model starts with the ice
123 % thickness in 'refdat' (presently measured 1997 surface),
124 % otherwise starts with no ice
125
126 climate = '\Input Files\Climat.txt'; % Specify climate data file
127 climdata = dlmread(climate, '\t'); % Read in climate data (temperature, ppt, etc)
128
129 reffile = '\Input Files\Trans_100_35_2007.txt'; % Specify reference data file
130 refdat = dlmread(reffile, '\t'); % Read in reference data (bed topography, etc)
131
132 %----- SET MASS BALANCE MODEL PARAMETERS
133
134 ddfs = 0.00694; % Degree day factor for snow
135
136 ddfi = 0.00822; % Degree day factor for ice
137
138 templapse = 0.0053; % Temperature lapse rate (deg C m^-1)
139
140 pptgrad = 0.37; % Precipitation gradient (1 per 100 m)
141
142 pptgradstart = 497; % Elevation from which ppt gradient employed (m a.s.l.)
143
144 snowthresh = 1.0; % Snow temperature threshold (deg C)
145
146 diurgrad = -0.0005; % Gradient used to calc diurnal temperature range (sigma)
147
148 diurint = 4.6699; % Intercept used to calc diurnal temperature range (sigma)
149
150 basalmelt = 0.8; % Basal melt due to geothermal heat flux (m w.e. yr^-1)
151
152 %----- SET PHYSICAL MODEL PARAMETERS
153
154 gap = 5.3e-15; % Glen's flow coeff A (s^-1 (kPa)^-3)
155
156 gn = 3; % Glen's flow exponent
157
158 rho = 910.0; % Density of ice (kg m^-3)
159
160 g = 9.81; % Gravity (m s^-2)
161
162 slide = 0.2; % Water lubrication factor
163
164 %----- SET/ESTABLISH TIME & DISTANCE PARAMETERS
165
166 startyear = 1997.0; % Set start yr for model run (earliest is 1958)
167
168 dt = 1/64; % Time step size (yr)
169
170 dx = 100.0; % Grid spacing (m)
171
172 xmax = (length(refdat(:,1))*dx)-dx; % Establish length of transect
173
174 x = 0:dx:xmax; % Set up x coordinate (m)
175
176 n = xmax / dx + 1; % Number of grid points
177
178 wsp = 35; % Grid point of watershed on transect (needed for 'total')
179
180 tmin = min(climdata(:,1)); % Start year of climate data
  
```

From this area, one can change all relevant parameters for both the degree-day and ice flow models. Once changes have been made, save the file (keeping the same name) and then run as before.

In order to change the input files, one needs to amend lines 123 (climate data) or 125 (reference glacier geometry – changing the size of δt). All files relative to these two variables are available in the 'Input Files' folder in the accompanying CD (Appendix 1.4.2). Changing the climate input is simply a case of changing the file name in line 123. However, to change the glacier geometry a few steps must be taken. The default file is 'Trans_100_35_2007.txt'. In this, and each of the other reference files, the first number (in this case '100') is the size of δt in metres and the second number (in this case '35') is the point along the transect where the watershed occurs (variable 'wsp' in the code). If changing the reference file, one must also change the corresponding values of δt (line 148) and wsp (line 153). Files for $\delta t = 200, 400, \text{ and } 800$ m are available in addition to the default file (100 m). It is only recommended that they be used should the code be taking too long to run or if wanting to run the model far into the future, as accuracy is, of course, reduced. Once changed, the file should be saved and then can be run as per before.

Within the first part of the parameter calibration area (from line 115), there are options for switching on or off some of the additions implemented by the author. To switch an option on, change the value of the relevant 'parameter' to '1'. To turn off, change to '0'. (N.B. to turn the 'Calibration GUI' option on or off, a change must be made at line 22 in addition to line 115)

If the model is set to produce output files, when the model is stopped by the user or it ends having reached the end of the available data in the climate input file, a total of 9 time-stamped Matlab array files will be generated. They can be split into the following:

- (a) Time-series files that provide values for each point along the transect and for each mass balance year the model is run:

[time stamp]_exposedice.mat	Values of 1 or 0. If 1 then there is no snow layer remaining at that grid point.
[time stamp]_nmbprofs.mat	Value (m w.e.) of net mass balance as calculated by the degree-day mass balance model.
[time stamp]_pddprofs.mat	The number of positive degree-days calculated by the mass balance model.

[time stamp]_sfracprofs.mat	The fraction of precipitation that falls as snow as calculated by the degree-day model.
[time stamp]_surfaceprofs.mat	The surface elevation in m.
[time stamp]_wateratbed.mat	The amount of water (m) that is assumed to reach the glacier bed.

(b) Time-series file that provides information on the glacier as a whole:

[time stamp]_overtime.mat	Values for glacier volume (km ³), glacier length with reference to watershed (m), total length of accumulation zone (m).
---------------------------	--

(c) Files with useful information relating to the model run:

[time stamp]_distance.mat	Enables efficient graphing of the files in (a) by providing the distance of each point on the transect with respect to the watershed.
[time stamp]_logfile.mat'	Provides details of 24 aspects of the model run (e.g. parameter values, names of input files, etc). Essential when dealing with multiple model runs or returning to the data at a later date.

Appendix 1.2

```
function iceflo(action)
% Ice dynamics model for valley glaciers

% Possible actions: initialize or close

% Information regarding the play status will be held in the axis user data
% according to the following table:
play= 1;
stop=-1;

if nargin<1,
    action='initialize';
end;

if strcmp(action,'initialize'),
    oldFigNumber=watchon;

%=====
% ----- FIGURE SET UP ----- %
%-----
    calibrating = 0;                % If calibrating againsts 2007 LiDAR data say '1'. This will
                                   % draw 2007 profile and calculate RMSE of run
    figNumber=figure('Name','Hagafellsjokull vestari Glacier Flow Model','position', ...
        [ 40 70 1200 900 ],'NumberTitle','off','Visible','off');
    axs1Hndl=axes('Units','normalized','Position',[ 0.07 0.065 0.36 0.29 ],'Visible','off');
    if calibrating == 1
        axs2Hndl=axes('Units','normalized','Position',[ 0.07 0.450 0.89 0.50 ],'Visible','off');
    else
        axs2Hndl=axes('Units','normalized','Position',[ 0.07 0.72 0.89 0.24 ],'Visible','off');
    end
    axs3Hndl=axes('Units','normalized','Position',[ 0.55 0.43 0.41 0.22 ],'Visible','off');
    axs4Hndl=axes('Units','normalized','Position',[ 0.07 0.43 0.41 0.22 ],'Visible','off');
    axs5Hndl=axes('Units','normalized','Position',[ 0.49 0.065 0.36 0.29 ],'Visible','off');
    axs6Hndl=axes('Units','normalized','Position',get(axs5Hndl,'Position'),'Visible','off');

    % ----- INFORMATION FOR ALL BUTTONS
    xPos=0.90;
    btnLen=0.08;
    btnWid=0.08;
    spacing=0.03;

    % ----- START BUTTON
    btnNumber=1;
    yPos=0.30-(btnNumber-1)*(btnWid+spacing);
    labelStr='START';
    cmdStr='start';
    callbackStr='iceflo(''start'')';
    btnPos=[xPos yPos-spacing btnLen btnWid];
    startHndl=uicontrol('Style','pushbutton','Units','normalized','Position',btnPos,'String', ...
        labelStr,'Interruptible','on','BackgroundColor',[0.0 0.8 0.0],'Callback',callbackStr);

    % ----- STOP BUTTON
    btnNumber=2;
    yPos=0.30-(btnNumber-1)*(btnWid+spacing);
    labelStr='STOP';
    callbackStr='set(gca, 'Userdata',-1)';
    btnPos=[xPos yPos-spacing btnLen btnWid];
    stopHndl=uicontrol('Style','pushbutton','Units','normalized','Position',btnPos,'String', ...
        labelStr,'Enable','off','BackgroundColor',[0.8 0.0 0.0],'Callback',callbackStr);

    % ----- CLOSE BUTTON
    btnNumber=3;
    yPos=0.30-(btnNumber-1)*(btnWid+spacing);
    labelStr='CLOSE';
    callbackStr='close(gcf)';
    btnPos=[xPos yPos-spacing btnLen btnWid];
    closeHndl=uicontrol('Style','pushbutton','Units','normalized','Position',btnPos,'String', ...
        labelStr,'BackgroundColor',[0.6 0.6 0.6],'call',callbackStr);

    % ----- UNCOVER THE FIGURE
    hndlList=[startHndl stopHndl closeHndl axs1Hndl axs2Hndl axs3Hndl axs4Hndl axs5Hndl axs6Hndl];
```

```

set(figNumber, 'Visible', 'on', 'UserData', hndlList);

watchoff(oldFigNumber);
figure(figNumber);

%-----
% ----- END OF FIGURE SET UP ----- %
%=====

elseif strcmp(action, 'start'),

%=====
% ----- COMMUNICATION OF FIGURE WITH REST OF CODE ----- %
%-----

figNumber=gcf;

hndlList=get(figNumber, 'UserData');
startHndl=hndlList(1);
stopHndl=hndlList(2);
closeHndl=hndlList(3);
axs1Hndl=hndlList(4);
axs2Hndl=hndlList(5);
axs3Hndl=hndlList(6);
axs4Hndl=hndlList(7);
axs5Hndl=hndlList(8);
axs6Hndl=hndlList(9);

set([startHndl closeHndl], 'Enable', 'off');
set(stopHndl, 'Enable', 'on');
set(figNumber, 'Backingstore', 'off');

%-----
% ----- END OF COMMUNICATION OF FIGURE WITH REST OF CODE ----- %
%=====

%=====
% ----- PARAMETER SET UP ----- %
%-----

% ----- READ IN CLIMATE DATA AND REFERENCE DATA
calibrating = 0; % If calibrating against 2007 LiDAR data say '1'. This will
% draw 2007 profile and provide data useful for calibration
show1997 = 0; % If '1' then will display 1997 reference surface
outputfiles = 1; % Determines whether output files will be generated by this
% run. If equals '1' then files will be generated
initial_ice = 1; % Initial ice cover. If '1' then model starts with the ice
% thickness in 'refdat' (presently measured 1997 surface),
% otherwise starts with no ice
climate = '\Input Files\Climate.txt'; % Specify climate data file
climdata = dlmread(climate, '\t'); % Read in climate data (temperature, ppt, etc)
reffile = '\Input Files\Trans_100_35_2007.txt'; % Specify reference data file
refdat = dlmread(reffile, '\t'); % Read in reference data (bed topography, etc)

% ----- SET MASS BALANCE MODEL PARAMETERS
ddfs = 0.00694; % Degree day factor for snow
ddfi = 0.00822; % Degree day factor for ice
templapse = 0.0053; % Temperature lapse rate (deg C m^-1)
pptgrad = 0.37; % Precipitation gradient (1 per 100 m)
pptgradstart = 497; % Elevation from which ppt gradient employed (m a.s.l.)
snowthresh = 1.0; % Snow temperature threshold (deg C)
diurgrad = -0.0005; % Gradient used to calc diurnal temperature range (sigma)
diurint = 4.6699; % Intercept used to calc diurnal temperature range (sigma)
basalmelt = 0.8; % Basal melt due to geothermal heat flux (m w.e. yr^-1)

% ----- SET PHYSICAL MODEL PARAMETERS
gap = 5.3e-15; % Glen's flow coeff A (s^-1 (kPa)^-3)
gn = 3; % Glen's flow exponent
rho = 910.0; % Density of ice (kg m^-3)
g = 9.81; % Gravity (m s^-2)
slide = 0.2; % Water lubrication factor

% ----- SET/ESTABLISH TIME & DISTANCE PARAMETERS
startyear = 1997.0; % Set start yr for model run (earliest is 1958)
dt = 1/64; % Time step size (yr)
dx = 100.0; % Grid spacing (m)

```

```

xmax = (length(refdat(:,1))*dx)-dx; % Establish length of transect
x = 0:dx:xmax; % Set up x coordinate (m)
n = xmax / dx + 1; % Number of grid points
wsp = 35; % Grid point of watershed on transect (needed for 'total')
tmin = min(climdata(:,1)); % Start year of climate data
tmax = max(climdata(:,1)); % Finish year of climate data
tperiod = tmax-tmin; % Time period of climate data (yr)
if dt < 1, t = startyear-dt; % As spin-up required for accurate first volume reading
else t = startyear;
end
tperiod2 = tmax-t; % Time period of run (yr)

% ----- CREATE MODEL MATRICES & MISCELLANEOUS
dist = x; % Distance along transect matrix
top = refdat(:,1); % Topography
rwid = refdat(:,2); % Reference width
rthk = refdat(:,3); % Reference thickness
cal2007 = refdat(:,4); % 2007 LiDAR surface
thk = zeros(n,1); % Ice thickness
sur = zeros(n,1); % Ice surface
wid = zeros(n,1); % Width
dif = zeros(n,1); % Diffusivity
nmb = zeros(n,1); % Net mass balance
runoff = zeros(n,1); % m w.e. of water deposited at this grid point in bal yr
bareice = zeros(n,1); % Whether all snow from current bal yr is ablated
pddmonitor = zeros(n,1); % To monitor output of degree day model
fracmonitor = zeros(n,1); % To monitor output of snow fraction calculation
ga = gap*0.031536; % Convert to units required by ice model (yr^-1 Pa^-n)
rmsnan = ~isnan(cal2007); % Remove NaNs from LiDAR data to allow rms error calculation

% ----- SET THE ICE THICKNESS TO REFERENCE FILE OR NO ICE
if (initial_ice == 1), % Set to ref thickness
    thk = rthk;
end % Else keep at no ice

% ----- ESTABLISH INITIAL ICE SURFACE FOR MODEL RUN
sur = thk + top;

% ----- SET UP OUTPUT FILE MATRICES & SET TIME STAMP OF RUN
surfaceprofs = zeros(tperiod,n); % Surface profile output matrix
nmbprofs = zeros(tperiod,n); % Net mass balance profile output matrix
totalvol = zeros(tperiod,1); % Total volume over time matrix
glength = zeros(tperiod,1); % Glacier length over time matrix
accumlength = zeros(tperiod,1); % Length of accumulation area over time
time = zeros(tperiod,1); % Time matrix
pddprofs = zeros(tperiod,n); % Positive degree days profile output matrix
fracprofs = zeros(tperiod,n); % Fraction of ppt as snow profile output matrix
wateratbed = zeros(tperiod,n); % Calculated water at bed (rain + surface abl + basal melt)
exposedice = zeros(tperiod,n); % Whether all snow removed & therefore if increased sliding
timestamp = datestr(now,30); % Time stamp for output files

% ----- ESTABLISH AXIS EXTREMES FOR GRAPHING IN FIGURE
hmax = max(top)+500; % Max likely elevation (m)
hmax = (ceil((hmax/100)))*100;
hmin = min(top)-150; % Min likely elevation (m)
hmin = roundn(hmin,2);
wmax = (max(rwid)/2)+1000; % Max likely width (m)
wmax = (ceil((wmax/1000)))*1000;
wmin = -wmax; % Min likely width (m)
bmax = 4.0; % Max likely net mass balance
bmin = -10.0; % Min likely net mass balance
vmin = 0; % Min likely ice volume
vmax = 50; % Max likely ice volume
xwsp = x-(wsp*dx)+dx; % Recalc x array for purposes of graphing from watershed
xwspmax = max(xwsp); % Max distance from watershed
xwspmin = min(xwsp); % Min distance from watershed
xwsps = (floor(xwsp/1000))*1000; % Rounding down the min for tick marks on graphs
xwsps = min(xwsps);
xwspe = (ceil(xwsp/1000))*1000; % Rounding up the max for tick marks on graphs
xwspe = max(xwspe);

%-----
% ----- END OF PARAMETER SET UP ----- %
%=====
%=====

```

```

% ----- GRAPHICS SET UP ----- %
%-----
% Set up ELEVATION vs MASS BALANCE axis with line types and text
axes(axs1Hndl);
set(axs1Hndl, ...
    'XLim',[bmin bmax],'YLim',[hmin hmax], ...
    'XTick',bmin:2:bmax,'YTick',hmin:200:hmax, ...
    'Drawmode','fast', ...
    'Visible','on', ...
    'YGrid','on', ...
    'NextPlot','add', ...
    'Userdata',play);
xlabel('Mass Balance (m w.e. yr^-1)');
ylabel('Elevation (m)');
cla;
mblne = line('linestyle','-','linewidth',1,'erase','xor','xdata',[],'ydata',[]);
%-----

% Set up THICKNESS vs DISTANCE axis with line types and text
axes(axs2Hndl);
set(axs2Hndl, ...
    'XLim',[xwspmin xwspmax],'YLim',[hmin hmax], ...
    'XTick',xwsp:2000:xwspe,'YTick',hmin:200:hmax, ...
    'Drawmode','fast', ...
    'Visible','on', ...
    'NextPlot','add', ...
    'Userdata',play);
xlabel('Distance from Watershed (m)');
ylabel('Elevation (m)');
cla;
hx1line=line('linestyle','-','linewidth',1,'markersize',1,'erase','xor','xdata',[],'ydata',[]);
hx2line=line('linestyle','-','linewidth',1,'markersize',1,'erase','none','xdata',[],'ydata',[]);

if calibrating == 1
    txtHndl=text(0.5,1.05,'\fontsize{16}Balance Yr ','HorizontalAlignment','center','EraseMode', ...
        'xor','units','normalized');
    hx3line=line('linestyle','-','linewidth',1,'markersize',1,'erase','none','xdata',[],'ydata',[]);
    hx4line=line('linestyle','-','linewidth',2,'markersize',1,'erase','normal','xdata',[], ...
        'ydata',[]);
    txtHndl2=text(0.8,0.96,' ','EraseMode','xor','units','normalized');
    txtHndl3=text(0.8,0.91,' ','EraseMode','xor','units','normalized');
    txtHndl4=text(0.8,0.86,' ','EraseMode','xor','units','normalized');
    txtHndl5=text(0.8,0.81,' ','EraseMode','xor','units','normalized');
    txtHndl6=text(0.8,0.76,' ','EraseMode','xor','units','normalized');
else
    txtHndl=text(0.5,1.08,'\fontsize{16}Balance Yr ','HorizontalAlignment','center','EraseMode', ...
        'xor','units','normalized');
end

if show1997 == 1
    hx5line=line('linestyle','-','linewidth',1,'markersize',1,'erase','none','xdata',[],'ydata',[]);
end
%-----

% Set up WIDTH vs DISTANCE axis with line types and text
axes(axs3Hndl);
if calibrating == 1
    set(axs3Hndl, 'Visible','off');
else
    set(axs3Hndl, ...
        'XLim',[xwspmin xwspmax],'YLim',[wmin wmax], ...
        'XTick',xwsp:2000:xwspe,'YTick',wmin:2000:wmax, ...
        'Drawmode','fast', ...
        'Visible','on', ...
        'YGrid','on', ...
        'NextPlot','add', ...
        'Userdata',play);
    xlabel('Distance from Watershed (m)');
    ylabel('Width (m)');
    cla;
    wxline = line('linestyle','-','linewidth',1,'markersize',1,'erase','xor','xdata',[],'ydata',[]);
end
%-----

% Set up MASS BALANCE vs DISTANCE axis with line types and text
axes(axs4Hndl);
if calibrating == 1
    set(axs4Hndl, 'Visible','off');
else

```

```

set(axes4Hndl, ...
    'XLim',[xwspmin xwspmax],'YLim',[bmin bmax], ...
    'XTick',xwsp:2000:xwspe,'YTick',bmin:2:bmax, ...
    'Drawmode','fast', ...
    'Visible','on', ...
    'YGrid','on', ...
    'NextPlot','add', ...
    'Userdata',play);
xlabel('Distance from Watershed (m)');
ylabel('Mass Balance (m w.e. yr-1)');
cla;
bxline = line('linestyle','-','linewidth',1,'erase','xor','xdata',[],'ydata',[]);
end

%-----
% Set up GLACIER LENGTH vs TIME axis with line types and text
if tperiod2 < 20, tgap = 2;           % Making the x axis scale markers appropriate for the
elseif tperiod2 < 50, tgap = 10;      % length of time of model run
elseif tperiod2 < 100, tgap = 20;
elseif tperiod2 < 500, tgap = 50;
elseif tperiod2 < 1000, tgap = 100;
elseif tperiod2 < 2000, tgap = 200;
elseif tperiod2 < 5000, tgap = 500;
end

if tgap < 50;
tminround1 = (floor(startyear/10))*10; % Round 'tmin' to start of decade
tmaxround1 = (ceil(tmax/10))*10;      % Round 'tmax' to end of decade
tminround2 = tminround1;              % Axis min limit
tmaxround2 = tmaxround1;              % Axis max limit
elseif tgap < 200
tminround1 = (floor(startyear/100))*100; % Round 'tmin' to start of century for tick marks
tmaxround1 = (ceil(tmax/100))*100;      % Round 'tmax' to end of century for tick marks
tminround2 = (floor(startyear/10))*10;  % Axis min limit
tmaxround2 = (ceil(tmax/10))*10;        % Axis max limit
else
tminround1 = (floor(startyear/1000))*1000; % Round 'tmin' to start of millennium for tick marks
tmaxround1 = (ceil(tmax/1000))*1000;      % Round 'tmax' to end of millennium for tick marks
tminround2 = (floor(startyear/100))*100;  % Axis min limit
tmaxround2 = (ceil(tmax/100))*100;        % Axis max limit
end

axes(axes5Hndl);
set(axes5Hndl, ...
    'XLim',[tminround2 tmaxround2],'YLim',[0.0 xmax+5000], ...
    'XTick',tminround1:tgap:tmaxround1,'YTick',0:4000:xmax+5000, ...
    'Drawmode','fast', ...
    'Visible','on', ...
    'XGrid','on', ...
    'NextPlot','add', ...
    'Userdata',play);
xlabel('Time (yr)');
ylabel('Length (m)');
cla;
lt1line = line('linestyle','-','linewidth',1,'erase','none','xdata',[],'ydata',[]);
lt2line = line('linestyle','-','linewidth',1,'erase','none','xdata',[],'ydata',[]);
text(0.03,0.13,'\fontsize{10} \color{blue}Glacier Length','EraseMode','none','units', ...
    'normalized');
text(0.03,0.07,'\fontsize{10} \color{red}Accum Zone Length','EraseMode','none','units', ...
    'normalized');

axes(axes6Hndl);
set(axes6Hndl, ...
    'YAxisLocation','right', ...
    'Color','none', ...
    'XLim',[tminround2 tmaxround2],'YLim',[vmin vmax], ...
    'XTick',tminround1:tgap:tmaxround1,'YTick',vmin:5:vmax, ...
    'Drawmode','fast', ...
    'Visible','on', ...
    'YGrid','off', ...
    'Userdata',play);
xlabel('Time (yr)');
ylabel('Ice Volume (km3)');
cla;
lt3line = line('linestyle','-','linewidth',1,'erase','none','xdata',[],'ydata',[]);
text(0.03,0.19,'\fontsize{10} \color{green}Ice Volume','EraseMode','none','units', ...
    'normalized');

```

```

%-----
% ----- END OF GRAPHICS SET UP ----- %
%=====

%-----
% ----- START NUMERICS ----- %
%-----

% ----- DEFINE WORK ARRAYS
A = zeros(n);
up = zeros(n,1);
dn = zeros(n,1);
con = zeros(n,1);

% ----- TAKE CARE OF BOUNDARY CONDITIONS
A(1,1) = 1.0;
A(n,n) = 1.0;
A(1,2) = 0.0;
A(n,n-1) = 0.0;

for i = 2:n-1
    xx(i) = (i-1) * dx;
    xx(2*n-i) = xx(i);
end

xx(1) = 0.0;
xx(n) = xmax;
xx(2*n-1) = 0.0;
width(1) = 0.0;
width(2*n-1) = 0.0;

xxwsp = xx-(wsp*dx)+dx;

%-----
% ----- END OF NUMERICS ----- %
%=====

%-----
% ----- MAIN TIME LOOP ----- %
%-----

while (t <= tmax) && (get(axes6Hndl,'UserData')==play)

% ----- RESET RUNNING TOTALS FOR VOLUME, LENGTH & ACCUMULATION ZONE TO ZERO FOR NEXT TIME STEP
total = 0.0;
length2 = 0.0;
acclen = 0.0;

tmb = floor(t);

% ----- CALCULATION OF NET MASS BALANCE ALONG TRANSECT & ICE PHYSICS MODEL
if tmb == t

    for i = 2:n-1

% ----- CALCULATE PPT GIVEN HEIGHT
pptht = climdata(tmb-(tmin-1),2) + climdata(tmb-(tmin-1),2)* ...
    ((sur(i)-pptgradstart)/100)*pptgrad;

% ----- CALCULATE DIURNAL TEMPERATURE RANGE FOR GIVEN ELEVATION
sigma = (diurgrad*sur(i))+diurint;

% ----- CALCULATE +VE DEGREE DAYS & FRACTION OF PPT AS SNOW
pdaynum = 0;
snowfrac = 0;

for montemp = [climdata(tmb-(tmin-1),3),climdata(tmb-(tmin-1),4), ...
    climdata(tmb-(tmin-1),5),climdata(tmb-(tmin-1),6),climdata(tmb-(tmin-1),7), ...
    climdata(tmb-(tmin-1),8),climdata(tmb-(tmin-1),9),climdata(tmb-(tmin-1),10), ...
    climdata(tmb-(tmin-1),11),climdata(tmb-(tmin-1),12),climdata(tmb-(tmin-1),13), ...
    climdata(tmb-(tmin-1),14)]

    montemp = montemp - templapse * (sur(i)-2);

    pddcur = quad(@pddcalc,0,40,[],[],montemp,sigma);

```

```

pddcur = ((365/12)/(sigma*sqrt(2*pi)))*pddcur;

pptcur = quad(@pptfrac,-50,snowthresh,[],[],montemp,sigma);
pptcur = ((1/12)/(sigma*sqrt(2*pi)))*pptcur;

pdaynum = pdaynum + pddcur;
snowfrac = snowfrac + pptcur;
end

pddmonitor(i) = pdaynum;
sfracmonitor(i) = snowfrac;

% ----- CALCULATE ACCUMULATION & RAINFALL
acc = snowfrac * pptht;
rain = (1-snowfrac) * pptht;

% ----- CALCULATE ABLATION & WHETHER BARE ICE IS REACHED
snowdays = acc / ddfs;

if (snowdays > pdaynum)
    abl = pdaynum * ddfs;
    bareice(i) = 0;
else
    abl = (snowdays * ddfs) + ((pdaynum - snowdays) * ddfi);
    bareice(i) = 1;
end

runoff(i) = abl + rain;

% ----- FIND RESULTING NET MASS BALANCE
nmb(i) = acc - abl;

end
end

for i = 2:n-1

% ----- FIND WIDTH FROM THICKNESS
wid(i) = rwid(i) * (thk(i) / rthk(i))^0.5 + 0.0001;

% ----- CALC DIFFUSIVITIES FOR FLOW & WIDTH CON/DIVERGENCE FACTOR GIVEN POINT ON TRANSECT
if bareice(i) == 0

    f1 = -2.0 * ga * ( rho * g )^gn / ( gn + 2 );
    f1 = dt * f1 / ( 2.0^gn * dx^(gn + 1) );
    f2 = dt / (2.0 * dx)^2;

    dif(i) = f1 * thk(i)^(gn+2) * (sur(i+1) - sur(i-1))^(gn-1);
    con(i) = f2 * dif(i) * (wid(i+1) - wid(i-1)) / wid(i);

else
    f1 = -2.0 * (ga + (ga * (runoff(i) + basalmelt) * slide)) * ( rho * g )^gn / ( gn + 2 );
    f1 = dt * f1 / ( 2.0^gn * dx^(gn + 1) );
    f2 = dt / (2.0 * dx)^2;

    dif(i) = f1 * thk(i)^(gn+2) * (sur(i+1) - sur(i-1))^(gn-1);
    con(i) = f2 * dif(i) * (wid(i+1) - wid(i-1)) / wid(i);

end

% ----- ESTABLISH IF CURRENT GRIDPOINT IS WITHIN WATERSHED
if i >= wsp

% ----- CALCULATE TOTAL ICE VOLUME IN THIS GLACIER SECTION
total = total + wid(i) * thk(i) + wid(i+1) * thk(i+1);

% ----- ESTABLISH LENGTH OF ICE EXTENT WITHIN WATERSHED
if (thk(i) > 0.1),
    length2 = length2 + dx;

% ----- ESTABLISH LENGTH OF ACCUMULATION ZONE WITHIN WATERSHED
if (nmb(i) > 0.0),
    acclen = acclen + dx;
end
end
end
end
end

```

```

% ----- CALCULATE TOTAL ICE VOLUME IN GIVEN GLACIER LENGTH
total = total * dx / 2.0e9;

% ----- ARRANGE STAGGERED GRID
for i = 2:n-1
    up(i) = dif(i+1) + dif(i);
    dn(i) = dif(i) + dif(i-1);
end

% ----- FORM TRIDIAGONAL MATRIX
A = diag(1.0 - up - dn, 0) + diag(up(1:n-1) + con(i), 1) + diag(dn(2:n) - con(i), -1);

% ----- UPDATE THE SOLUTION
sur = A \ sur + dt * (nmb - basalmelt);
thk = max(0.0, sur - top);

% ----- HANDLE LOWER GRADIENT BC
thk(1) = 0.0;
thk(n) = thk(n-1);

% ----- ESTABLISH NEW GLACIER SURFACE
sur = thk + top;

% ----- MIRROR IMAGE WIDTH FOR GRAPHING PURPOSES
for i = 2:n-1
    width(i) = wid(i) / 2.0;
    width(2*n-i) = -width(i);
end

% ----- IF T IS INT RECORD OUTPUT PARAMETERS & SAVE FILES THEN EXTRACT DATA FOR FIGURE & DRAW IT
if t == tmb
    nmbprofs(t,:) = nmb';
    surfaceprofs(t,:) = sur';
    pddprofs(t,:) = pddmonitor';
    sfracprofs(t,:) = sfracmonitor';
    wateratbed(t,:) = runoff' + basalmelt;
    exposedice(t,:) = bareice';
    totalvol(t,1) = total;
    glength(t,1) = length2;
    accumulength(t,1) = acclen;
    time(t,1) = t;
    overtime = [time glength accumulength totalvol];

    if calibrating == 1
        surrms = sur(rmsnan);
        surcal2007 = cal2007(rmsnan);
        rmsererror = sqrt(sum((surcal2007(:)-surrms(:)).^2)/numel(surcal2007));

logfile = struct('Time_of_model_run',timestamp,'RMSE_of_run',rmsererror,'Climate_data_file', ...
climate,'Reference_data_file',reffile,'Initial_ice_cover',initial_ice, ...
'Start_year_for_model_run',t,'Time_step_size_yrs',dt,'Maximum_run_time', ...
tmax-startyear+1,'Grid_spacing',dx,'Number_of_gridpoints',n,'Gridpoint_of_watershed', ...
wsp,'ddfs',ddfs,'ddfi',ddfi,'Temp_lapse_rate',templapse,'Precipitation_gradient', ...
pptgrad,'Elevation_from_which_ppt_grad_employed',pptgradstart,'Snow_threshold_temperature',
...
snowthresh,'Diurnal_temp_range_grad',diurgrad,'Diurnal_temp_range_intercept',diurint, ...
'Basal_melt_rate',basalmelt,'Meltwater_lubrication_factor',slide, ...
'Glens_flow_coefficient',gap,'Glens_flow_exponent',gn,'Density_of_ice',rho,'Gravity',g);

set(txtHndl2,'string',['Time of run ', num2str(timestamp)]);
set(txtHndl3,'string',['Flow coefficient = ', num2str(gap)]);
set(txtHndl4,'string',['Basal melt rate = ', num2str(basalmelt),' m w.e. yr^-1']);
set(txtHndl5,'string',['Meltwater factor = ', num2str(slide)]);
set(txtHndl6,'string',['RMSE = ', num2str(rmsererror)]);
set(hx3line,'xdata',xwsp(1:n),'ydata',cal2007(1:n),'color','c')
set(hx4line,'xdata',xwsp(1:n),'ydata',bareice(1:n)*hmin,'color','r')

else
logfile = struct('Time_of_model_run',timestamp,'Climate_data_file',climate, ...
'Reference_data_file',reffile,'Initial_ice_cover',initial_ice,'Start_year_for_model_run' ...
,t,'Time_step_size_yrs',dt,'Maximum_run_time',tmax-startyear+1,'Grid_spacing',dx, ...
'Number_of_gridpoints',n,'Gridpoint_of_watershed',wsp,'ddfs',ddfs,'ddfi',ddfi, ...
'Temp_lapse_rate',templapse,'Precipitation_gradient',pptgrad, ...
'Elevation_from_which_ppt_grad_employed',pptgradstart,'Snow_threshold_temperature', ...
snowthresh,'Diurnal_temp_range_grad',diurgrad,'Diurnal_temp_range_intercept',diurint, ...
'Basal_melt_rate',basalmelt,'Meltwater_lubrication_factor',slide, ...

```

```

'Glens_flow_coefficient',gap,'Glens_flow_exponent',gn,'Density_of_ice',rho,'Gravity',g);
end

if outputfiles == 1
    save([ timestamp '_surfaceprofs.mat'], 'surfaceprofs');
    save([ timestamp '_nmbprofs.mat'], 'nmbprofs');
    save([ timestamp '_pddprofs.mat'], 'pddprofs');
    save([ timestamp '_sfracprofs.mat'], 'sfracprofs');
    save([ timestamp '_distance.mat'], 'dist');
    save([ timestamp '_overtime.mat'], 'overtime');
    save([ timestamp '_wateratbed.mat'], 'wateratbed');
    save([ timestamp '_exposedice.mat'], 'exposedice');
    save([ timestamp '_logfile.mat'], 'logfile');
end

if calibrating ~= 1
set(bxline, 'xdata', xwsp(2:n-1), 'ydata', nmb(2:n-1), 'color', 'r')
set(wxline, 'xdata', xxwsp, 'ydata', width, 'color', 'r')
end

if show1997 == 1
set(hx5line, 'xdata', xwsp(1:n), 'ydata', top+rthk, 'color', [1 0.5 0])
end

set(mbline, 'xdata', nmb(wsp:n-1), 'ydata', sur(wsp:n-1), 'color', 'r')
set(txtHndl, 'string', ['\fontsize{16}Balance Yr ', num2str(t-1), ' - ', num2str(t)]);
set(hx1line, 'xdata', xwsp, 'ydata', sur, 'color', 'k')
set(hx2line, 'xdata', xwsp(1:n), 'ydata', top(1:n), 'color', 'g')
set(lt1line, 'xdata', overtime(startyear:t,1), 'ydata', overtime(startyear:t,2), 'color', 'b')
set(lt2line, 'xdata', overtime(startyear:t,1), 'ydata', overtime(startyear:t,3), 'color', 'r')
set(lt3line, 'xdata', overtime(startyear:t,1), 'ydata', overtime(startyear:t,4), 'color', 'g')
drawnow;
end

% ----- INCREMENT TIME FOR NEXT YEAR'S RUN
t = t + dt;

end;

%-----
% ----- END OF MAIN TIME LOOP ----- %
%=====

% ----- CREATE TIMESTAMPED FOLDER FOR OUTPUT FILES
if outputfiles == 1

newfolder = fullfile('C:', 'Documents and Settings', 'Plant', 'My Documents', 'Cambridge Work', ...
    'Langjokull Data', 'Ice Model', timestamp);
if (exist(newfolder) == 0)
    mkdir(newfolder);
end
end

% ----- DISABLE 'STOP' BUTTON & ENABLE 'CLOSE' BUTTON ON GUI
set([startHndl closeHndl], 'Enable', 'on');
set(stopHndl, 'Enable', 'off');

end;

% ----- END OF SCRIPT ----- %

```

Appendix 1.3

Transect Point	Bed Topog. (m a.s.l.)	Glacier Width (m)	1997 Ice Thickn. (m)	2007 Surface Elev. (m a.s.l.)	Transect Point	Bed Topog. (m a.s.l.)	Glacier Width (m)	1997 Ice Thickn. (m)	2007 Surface Elev. (m a.s.l.)	Transect Point	Bed Topog. (m a.s.l.)	Glacier Width (m)	1997 Ice Thickn. (m)	2007 Surface Elev. (m a.s.l.)
1	982.69	2872	39.18	NaN	86	794.89	7743	419.69	1204.51	171	614.45	6185	284.46	879.86
2	990	2938	41	NaN	87	799.23	7732	412.51	1201.92	172	612.47	6185	283	874.27
3	997.43	3044	43.98	NaN	88	802.96	7720	405.92	1199.01	173	610.25	6185	281.4	869.29
4	1004.2	3158	47.37	NaN	89	805.68	7709	400.26	1195.68	174	608.16	6186	279.29	864.86
5	1009.66	3302	51.8	NaN	90	808.69	7698	394.12	1191.89	175	606.46	6186	276.8	860.89
6	1013.62	3502	58.22	NaN	91	811.42	7687	388.01	1188.03	176	605.09	6186	273.84	857.07
7	1016.58	3772	67.57	NaN	92	814.41	7675	381.44	1184.22	177	603.52	6187	270.76	853.37
8	1019.05	4124	80.73	NaN	93	817.65	7664	374.55	1180.29	178	601.37	6187	267.94	849.62
9	1021.38	4502	96.25	NaN	94	820.8	7653	367.91	1176.24	179	598.48	6188	265.84	844.85
10	1023.68	4822	110.42	NaN	95	823.75	7642	361.52	1172.51	180	595.35	6188	264.03	839.8
11	1025.67	5066	121.87	NaN	96	825.98	7630	356.08	1169.34	181	592.42	6188	262.27	834.77
12	1027.48	5224	129.57	NaN	97	827.19	7619	351.93	1166.62	182	590.19	6189	260.16	830.61
13	1028.93	5376	137.2	NaN	98	827.63	7608	348.87	1164.35	183	588.35	6189	257.8	826.99
14	1029.8	5560	146.74	NaN	99	827.68	7597	346.37	1162.53	184	586.61	6189	255.4	822.98
15	1030.39	5734	156.11	NaN	100	827.91	7586	344.05	1160.82	185	584.87	6190	252.85	818.44
16	1031.8	5868	163.45	NaN	101	827.98	7574	341.99	1158.98	186	583.2	6190	250.1	813.2
17	1034.84	5950	168.06	NaN	102	827.58	7563	340.38	1156.56	187	581.58	6190	247.06	807.07
18	1039.64	6004	171.14	NaN	103	826.28	7552	339.47	1153.44	188	580.14	6191	243.54	NaN
19	1045.44	6056	174.08	NaN	104	823.96	7541	339.19	1149.62	189	578.71	6191	239.81	NaN
20	1051.32	6072	175.03	NaN	105	820.72	7529	339.39	1145.53	190	577.34	6191	235.98	790.59
21	1056.71	6048	173.71	NaN	106	816.88	7518	339.91	1141.37	191	576.08	6192	231.99	784.31
22	1061.68	6030	172.59	NaN	107	812.71	7507	340.54	1137.61	192	575	6192	227.21	778.56
23	1066.43	6018	171.92	NaN	108	808.41	7496	341.06	1134.55	193	574.02	6193	221.86	773.13
24	1070.54	6036	173.01	NaN	109	803.56	7484	342.07	1132.31	194	572.93	6193	217.72	767.42
25	1073.54	6088	175.95	NaN	110	798.84	7473	342.89	1130.25	195	571.51	6193	215.2	762.35
26	1075.32	6170	180.77	NaN	111	795.11	7462	342.68	1127.57	196	569.78	6194	212.33	757.31
27	1076.31	6268	186.6	NaN	112	793.54	7451	340.53	1124.15	197	568.21	6194	207.99	752.49
28	1077.15	6366	192.44	NaN	113	794.3	7440	336.46	1120.21	198	566.33	6194	203.45	747.4
29	1078.16	6460	198.18	NaN	114	796.49	7428	331.27	1116.37	199	564.31	6195	199.61	742.49
30	1079.57	6548	203.52	NaN	115	799.22	7417	325.48	1112.76	200	561.98	6195	196.93	736.88
31	1080.81	6630	208.74	NaN	116	801.49	7406	320.03	1109.18	201	559.25	6195	194.23	731.25
32	1081.64	6708	213.62	NaN	117	802.9	7395	315.3	1105.23	202	556.25	6196	190.75	725.26
33	1081.96	6786	218.71	NaN	118	803.73	7383	311.08	1100.92	203	552.91	6196	188.04	719.03
34	1082.13	6864	223.64	NaN	119	804.1	7372	307.33	1096.65	204	549.33	6196	186.17	712.55
35	1082.21	6891	228.58	NaN	120	803.46	7361	304.47	1092.9	205	545.44	6197	184.01	705.54
36	1082.1	6919	233.63	NaN	121	801.5	7350	302.92	1089.22	206	541.22	6197	181.94	698.59
37	1081.27	6946	239.03	1310.19	122	797.79	7338	302.99	1085.21	207	537.1	6198	181.27	691.76
38	1079.5	6973	244.47	1313.7	123	792.74	7327	304.48	1080.92	208	533.16	6198	181.53	685.57
39	1077.05	7000	250.17	1317.18	124	787.06	7316	306.95	1076.47	209	529.81	6198	179.58	680.37
40	1073.8	7028	256.04	1320.11	125	781.4	7300	309.47	1072.07	210	526.97	6199	175.43	674.25
41	1069.73	7055	262.28	1322.28	126	776.17	7280	311.45	1067.69	211	524.37	6199	170.83	667.75
42	1064.28	7082	269.45	1323.52	127	771.28	7240	313.04	1063.25	212	521.88	6199	166.41	660.48
43	1057.45	7109	277.39	1323.7	128	766.56	7200	314.43	1059.75	213	519.08	6200	162.62	652.05
44	1050.35	7137	284.49	1322.77	129	761.94	7180	315.79	1056.48	214	515.84	6200	160	644.54
45	1044.13	7164	289.88	1320.87	130	757.44	7140	317.09	1053.8	215	512.25	6168	158.33	637.56
46	1039.66	7191	292.23	1318.67	131	752.78	7100	318.39	1051.54	216	508.58	6130	156.43	631
47	1036.25	7218	292.94	1316.16	132	748.18	7060	319.65	1048.94	217	505.23	6074	153.56	624.32
48	1032.83	7246	293.1	1313.71	133	744.09	7040	320.02	1046.32	218	502.74	5996	149.64	617.34
49	1028.34	7273	294.1	1311.01	134	741.19	7000	319.04	1043.08	219	500.8	5905	145.12	610.18
50	1022.22	7300	296.5	1308.39	135	740.34	6960	316.07	1040.06	220	498.88	5811	140.57	602.72
51	1015.06	7327	300.1	1305.73	136	741.08	6940	311.54	1037.31	221	496.65	5717	136.03	592.86
52	1007.88	7355	304.16	NaN	137	742.59	6900	306.14	1034.24	222	493.88	5612	131.09	582.94
53	1001.68	7382	307.37	1300.19	138	743.62	6860	301.04	1030.62	223	491.51	5476	124.82	572.86
54	996.56	7409	309.27	1296.99	139	743.5	6840	297.02	1026.08	224	489.67	5321	117.84	NaN
55	992.03	7437	310.6	1294.02	140	742.23	6800	294.17	1021.19	225	488.07	5164	110.99	NaN
56	988.13	7464	311.47	1291.15	141	740.41	6760	291.88	1016.29	226	485.92	5031	105.35	NaN
57	985.01	7491	311.59	1288.67	142	738.2	6720	289.92	1011.86	227	482.3	4950	101.97	NaN
58	983.29	7518	310.22	1286.23	143	735.77	6700	288.02	1007.23	228	477.75	4906	100.19	NaN
59	982.86	7546	307.34	1283.26	144	733.12	6660	286.06	1002.05	229	472.27	4838	97.42	NaN
60	982.56	7573	303.99	1279.88	145	730.18	6620	284.22	996.75	230	466.83	4715	92.55	NaN
61	981.11	7600	301.81	1276.35	146	726.91	6600	282.71	991.91	231	461.4	4579	87.29	NaN
62	978.42	7627	301.19	1272.63	147	722.88	6560	282.24	986.86	232	455.82	4442	82.14	NaN
63	974.85	7655	301.35	1268.62	148	717.68	6520	283.11	981.89	233	451.19	4253	75.3	NaN
64	969.67	7682	302.78	1264.9	149	711.23	6500	285.05	976.7	234	448.46	3971	65.65	NaN
65	962.06	7709	306.3	1261.1	150	704.35	6460	286.5	971.37	235	448.4	3578	53.28	NaN
66	951.71	7736	312.41	1257.25	151	697.87	6420	286.75	965.93	236	451.09	3039	38.45	NaN
67	938.93	7764	320.95	1253.8	152	692.74	6400	285.55	960.21	237	455.39	2370	23.37	NaN
68	924.21	7791	331.55	1250.67	153	688.73	6360	283.7	954.48	238	459.78	1662	11.5	NaN
69	907.99	7818	343.75	1247.25	154	685.1	6320	281.91	949.07	239	462.09	49	0.01	NaN
70	889.54	7845	358.31	1243.24	155	681.14	6280	280.83	944.61	240	462.17	49	0.01	NaN
71	868.57	7873	375.81	1237.88	156	676.41	6260	280.81	940.97	241	460.58	49	0.01	NaN
72	846.54	7900	394.92	1231.56	157	670.87	6220	282.07	937.83	242	457.49	49	0.01	NaN
73	825.98	7889	413	1225.11	158	665.12	6180	283.84	934.63	243	454.17	49	0.01	NaN
74	806.46	7878	430.45	1220.86	159	659.69	6180	285.59	931.39	244	451.23	49	0.01	449.1
75	787.66	7866	447.48	1220.3	160	654.81	6181	287.04	927.82	245	449.13	49	0.01	449.17
76	771.96	7855	461.79	1220.6	161	650.4	6181	288.44	924.04	246	448.27	49	0.01	449.26
77	762.09	7844	470.44	1220.9	162	646.41	6181	289.51	919.81	247	448.39	49	0.01	449.4
78	760.12	7833	471.15	1220.64	163	642.76	6182	289.86	915.5	248	448.9	49	0.01	NaN
79	764.51	7821	465.46	1219.68	164	639.28	6182	289.41	910.91	249	449.36	49	0.01	NaN
80	771.52	7810	456.91	1218.24	165	635.67	6183	288.59	906.54	250	449.67	49	0.01	NaN
81	777.18	7799	449.35	1216.28	166	631.57	6							

Appendix 1.4

Appendix 1.4.1

Balance Yr	Annual Ppt (m)	Oct (oC)	Nov (oC)	Dec (oC)	Jan (oC)	Feb (oC)	Mar (oC)	Apr (oC)	May (oC)	Jun (oC)	Jul (oC)	Aug (oC)	Sep (oC)
1958	1.073	2.44	0.85	-2.84	-5.63	-5.67	-2.83	2.33	1.96	7.95	9.88	7.46	8.38
1959	1.72	3.75	2.68	-2.89	-8.36	-0.12	1	-1.51	4.82	6.55	8.97	7.4	6.3
1960	1.232	4.91	-2.31	-2.55	-1.66	-5.44	0	1.92	5.45	7.58	8.99	7.61	5.81
1961	1.224	1.8	0.63	-2.54	-1.58	-2.68	-2.2	-0.87	5.69	6.39	8.38	7.38	6.38
1962	1.181	2.7	-1.01	-5.29	-2	-3.25	-6.77	1.16	3.68	6.77	8.72	7.52	4.67
1963	1.211	2.18	-2.74	-3.33	-3.89	-2.03	1.6	0.85	2.56	8.26	7.77	7.24	3.1
1964	1.275	2.57	-5.03	-1.14	0.17	-0.1	2.68	1.87	5.24	6.81	8	6.82	3.9
1965	1.052	2.91	0.98	-4.89	-3.41	0.79	-5.56	0.73	5.11	7.12	9.57	7.61	4.4
1966	1.153	4.78	-2.9	-5.51	-5.57	-6.14	-3.67	0.91	3.45	8.24	8.45	7.89	5.28
1967	1.168	-0.11	-2.68	-4.77	-2.12	-1.31	-7.5	0.29	3.68	6.98	8.36	7.74	5.64
1968	1.322	-0.24	-2.8	-3.96	-4.38	-5.78	-2.76	1.52	3.81	7.3	9.68	7.95	6.8
1969	1.278	-0.54	1.88	-2.22	-4.75	-6.27	-0.96	1.31	6.23	8.13	7.52	8.82	3.95
1970	1.173	2.34	-4.67	-1.94	-2.84	-5.85	-4.56	1.67	5.14	7.17	6.79	7.66	4.43
1971	1.298	0.57	-2.91	-0.9	-6.93	-1.79	-0.15	1.24	5.36	7.5	8.91	7.55	5.63
1972	1.517	1.56	-1.65	-2.59	0.1	-0.59	-0.45	0.54	5.27	6.72	8.04	6.86	5.66
1973	1.675	1.89	-2.5	-0.64	0.53	-5.84	-0.72	0.62	2.8	5.31	8.05	7.36	5.99
1974	1.579	1.52	-5.36	-7.83	-1.08	-3.17	1.59	4.02	5.41	7.45	8.41	7.69	3.18
1975	1.347	1.92	-0.18	-5.88	-7.12	-0.43	-3.07	-0.37	3.68	5.45	8.01	8.49	2.76
1976	1.837	3.14	-0.98	-3.43	-6.11	-2.23	-0.94	0.37	4.01	7.1	9.42	7.51	5.5
1977	1.034	3.18	-0.09	-4.89	-5.07	-4.33	0.28	-1.09	4.93	6.06	8.99	7.82	4.63
1978	1.132	2.36	-4.3	-1.67	-5.32	-4.4	-1.83	1.72	4.09	5.5	8.97	8.69	4.78
1979	1.173	1.58	-1.94	-2.48	-7.5	-3.84	-0.66	-0.66	6.43	7.56	7.22	2.44	4.4
1980	1.212	1.91	-2.24	-3.06	-3.76	-1.67	-2.39	1.03	4.81	7.74	8.94	8.53	5.39
1981	1.31	-2.14	-2.5	-4.93	-5.93	-4.48	-4.23	1.49	3.98	6.27	7.95	8.47	4.62
1982	1.277	-2.65	-3.39	-6.01	-5.31	-0.15	-2.46	0.92	2.87	8.09	8.96	7.08	3.03
1983	1.522	2.19	-3.32	-4.66	-5.83	-1.45	-3.02	-3.48	3.23	6.25	7.52	7.26	3.83
1984	1.655	0.86	-1.55	-3.58	-7.87	-2.34	-1.14	1.15	4.17	8.28	10.28	8.82	4.96
1985	1.034	0.28	-2.03	-1.91	-4.49	-2.98	-3.53	0.63	4.37	7.33	7.97	7.82	3.72
1986	1.205	3.88	-3.2	-5.94	-3.78	-2.77	-2.1	0.83	2.52	6.69	8.37	7.61	4.62
1987	1.322	-0.61	-2.31	-4.21	0.36	-2.01	-2.41	0.28	4.53	7.83	9.28	8.54	5.11
1988	1.08	-0.6	1.68	1.26	-6.74	-4.68	-3.83	-2.68	5	6.95	8.79	8.73	4.57
1989	1.807	1.52	0.72	-2.13	-2.54	-6.11	-3.81	-1.06	2.61	6.42	8.19	7.79	4.59
1990	1.204	2.4	-1.11	-3.35	-2.59	-4.42	-4.82	-2.79	5.39	7.51	9.28	8.74	3.72
1991	1.403	2.31	0.38	-3.37	-1.62	-1.29	-0.95	-1.8	5.08	7.51	11.36	8.75	4.94
1992	1.824	2.11	-2.66	-1.9	0.12	-3.04	-2.42	-0.24	3.49	5.9	7.84	7.43	4.42
1993	1.439	1.26	-2.29	-3.47	-6.13	-2.09	-0.92	1.02	3.01	6.58	7.17	7.2	6.75
1994	1.278	1.29	1.63	-5.49	-5.88	-2.21	-4.44	-1.67	4.29	5.86	10.07	8.67	4.04
1995	1.317	0.74	-0.73	-4.15	-5.16	-6.21	-5.29	-1.75	3.93	7.44	8.09	9.01	5.26
1996	1.305	0.75	-1.37	-3.84	-0.84	-3.8	-0.17	1.92	4.77	7.77	9.03	8.05	8.48
1997	1.348	1.67	-6.38	-3.19	-2.56	-4.18	-3.55	1.74	3.4	6.36	10.1	8.82	5.63
1998	1.188	2.93	1.33	-0.2	-2.53	-4.16	-4.39	0.78	4.83	7.13	8.2	8.97	5.3
1999	1.379	-0.67	-0.96	-2.03	-3.07	-4.55	-4.93	-0.7	4.33	7.1	9.11	9.22	5.7
2000	1.396	2.91	-0.86	-4.37	-2.04	-3.85	-2.23	-1.99	4.25	6.8	10.22	8.89	6.29
2001	1.007	2.08	-2.25	-3	-1.51	-3.32	-4.32	0.96	4.41	6.8	8.69	8.64	6.78
2002	1.312	3.4	-1.35	-0.28	-2.06	-7.27	-2.79	1.73	4.13	8.47	8.58	8.37	6.56
2003	1.303	2.25	1.07	1.62	-2.05	-0.51	1.22	3.9	4.34	8.46	9.98	11.15	6.01
2004	1.391	2.75	-0.63	-2.88	-3.95	-1.81	1.52	2.8	5.04	8.66	10.08	10.75	6.81
2005	1.413	1.35	-1.53	-3.68	-4.05	-1.71	1.42	1.8	3.94	7.86	10.28	8.15	2.81
2006	1.5	-0.05	-0.73	-0.38	-0.35	0.7	-1.69	0	3.94	7.26	9.28	9.75	7.11
2007	1.3	2.25	1.07	1.62	-2.05	-0.51	1.22	3.9	4.34	8.46	9.98	11.15	6.01

Appendix 1.4.2

Balance Yr	Annual Ppt (m)	Oct (oC)	Nov (oC)	Dec (oC)	Jan (oC)	Feb (oC)	Mar (oC)	Apr (oC)	May (oC)	Jun (oC)	Jul (oC)	Aug (oC)	Sep (oC)
2008	1.309	1.44	-1.92	-3.48	-3.91	-3.08	-2.57	0.41	4.1	7	8.5	7.84	4.58
VALUES ARE CONSTANT OVER TIME													
2109	1.309	1.44	-1.92	-3.48	-3.91	-3.08	-2.57	0.41	4.1	7	8.5	7.84	4.58

Appendix 1.4.3

Balance Yr	Annual Ppt (m)	Oct (oC)	Nov (oC)	Dec (oC)	Jan (oC)	Feb (oC)	Mar (oC)	Apr (oC)	May (oC)	Jun (oC)	Jul (oC)	Aug (oC)	Sep (oC)
2008	1.335	1.34	-1.39	-2.72	-3.57	-3.04	-2.55	0.33	3.95	7.19	9	8.61	5.14
VALUES ARE CONSTANT OVER TIME													
2109	1.335	1.34	-1.39	-2.72	-3.57	-3.04	-2.55	0.33	3.95	7.19	9	8.61	5.14

Appendix 1.4.4

Balance Yr	Annual Ppt (m)	Oct (oC)	Nov (oC)	Dec (oC)	Jan (oC)	Feb (oC)	Mar (oC)	Apr (oC)	May (oC)	Jun (oC)	Jul (oC)	Aug (oC)	Sep (oC)
2008	1.305	2.44	-0.79	-2.8	-3.44	-2.44	-2.29	0.76	4.51	7.6	8.88	8.42	4.91
2009	1.305	2.47	-0.76	-2.78	-3.43	-2.42	-2.28	0.77	4.52	7.62	8.89	8.44	4.92
2010	1.305	2.5	-0.72	-2.76	-3.41	-2.4	-2.27	0.78	4.54	7.64	8.9	8.45	4.93
2011	1.305	2.53	-0.69	-2.73	-3.4	-2.38	-2.26	0.79	4.55	7.66	8.91	8.47	4.94
2012	1.304	2.56	-0.65	-2.71	-3.39	-2.36	-2.25	0.8	4.56	7.68	8.92	8.49	4.95
2013	1.304	2.59	-0.62	-2.69	-3.37	-2.34	-2.24	0.81	4.58	7.7	8.94	8.51	4.96
2014	1.304	2.62	-0.58	-2.67	-3.36	-2.32	-2.24	0.82	4.59	7.71	8.95	8.53	4.97
2015	1.304	2.65	-0.55	-2.65	-3.34	-2.3	-2.23	0.84	4.6	7.73	8.96	8.54	4.98
2016	1.304	2.68	-0.51	-2.63	-3.33	-2.28	-2.22	0.85	4.61	7.75	8.97	8.56	4.99
2017	1.304	2.72	-0.48	-2.61	-3.31	-2.26	-2.21	0.86	4.63	7.77	8.98	8.58	5
2018	1.304	2.75	-0.44	-2.58	-3.3	-2.24	-2.2	0.87	4.64	7.79	8.99	8.6	5.01
2019	1.304	2.78	-0.4	-2.56	-3.28	-2.22	-2.19	0.88	4.65	7.81	9.01	8.62	5.02
2020	1.304	2.81	-0.37	-2.54	-3.27	-2.2	-2.18	0.89	4.67	7.83	9.02	8.63	5.03
2021	1.303	2.84	-0.33	-2.52	-3.25	-2.18	-2.17	0.9	4.68	7.85	9.03	8.65	5.04
2022	1.306	2.87	-0.31	-2.49	-3.22	-2.16	-2.16	0.92	4.7	7.85	9.06	8.69	5.08
2023	1.309	2.9	-0.29	-2.47	-3.18	-2.14	-2.14	0.93	4.72	7.86	9.08	8.73	5.13
2024	1.311	2.94	-0.27	-2.44	-3.15	-2.12	-2.13	0.94	4.74	7.87	9.11	8.77	5.17
2025	1.314	2.97	-0.25	-2.41	-3.11	-2.1	-2.11	0.96	4.76	7.87	9.14	8.81	5.21
2026	1.316	3	-0.23	-2.39	-3.08	-2.08	-2.1	0.97	4.78	7.88	9.17	8.85	5.26
2027	1.319	3.03	-0.21	-2.36	-3.04	-2.05	-2.08	0.98	4.8	7.89	9.19	8.89	5.3
2028	1.322	3.06	-0.19	-2.33	-3.01	-2.03	-2.06	1	4.83	7.9	9.22	8.93	5.34
2029	1.324	3.09	-0.17	-2.3	-2.97	-2.01	-2.05	1.01	4.85	7.9	9.25	8.97	5.38
2030	1.327	3.13	-0.15	-2.28	-2.94	-1.99	-2.03	1.03	4.87	7.91	9.27	9.01	5.43
2031	1.329	3.16	-0.13	-2.25	-2.9	-1.97	-2.02	1.04	4.89	7.92	9.3	9.05	5.47
2032	1.332	3.19	-0.1	-2.22	-2.87	-1.95	-2	1.05	4.91	7.93	9.33	9.09	5.51
2033	1.335	3.22	-0.08	-2.2	-2.83	-1.93	-1.99	1.07	4.93	7.93	9.35	9.13	5.56
2034	1.337	3.25	-0.06	-2.17	-2.8	-1.91	-1.97	1.08	4.95	7.94	9.38	9.17	5.6
2035	1.34	3.28	-0.04	-2.14	-2.76	-1.89	-1.96	1.1	4.97	7.95	9.41	9.21	5.64
2036	1.342	3.32	-0.02	-2.12	-2.73	-1.87	-1.94	1.11	4.99	7.96	9.44	9.25	5.69
2037	1.345	3.35	0	-2.09	-2.69	-1.84	-1.92	1.12	5.02	7.96	9.46	9.29	5.73
2038	1.348	3.38	0.02	-2.06	-2.66	-1.82	-1.91	1.14	5.04	7.97	9.49	9.33	5.77
2039	1.35	3.41	0.04	-2.03	-2.62	-1.8	-1.89	1.15	5.06	7.98	9.52	9.37	5.81
2040	1.353	3.44	0.06	-2.01	-2.59	-1.78	-1.88	1.16	5.08	7.98	9.54	9.41	5.86
2041	1.355	3.47	0.08	-1.98	-2.55	-1.76	-1.86	1.18	5.1	7.99	9.57	9.45	5.9
2042	1.358	3.51	0.11	-1.95	-2.52	-1.74	-1.85	1.19	5.12	8	9.6	9.5	5.94
2043	1.36	3.54	0.13	-1.93	-2.48	-1.72	-1.83	1.21	5.14	8.01	9.62	9.54	5.99
2044	1.363	3.57	0.15	-1.9	-2.45	-1.7	-1.82	1.22	5.16	8.01	9.65	9.58	6.03
2045	1.366	3.6	0.17	-1.87	-2.41	-1.68	-1.8	1.23	5.18	8.02	9.68	9.62	6.07
2046	1.368	3.63	0.19	-1.85	-2.38	-1.66	-1.78	1.25	5.2	8.03	9.71	9.66	6.12
2047	1.371	3.66	0.21	-1.82	-2.34	-1.63	-1.77	1.26	5.23	8.04	9.73	9.7	6.16
2048	1.373	3.7	0.23	-1.79	-2.31	-1.61	-1.75	1.27	5.25	8.04	9.76	9.74	6.2
2049	1.376	3.73	0.25	-1.76	-2.27	-1.59	-1.74	1.29	5.27	8.05	9.79	9.78	6.24
2050	1.379	3.76	0.27	-1.74	-2.24	-1.57	-1.72	1.3	5.29	8.06	9.81	9.82	6.29
2051	1.381	3.79	0.29	-1.71	-2.2	-1.55	-1.71	1.32	5.31	8.06	9.84	9.86	6.33
2052	1.384	3.82	0.31	-1.68	-2.17	-1.53	-1.69	1.33	5.33	8.07	9.87	9.9	6.37
2053	1.386	3.85	0.34	-1.66	-2.13	-1.51	-1.68	1.34	5.35	8.08	9.89	9.94	6.42
2054	1.389	3.89	0.36	-1.63	-2.1	-1.49	-1.66	1.36	5.37	8.09	9.92	9.98	6.46
2055	1.392	3.92	0.38	-1.6	-2.06	-1.47	-1.64	1.37	5.39	8.09	9.95	10.02	6.5
2056	1.394	3.95	0.4	-1.58	-2.03	-1.45	-1.63	1.39	5.41	8.1	9.98	10.06	6.55
2057	1.395	3.96	0.44	-1.56	-2.02	-1.43	-1.59	1.42	5.44	8.13	10.01	10.08	6.56
2058	1.397	3.98	0.47	-1.54	-2.01	-1.41	-1.55	1.45	5.47	8.16	10.05	10.1	6.57
2059	1.398	4	0.51	-1.52	-1.99	-1.39	-1.51	1.48	5.5	8.18	10.09	10.12	6.59
2060	1.399	4.01	0.55	-1.5	-1.98	-1.37	-1.47	1.52	5.53	8.21	10.12	10.14	6.6
2061	1.401	4.03	0.59	-1.48	-1.97	-1.35	-1.44	1.55	5.56	8.24	10.16	10.16	6.61
2062	1.402	4.04	0.62	-1.46	-1.96	-1.33	-1.4	1.58	5.59	8.26	10.2	10.17	6.63
2063	1.403	4.06	0.66	-1.44	-1.95	-1.31	-1.36	1.61	5.62	8.29	10.23	10.19	6.64
2064	1.404	4.07	0.7	-1.42	-1.94	-1.3	-1.32	1.65	5.65	8.32	10.27	10.21	6.66
2065	1.406	4.09	0.73	-1.4	-1.93	-1.28	-1.28	1.68	5.68	8.35	10.31	10.23	6.67
2066	1.407	4.1	0.77	-1.38	-1.92	-1.26	-1.24	1.71	5.71	8.37	10.35	10.25	6.68
2067	1.408	4.12	0.81	-1.36	-1.91	-1.24	-1.2	1.75	5.74	8.4	10.38	10.27	6.7
2068	1.409	4.14	0.85	-1.34	-1.9	-1.22	-1.17	1.78	5.77	8.43	10.42	10.29	6.71
2069	1.411	4.15	0.88	-1.32	-1.88	-1.2	-1.13	1.81	5.8	8.45	10.46	10.31	6.72
2070	1.412	4.17	0.92	-1.29	-1.87	-1.18	-1.09	1.84	5.83	8.48	10.49	10.33	6.74
2071	1.413	4.18	0.96	-1.27	-1.86	-1.16	-1.05	1.88	5.86	8.51	10.53	10.35	6.75
2072	1.414	4.2	1	-1.25	-1.85	-1.15	-1.01	1.91	5.89	8.53	10.57	10.37	6.77
2073	1.416	4.21	1.03	-1.23	-1.84	-1.13	-0.97	1.94	5.92	8.56	10.6	10.39	6.78
2074	1.417	4.23	1.07	-1.21	-1.83	-1.11	-0.93	1.98	5.95	8.59	10.64	10.41	6.79
2075	1.418	4.24	1.11	-1.19	-1.82	-1.09	-0.9	2.01	5.98	8.62	10.68	10.43	6.81
2076	1.419	4.26	1.15	-1.17	-1.81	-1.07	-0.86	2.04	6.01	8.64	10.71	10.45	6.82
2077	1.421	4.28	1.18	-1.15	-1.8	-1.05	-0.82	2.07	6.04	8.67	10.75	10.47	6.83
2078	1.422	4.29	1.22	-1.13	-1.78	-1.03	-0.78	2.11	6.07	8.7	10.79	10.49	6.85
2079	1.423	4.31	1.26	-1.11	-1.77	-1.01	-0.74	2.14	6.1	8.72	10.83	10.51	6.86
2080	1.424	4.32	1.3	-1.09	-1.76	-1	-0.7	2.17	6.13	8.75	10.86	10.53	6.87
2081	1.426	4.34	1.33	-1.07	-1.75	-0.98	-0.66	2.2	6.16	8.78	10.9	10.55	6.89
2082	1.427	4.35	1.37	-1.05	-1.74	-0.96	-0.63	2.24	6.19	8.81	10.94	10.57	6.9
2083	1.428	4.37	1.41	-1.03	-1.73	-0.94	-0.59	2.27	6.22	8.83	10.97	10.59	6.92
2084	1.429	4.39	1.44	-1.01	-1.72	-0.92	-0.55	2.3	6.25	8.86	11.01	10.61	6.93
2085	1.431	4.4	1.48	-0.99	-1.71	-0.9	-0.51	2.34	6.28	8.89	11.05	10.63	6.94
2086	1.432	4.42	1.52	-0.97	-1.7	-0.88	-0.47	2.37	6.31	8.91	11.08	10.65	6.96

2087	1.433	4.43	1.56	-0.95	-1.69	-0.87	-0.43	2.4	6.34	8.94	11.12	10.67	6.97
2088	1.435	4.45	1.59	-0.93	-1.67	-0.85	-0.4	2.43	6.37	8.97	11.16	10.69	6.98
2089	1.436	4.46	1.63	-0.91	-1.66	-0.83	-0.36	2.47	6.4	9	11.19	10.71	7
2090	1.437	4.48	1.67	-0.89	-1.65	-0.81	-0.32	2.5	6.43	9.02	11.23	10.73	7.01
2091	1.438	4.49	1.71	-0.87	-1.64	-0.79	-0.28	2.53	6.46	9.05	11.27	10.75	7.03
2092	1.44	4.51	1.74	-0.85	-1.63	-0.77	-0.24	2.57	6.49	9.08	11.3	10.76	7.04
2093	1.441	4.53	1.78	-0.83	-1.62	-0.75	-0.2	2.6	6.51	9.1	11.34	10.78	7.05
2094	1.442	4.54	1.82	-0.81	-1.61	-0.73	-0.16	2.63	6.54	9.13	11.38	10.8	7.07
2095	1.443	4.56	1.86	-0.79	-1.6	-0.72	-0.13	2.66	6.57	9.16	11.42	10.82	7.08
2096	1.445	4.57	1.89	-0.77	-1.59	-0.7	-0.09	2.7	6.6	9.18	11.45	10.84	7.09
2097	1.446	4.59	1.93	-0.75	-1.58	-0.68	-0.05	2.73	6.63	9.21	11.49	10.86	7.11
2098	1.447	4.6	1.97	-0.73	-1.56	-0.66	-0.01	2.76	6.66	9.24	11.53	10.88	7.12
2099	1.448	4.62	2.01	-0.71	-1.55	-0.64	0.03	2.79	6.69	9.27	11.56	10.9	7.13
2100	1.45	4.63	2.04	-0.69	-1.54	-0.62	0.07	2.83	6.72	9.29	11.6	10.92	7.15
2101	1.451	4.65	2.08	-0.67	-1.53	-0.6	0.11	2.86	6.75	9.32	11.64	10.94	7.16
2102	1.452	4.67	2.12	-0.65	-1.52	-0.58	0.14	2.89	6.78	9.35	11.67	10.96	7.18
2103	1.453	4.68	2.15	-0.63	-1.51	-0.57	0.18	2.93	6.81	9.37	11.71	10.98	7.19
2104	1.455	4.7	2.19	-0.61	-1.5	-0.55	0.22	2.96	6.84	9.4	11.75	11	7.2
2105	1.456	4.71	2.23	-0.59	-1.49	-0.53	0.26	2.99	6.87	9.43	11.78	11.02	7.22
2106	1.457	4.73	2.27	-0.57	-1.48	-0.51	0.3	3.02	6.9	9.46	11.82	11.04	7.23
2107	1.458	4.74	2.3	-0.55	-1.47	-0.49	0.34	3.06	6.93	9.48	11.86	11.06	7.24
2108	1.46	4.76	2.34	-0.53	-1.45	-0.47	0.38	3.09	6.96	9.51	11.9	11.08	7.26
2109	1.461	4.77	2.38	-0.51	-1.44	-0.45	0.41	3.12	6.99	9.54	11.93	11.1	7.27

Appendix 1.4.5

Balance Yr	Annual Ppt (m)	Oct (oC)	Nov (oC)	Dec (oC)	Jan (oC)	Feb (oC)	Mar (oC)	Apr (oC)	May (oC)	Jun (oC)	Jul (oC)	Aug (oC)	Sep (oC)
2008	1.341	2.24	-0.58	-2.93	-3.36	-2.72	-2.3	0.88	4.56	7.36	9.2	8.55	4.86
2009	1.342	2.26	-0.54	-2.92	-3.34	-2.71	-2.29	0.89	4.57	7.37	9.22	8.58	4.87
2010	1.344	2.29	-0.5	-2.9	-3.32	-2.7	-2.28	0.91	4.59	7.38	9.24	8.6	4.88
2011	1.345	2.31	-0.46	-2.88	-3.3	-2.69	-2.27	0.92	4.6	7.39	9.26	8.62	4.89
2012	1.346	2.34	-0.42	-2.87	-3.29	-2.68	-2.27	0.94	4.62	7.41	9.28	8.64	4.9
2013	1.347	2.36	-0.38	-2.85	-3.27	-2.66	-2.26	0.95	4.63	7.42	9.3	8.66	4.91
2014	1.348	2.39	-0.33	-2.83	-3.25	-2.65	-2.25	0.97	4.64	7.43	9.33	8.69	4.92
2015	1.349	2.41	-0.29	-2.81	-3.23	-2.64	-2.24	0.98	4.66	7.44	9.35	8.71	4.93
2016	1.35	2.44	-0.25	-2.8	-3.22	-2.63	-2.23	1	4.67	7.45	9.37	8.73	4.94
2017	1.351	2.46	-0.21	-2.78	-3.2	-2.62	-2.22	1.01	4.69	7.46	9.39	8.75	4.95
2018	1.352	2.49	-0.17	-2.76	-3.18	-2.61	-2.21	1.03	4.7	7.47	9.41	8.78	4.95
2019	1.353	2.51	-0.13	-2.75	-3.16	-2.6	-2.21	1.04	4.72	7.48	9.43	8.8	4.96
2020	1.354	2.54	-0.08	-2.73	-3.15	-2.59	-2.2	1.06	4.73	7.49	9.46	8.82	4.97
2021	1.355	2.57	-0.04	-2.71	-3.13	-2.57	-2.19	1.07	4.75	7.51	9.48	8.84	4.98
2022	1.356	2.57	-0.02	-2.69	-3.12	-2.56	-2.19	1.08	4.76	7.52	9.48	8.87	5
2023	1.357	2.58	-0.01	-2.67	-3.11	-2.54	-2.2	1.09	4.77	7.53	9.48	8.9	5.01
2024	1.358	2.59	0.01	-2.65	-3.1	-2.52	-2.21	1.09	4.78	7.54	9.48	8.94	5.03
2025	1.359	2.6	0.03	-2.63	-3.09	-2.51	-2.21	1.1	4.79	7.55	9.48	8.97	5.04
2026	1.36	2.6	0.05	-2.61	-3.08	-2.49	-2.22	1.11	4.8	7.56	9.48	9	5.05
2027	1.361	2.61	0.07	-2.59	-3.08	-2.47	-2.22	1.12	4.81	7.57	9.48	9.03	5.07
2028	1.363	2.62	0.09	-2.57	-3.07	-2.46	-2.23	1.12	4.82	7.58	9.48	9.06	5.08
2029	1.364	2.63	0.11	-2.55	-3.06	-2.44	-2.23	1.13	4.83	7.59	9.48	9.09	5.1
2030	1.365	2.64	0.13	-2.53	-3.05	-2.42	-2.24	1.14	4.84	7.6	9.48	9.12	5.11
2031	1.366	2.64	0.14	-2.51	-3.04	-2.41	-2.24	1.14	4.85	7.61	9.47	9.15	5.13
2032	1.367	2.65	0.16	-2.49	-3.03	-2.39	-2.25	1.15	4.86	7.62	9.47	9.18	5.14
2033	1.368	2.66	0.18	-2.46	-3.02	-2.37	-2.26	1.16	4.87	7.63	9.47	9.21	5.16
2034	1.369	2.67	0.2	-2.44	-3.01	-2.36	-2.26	1.16	4.88	7.64	9.47	9.24	5.17
2035	1.37	2.67	0.22	-2.42	-3	-2.34	-2.27	1.17	4.89	7.65	9.47	9.28	5.18
2036	1.371	2.68	0.24	-2.4	-2.99	-2.32	-2.27	1.18	4.91	7.66	9.47	9.31	5.2
2037	1.373	2.69	0.26	-2.38	-2.98	-2.31	-2.28	1.19	4.92	7.66	9.47	9.34	5.21
2038	1.374	2.7	0.28	-2.36	-2.97	-2.29	-2.28	1.19	4.93	7.67	9.47	9.37	5.23
2039	1.375	2.71	0.29	-2.34	-2.97	-2.27	-2.29	1.2	4.94	7.68	9.47	9.4	5.24
2040	1.376	2.71	0.31	-2.32	-2.96	-2.25	-2.29	1.21	4.95	7.69	9.47	9.43	5.26
2041	1.377	2.72	0.33	-2.3	-2.95	-2.24	-2.3	1.21	4.96	7.7	9.47	9.46	5.27
2042	1.378	2.73	0.35	-2.28	-2.94	-2.22	-2.3	1.22	4.97	7.71	9.47	9.49	5.29
2043	1.379	2.74	0.37	-2.26	-2.93	-2.2	-2.31	1.23	4.98	7.72	9.47	9.52	5.3
2044	1.38	2.74	0.39	-2.24	-2.92	-2.19	-2.32	1.24	4.99	7.73	9.47	9.55	5.32
2045	1.382	2.75	0.41	-2.22	-2.91	-2.17	-2.32	1.24	5	7.74	9.47	9.58	5.33
2046	1.383	2.76	0.43	-2.2	-2.9	-2.15	-2.33	1.25	5.01	7.75	9.47	9.62	5.34
2047	1.384	2.77	0.44	-2.18	-2.89	-2.14	-2.33	1.26	5.02	7.76	9.47	9.65	5.36
2048	1.385	2.78	0.46	-2.15	-2.88	-2.12	-2.34	1.26	5.03	7.77	9.47	9.68	5.37
2049	1.386	2.78	0.48	-2.13	-2.87	-2.1	-2.34	1.27	5.04	7.78	9.47	9.71	5.39
2050	1.387	2.79	0.5	-2.11	-2.86	-2.09	-2.35	1.28	5.06	7.79	9.47	9.74	5.4
2051	1.388	2.8	0.52	-2.09	-2.86	-2.07	-2.35	1.29	5.07	7.8	9.47	9.77	5.42
2052	1.389	2.81	0.54	-2.07	-2.85	-2.05	-2.36	1.29	5.08	7.81	9.47	9.8	5.43
2053	1.39	2.81	0.56	-2.05	-2.84	-2.04	-2.37	1.3	5.09	7.82	9.47	9.83	5.45
2054	1.392	2.82	0.58	-2.03	-2.83	-2.02	-2.37	1.31	5.1	7.83	9.47	9.86	5.46
2055	1.393	2.83	0.59	-2.01	-2.82	-2	-2.38	1.31	5.11	7.84	9.47	9.89	5.47
2056	1.394	2.84	0.61	-1.99	-2.81	-1.99	-2.38	1.32	5.12	7.85	9.47	9.92	5.49
2057	1.394	2.88	0.64	-1.95	-2.77	-1.94	-2.32	1.36	5.16	7.89	9.51	9.96	5.53
2058	1.394	2.91	0.67	-1.91	-2.73	-1.9	-2.26	1.41	5.19	7.94	9.55	10	5.56
2059	1.394	2.95	0.7	-1.87	-2.69	-1.85	-2.2	1.45	5.23	7.98	9.59	10.04	5.6
2060	1.394	2.99	0.72	-1.82	-2.65	-1.81	-2.14	1.49	5.27	8.02	9.63	10.08	5.64
2061	1.394	3.03	0.75	-1.78	-2.62	-1.76	-2.08	1.54	5.3	8.06	9.67	10.12	5.68

2062	1.394	3.06	0.78	-1.74	-2.58	-1.72	-2.02	1.58	5.34	8.1	9.71	10.16	5.72
2063	1.394	3.1	0.81	-1.7	-2.54	-1.67	-1.96	1.63	5.38	8.14	9.75	10.19	5.75
2064	1.394	3.14	0.83	-1.66	-2.5	-1.63	-1.9	1.67	5.41	8.18	9.79	10.23	5.79
2065	1.394	3.18	0.86	-1.62	-2.46	-1.58	-1.83	1.71	5.45	8.22	9.83	10.27	5.83
2066	1.394	3.22	0.89	-1.58	-2.42	-1.54	-1.77	1.76	5.49	8.26	9.87	10.31	5.87
2067	1.394	3.25	0.92	-1.54	-2.38	-1.49	-1.71	1.8	5.52	8.3	9.91	10.35	5.9
2068	1.394	3.29	0.94	-1.5	-2.34	-1.45	-1.65	1.84	5.56	8.34	9.95	10.39	5.94
2069	1.394	3.33	0.97	-1.45	-2.3	-1.4	-1.59	1.89	5.6	8.38	9.99	10.43	5.98
2070	1.394	3.37	1	-1.41	-2.26	-1.36	-1.53	1.93	5.63	8.43	10.03	10.46	6.02
2071	1.394	3.41	1.03	-1.37	-2.23	-1.31	-1.47	1.97	5.67	8.47	10.07	10.5	6.05
2072	1.394	3.44	1.06	-1.33	-2.19	-1.27	-1.41	2.02	5.71	8.51	10.12	10.54	6.09
2073	1.394	3.48	1.08	-1.29	-2.15	-1.22	-1.35	2.06	5.74	8.55	10.16	10.58	6.13
2074	1.394	3.52	1.11	-1.25	-2.11	-1.18	-1.29	2.1	5.78	8.59	10.2	10.62	6.17
2075	1.394	3.56	1.14	-1.21	-2.07	-1.13	-1.23	2.15	5.82	8.63	10.24	10.66	6.2
2076	1.394	3.59	1.17	-1.17	-2.03	-1.09	-1.16	2.19	5.86	8.67	10.28	10.69	6.24
2077	1.394	3.63	1.19	-1.12	-1.99	-1.04	-1.1	2.23	5.89	8.71	10.32	10.73	6.28
2078	1.394	3.67	1.22	-1.08	-1.95	-1	-1.04	2.28	5.93	8.75	10.36	10.77	6.32
2079	1.394	3.71	1.25	-1.04	-1.91	-0.95	-0.98	2.32	5.97	8.79	10.4	10.81	6.36
2080	1.394	3.75	1.28	-1	-1.87	-0.91	-0.92	2.37	6	8.83	10.44	10.85	6.39
2081	1.394	3.78	1.3	-0.96	-1.84	-0.86	-0.86	2.41	6.04	8.87	10.48	10.89	6.43
2082	1.394	3.82	1.33	-0.92	-1.8	-0.82	-0.8	2.45	6.08	8.92	10.52	10.93	6.47
2083	1.394	3.86	1.36	-0.88	-1.76	-0.77	-0.74	2.5	6.11	8.96	10.56	10.96	6.51
2084	1.394	3.9	1.39	-0.84	-1.72	-0.73	-0.68	2.54	6.15	9	10.6	11	6.54
2085	1.394	3.94	1.41	-0.8	-1.68	-0.68	-0.62	2.58	6.19	9.04	10.64	11.04	6.58
2086	1.394	3.97	1.44	-0.75	-1.64	-0.64	-0.56	2.63	6.22	9.08	10.68	11.08	6.62
2087	1.394	4.01	1.47	-0.71	-1.6	-0.59	-0.5	2.67	6.26	9.12	10.72	11.12	6.66
2088	1.394	4.05	1.5	-0.67	-1.56	-0.55	-0.43	2.71	6.3	9.16	10.76	11.16	6.69
2089	1.394	4.09	1.53	-0.63	-1.52	-0.5	-0.37	2.76	6.33	9.2	10.8	11.2	6.73
2090	1.394	4.13	1.55	-0.59	-1.49	-0.46	-0.31	2.8	6.37	9.24	10.84	11.23	6.77
2091	1.395	4.16	1.58	-0.55	-1.45	-0.41	-0.25	2.84	6.41	9.28	10.88	11.27	6.81
2092	1.395	4.2	1.61	-0.51	-1.41	-0.36	-0.19	2.89	6.44	9.32	10.92	11.31	6.84
2093	1.395	4.24	1.64	-0.47	-1.37	-0.32	-0.13	2.93	6.48	9.36	10.96	11.35	6.88
2094	1.395	4.28	1.66	-0.42	-1.33	-0.27	-0.07	2.97	6.52	9.41	11	11.39	6.92
2095	1.395	4.31	1.69	-0.38	-1.29	-0.23	-0.01	3.02	6.55	9.45	11.04	11.43	6.96
2096	1.395	4.35	1.72	-0.34	-1.25	-0.18	0.05	3.06	6.59	9.49	11.08	11.47	7
2097	1.395	4.39	1.75	-0.3	-1.21	-0.14	0.11	3.11	6.63	9.53	11.13	11.5	7.03
2098	1.395	4.43	1.77	-0.26	-1.17	-0.09	0.17	3.15	6.66	9.57	11.17	11.54	7.07
2099	1.395	4.47	1.8	-0.22	-1.13	-0.05	0.24	3.19	6.7	9.61	11.21	11.58	7.11
2100	1.395	4.5	1.83	-0.18	-1.1	0	0.3	3.24	6.74	9.65	11.25	11.62	7.15
2101	1.395	4.54	1.86	-0.14	-1.06	0.04	0.36	3.28	6.77	9.69	11.29	11.66	7.18
2102	1.395	4.58	1.89	-0.1	-1.02	0.09	0.42	3.32	6.81	9.73	11.33	11.7	7.22
2103	1.395	4.62	1.91	-0.05	-0.98	0.13	0.48	3.37	6.85	9.77	11.37	11.73	7.26
2104	1.395	4.66	1.94	-0.01	-0.94	0.18	0.54	3.41	6.89	9.81	11.41	11.77	7.3
2105	1.395	4.69	1.97	0.03	-0.9	0.22	0.6	3.45	6.92	9.85	11.45	11.81	7.33
2106	1.395	4.73	2	0.07	-0.86	0.27	0.66	3.5	6.96	9.9	11.49	11.85	7.37
2107	1.395	4.77	2.02	0.11	-0.82	0.31	0.72	3.54	7	9.94	11.53	11.89	7.41
2108	1.395	4.81	2.05	0.15	-0.78	0.36	0.78	3.58	7.03	9.98	11.57	11.93	7.45
2109	1.395	4.84	2.08	0.19	-0.74	0.4	0.84	3.63	7.07	10.02	11.61	11.97	7.48

Appendix 1.4.6

Balance Yr	Annual Ppt (m)	Oct (oC)	Nov (oC)	Dec (oC)	Jan (oC)	Feb (oC)	Mar (oC)	Apr (oC)	May (oC)	Jun (oC)	Jul (oC)	Aug (oC)	Sep (oC)
2008	1.33	1.99	-1.04	-3.18	-3.36	-2.41	-2.34	0.87	4.68	7.22	8.71	8.62	4.89
2009	1.33	2.01	-1.01	-3.17	-3.34	-2.39	-2.33	0.88	4.7	7.23	8.72	8.65	4.9
2010	1.331	2.03	-0.98	-3.16	-3.32	-2.37	-2.33	0.9	4.72	7.24	8.72	8.67	4.91
2011	1.332	2.05	-0.96	-3.15	-3.3	-2.35	-2.32	0.91	4.74	7.24	8.73	8.7	4.92
2012	1.332	2.06	-0.93	-3.14	-3.29	-2.33	-2.31	0.93	4.75	7.25	8.73	8.72	4.93
2013	1.333	2.08	-0.9	-3.13	-3.27	-2.31	-2.31	0.94	4.77	7.26	8.74	8.74	4.94
2014	1.334	2.1	-0.88	-3.12	-3.25	-2.29	-2.3	0.95	4.79	7.26	8.75	8.77	4.95
2015	1.334	2.12	-0.85	-3.11	-3.24	-2.26	-2.29	0.97	4.81	7.27	8.75	8.79	4.96
2016	1.335	2.13	-0.82	-3.1	-3.22	-2.24	-2.28	0.98	4.83	7.28	8.76	8.82	4.97
2017	1.336	2.15	-0.79	-3.09	-3.2	-2.22	-2.28	1	4.85	7.29	8.77	8.84	4.98
2018	1.336	2.17	-0.77	-3.08	-3.18	-2.2	-2.27	1.01	4.86	7.29	8.77	8.87	4.99
2019	1.337	2.19	-0.74	-3.08	-3.17	-2.18	-2.26	1.03	4.88	7.3	8.78	8.89	5
2020	1.338	2.2	-0.71	-3.07	-3.15	-2.16	-2.26	1.04	4.9	7.31	8.79	8.92	5.01
2021	1.338	2.22	-0.68	-3.06	-3.13	-2.14	-2.25	1.06	4.92	7.31	8.79	8.94	5.02
2022	1.339	2.24	-0.66	-3.02	-3.11	-2.14	-2.23	1.07	4.93	7.32	8.81	8.96	5.05
2023	1.339	2.25	-0.63	-2.99	-3.1	-2.13	-2.2	1.08	4.93	7.34	8.82	8.97	5.08
2024	1.34	2.26	-0.61	-2.96	-3.08	-2.13	-2.18	1.09	4.94	7.35	8.84	8.99	5.1
2025	1.341	2.28	-0.59	-2.93	-3.07	-2.13	-2.16	1.1	4.95	7.36	8.85	9	5.13
2026	1.341	2.29	-0.56	-2.9	-3.05	-2.12	-2.14	1.12	4.96	7.37	8.87	9.02	5.16
2027	1.342	2.31	-0.54	-2.87	-3.03	-2.12	-2.12	1.13	4.96	7.38	8.88	9.03	5.18
2028	1.342	2.32	-0.51	-2.84	-3.02	-2.12	-2.09	1.14	4.97	7.4	8.9	9.05	5.21
2029	1.343	2.34	-0.49	-2.8	-3	-2.12	-2.07	1.15	4.98	7.41	8.91	9.06	5.24
2030	1.343	2.35	-0.46	-2.77	-2.98	-2.11	-2.05	1.17	4.99	7.42	8.93	9.08	5.26
2031	1.344	2.36	-0.44	-2.74	-2.97	-2.11	-2.03	1.18	4.99	7.43	8.94	9.09	5.29
2032	1.344	2.38	-0.42	-2.71	-2.95	-2.11	-2.01	1.19	5	7.44	8.96	9.11	5.32
2033	1.345	2.39	-0.39	-2.68	-2.94	-2.1	-1.98	1.2	5.01	7.46	8.97	9.13	5.34
2034	1.345	2.41	-0.37	-2.65	-2.92	-2.1	-1.96	1.22	5.02	7.47	8.99	9.14	5.37
2035	1.346	2.42	-0.34	-2.61	-2.9	-2.1	-1.94	1.23	5.02	7.48	9	9.16	5.4
2036	1.347	2.44	-0.32	-2.58	-2.89	-2.09	-1.92	1.24	5.03	7.49	9.01	9.17	5.42

2037	1.347	2.45	-0.29	-2.55	-2.87	-2.09	-1.9	1.25	5.04	7.5	9.03	9.19	5.45
2038	1.348	2.46	-0.27	-2.52	-2.85	-2.09	-1.88	1.26	5.05	7.51	9.04	9.2	5.48
2039	1.348	2.48	-0.24	-2.49	-2.84	-2.09	-1.85	1.28	5.05	7.53	9.06	9.22	5.5
2040	1.349	2.49	-0.22	-2.46	-2.82	-2.08	-1.83	1.29	5.06	7.54	9.07	9.23	5.53
2041	1.349	2.51	-0.2	-2.42	-2.81	-2.08	-1.81	1.3	5.07	7.55	9.09	9.25	5.56
2042	1.35	2.52	-0.17	-2.39	-2.79	-2.08	-1.79	1.31	5.08	7.56	9.1	9.26	5.58
2043	1.35	2.54	-0.15	-2.36	-2.77	-2.07	-1.77	1.33	5.08	7.57	9.12	9.28	5.61
2044	1.351	2.55	-0.12	-2.33	-2.76	-2.07	-1.74	1.34	5.09	7.59	9.13	9.3	5.64
2045	1.351	2.56	-0.1	-2.3	-2.74	-2.07	-1.72	1.35	5.1	7.6	9.15	9.31	5.66
2046	1.352	2.58	-0.07	-2.27	-2.72	-2.06	-1.7	1.36	5.11	7.61	9.16	9.33	5.69
2047	1.353	2.59	-0.05	-2.24	-2.71	-2.06	-1.68	1.38	5.11	7.62	9.18	9.34	5.72
2048	1.353	2.61	-0.03	-2.2	-2.69	-2.06	-1.66	1.39	5.12	7.63	9.19	9.36	5.75
2049	1.354	2.62	0	-2.17	-2.67	-2.06	-1.63	1.4	5.13	7.65	9.21	9.37	5.77
2050	1.354	2.64	0.02	-2.14	-2.66	-2.05	-1.61	1.41	5.14	7.66	9.22	9.39	5.8
2051	1.355	2.65	0.05	-2.11	-2.64	-2.05	-1.59	1.42	5.14	7.67	9.24	9.4	5.83
2052	1.355	2.66	0.07	-2.08	-2.63	-2.05	-1.57	1.44	5.15	7.68	9.25	9.42	5.85
2053	1.356	2.68	0.1	-2.05	-2.61	-2.04	-1.55	1.45	5.16	7.69	9.27	9.43	5.88
2054	1.356	2.69	0.12	-2.01	-2.59	-2.04	-1.52	1.46	5.17	7.7	9.28	9.45	5.91
2055	1.357	2.71	0.15	-1.98	-2.58	-2.04	-1.5	1.47	5.17	7.72	9.3	9.47	5.93
2056	1.357	2.72	0.17	-1.95	-2.56	-2.03	-1.48	1.49	5.18	7.73	9.31	9.48	5.96
2057	1.358	2.74	0.19	-1.94	-2.54	-2.01	-1.47	1.5	5.2	7.75	9.34	9.5	5.97
2058	1.359	2.76	0.21	-1.93	-2.52	-1.99	-1.47	1.51	5.21	7.76	9.36	9.52	5.98
2059	1.36	2.77	0.22	-1.91	-2.5	-1.97	-1.46	1.53	5.22	7.78	9.38	9.54	5.98
2060	1.361	2.79	0.24	-1.9	-2.47	-1.95	-1.46	1.54	5.24	7.8	9.41	9.56	5.99
2061	1.362	2.81	0.26	-1.89	-2.45	-1.93	-1.45	1.55	5.25	7.82	9.43	9.58	6
2062	1.363	2.83	0.28	-1.88	-2.43	-1.91	-1.44	1.57	5.26	7.84	9.45	9.6	6.01
2063	1.364	2.84	0.3	-1.86	-2.41	-1.89	-1.44	1.58	5.28	7.85	9.48	9.62	6.02
2064	1.365	2.86	0.32	-1.85	-2.39	-1.87	-1.43	1.59	5.29	7.87	9.5	9.64	6.02
2065	1.366	2.88	0.33	-1.84	-2.37	-1.85	-1.43	1.61	5.3	7.89	9.53	9.66	6.03
2066	1.367	2.89	0.35	-1.83	-2.34	-1.83	-1.42	1.62	5.32	7.91	9.55	9.68	6.04
2067	1.368	2.91	0.37	-1.81	-2.32	-1.81	-1.41	1.63	5.33	7.92	9.57	9.69	6.05
2068	1.369	2.93	0.39	-1.8	-2.3	-1.78	-1.41	1.65	5.34	7.94	9.6	9.71	6.05
2069	1.37	2.95	0.41	-1.79	-2.28	-1.76	-1.4	1.66	5.36	7.96	9.62	9.73	6.06
2070	1.371	2.96	0.43	-1.78	-2.26	-1.74	-1.4	1.67	5.37	7.98	9.64	9.75	6.07
2071	1.372	2.98	0.44	-1.77	-2.24	-1.72	-1.39	1.69	5.39	8	9.67	9.77	6.08
2072	1.373	3	0.46	-1.75	-2.21	-1.7	-1.38	1.7	5.4	8.01	9.69	9.79	6.09
2073	1.374	3.02	0.48	-1.74	-2.19	-1.68	-1.38	1.72	5.41	8.03	9.72	9.81	6.09
2074	1.375	3.03	0.5	-1.73	-2.17	-1.66	-1.37	1.73	5.43	8.05	9.74	9.83	6.1
2075	1.376	3.05	0.52	-1.72	-2.15	-1.64	-1.37	1.74	5.44	8.07	9.76	9.85	6.11
2076	1.377	3.07	0.54	-1.7	-2.13	-1.62	-1.36	1.76	5.45	8.08	9.79	9.87	6.12
2077	1.377	3.09	0.55	-1.69	-2.11	-1.6	-1.35	1.77	5.47	8.1	9.81	9.89	6.13
2078	1.378	3.1	0.57	-1.68	-2.08	-1.58	-1.35	1.78	5.48	8.12	9.84	9.91	6.13
2079	1.379	3.12	0.59	-1.67	-2.06	-1.56	-1.34	1.8	5.49	8.14	9.86	9.93	6.14
2080	1.38	3.14	0.61	-1.65	-2.04	-1.54	-1.34	1.81	5.51	8.16	9.88	9.95	6.15
2081	1.381	3.15	0.63	-1.64	-2.02	-1.51	-1.33	1.82	5.52	8.17	9.91	9.97	6.16
2082	1.382	3.17	0.65	-1.63	-2	-1.49	-1.32	1.84	5.53	8.19	9.93	9.99	6.17
2083	1.383	3.19	0.66	-1.62	-1.98	-1.47	-1.32	1.85	5.55	8.21	9.95	10.01	6.17
2084	1.384	3.21	0.68	-1.6	-1.95	-1.45	-1.31	1.86	5.56	8.23	9.98	10.03	6.18
2085	1.385	3.22	0.7	-1.59	-1.93	-1.43	-1.31	1.88	5.57	8.25	10	10.05	6.19
2086	1.386	3.24	0.72	-1.58	-1.91	-1.41	-1.3	1.89	5.59	8.26	10.03	10.06	6.2
2087	1.387	3.26	0.74	-1.57	-1.89	-1.39	-1.29	1.9	5.6	8.28	10.05	10.08	6.21
2088	1.388	3.28	0.76	-1.55	-1.87	-1.37	-1.29	1.92	5.62	8.3	10.07	10.1	6.21
2089	1.389	3.29	0.78	-1.54	-1.85	-1.35	-1.28	1.93	5.63	8.32	10.1	10.12	6.22
2090	1.39	3.31	0.79	-1.53	-1.83	-1.33	-1.28	1.94	5.64	8.33	10.12	10.14	6.23
2091	1.391	3.33	0.81	-1.52	-1.8	-1.31	-1.27	1.96	5.66	8.35	10.14	10.16	6.24
2092	1.392	3.35	0.83	-1.51	-1.78	-1.29	-1.26	1.97	5.67	8.37	10.17	10.18	6.25
2093	1.393	3.36	0.85	-1.49	-1.76	-1.27	-1.26	1.98	5.68	8.39	10.19	10.2	6.25
2094	1.394	3.38	0.87	-1.48	-1.74	-1.24	-1.25	2	5.7	8.41	10.22	10.22	6.26
2095	1.395	3.4	0.89	-1.47	-1.72	-1.22	-1.25	2.01	5.71	8.42	10.24	10.24	6.27
2096	1.396	3.41	0.9	-1.46	-1.7	-1.2	-1.24	2.03	5.72	8.44	10.26	10.26	6.28
2097	1.396	3.43	0.92	-1.44	-1.67	-1.18	-1.23	2.04	5.74	8.46	10.29	10.28	6.29
2098	1.397	3.45	0.94	-1.43	-1.65	-1.16	-1.23	2.05	5.75	8.48	10.31	10.3	6.29
2099	1.398	3.47	0.96	-1.42	-1.63	-1.14	-1.22	2.07	5.76	8.5	10.33	10.32	6.3
2100	1.399	3.48	0.98	-1.41	-1.61	-1.12	-1.22	2.08	5.78	8.51	10.36	10.34	6.31
2101	1.4	3.5	1	-1.39	-1.59	-1.1	-1.21	2.09	5.79	8.53	10.38	10.36	6.32
2102	1.401	3.52	1.01	-1.38	-1.57	-1.08	-1.2	2.11	5.81	8.55	10.41	10.38	6.32
2103	1.402	3.54	1.03	-1.37	-1.54	-1.06	-1.2	2.12	5.82	8.57	10.43	10.4	6.33
2104	1.403	3.55	1.05	-1.36	-1.52	-1.04	-1.19	2.13	5.83	8.58	10.45	10.42	6.34
2105	1.404	3.57	1.07	-1.34	-1.5	-1.02	-1.19	2.15	5.85	8.6	10.48	10.43	6.35
2106	1.405	3.59	1.09	-1.33	-1.48	-1	-1.18	2.16	5.86	8.62	10.5	10.45	6.36
2107	1.406	3.6	1.11	-1.32	-1.46	-0.97	-1.17	2.17	5.87	8.64	10.52	10.47	6.36
2108	1.407	3.62	1.12	-1.31	-1.44	-0.95	-1.17	2.19	5.89	8.66	10.55	10.49	6.37
2109	1.408	3.64	1.14	-1.29	-1.41	-0.93	-1.16	2.2	5.9	8.67	10.57	10.51	6.38

APPENDIX 2

Appendix 2.1 Results from Ice flow model calibration

Round 1				Round 2				Round 3			
A_0 ($\times 10^{15}$ s^{-1} (kPa) $^{-3}$)	Basal Melt Rate (m yr $^{-1}$)	Water Lubrication Factor	RMSE (m)	A_0 ($\times 10^{15}$ s^{-1} (kPa) $^{-3}$)	Basal Melt Rate (m yr $^{-1}$)	Water Lubrication Factor	RMSE (m)	A_0 ($\times 10^{15}$ s^{-1} (kPa) $^{-3}$)	Basal Melt Rate (m yr $^{-1}$)	Water Lubrication Factor	RMSE (m)
6.8	0.6	0.0	7.831	5.5	0.6	0.1	5.849	5.4	0.7	0.1	5.621
6.8	0.6	0.1	5.493	5.5	0.6	0.2	4.950	5.4	0.7	0.2	4.550
6.8	0.6	0.2	6.101	5.5	0.6	0.3	5.967	5.4	0.7	0.3	5.589
6.8	0.6	0.3	8.301	5.5	0.8	0.1	5.408	5.4	0.8	0.1	5.492
6.8	0.8	0.0	7.546	5.5	0.8	0.2	4.452	5.4	0.8	0.2	4.426
6.8	0.8	0.1	5.036	5.5	0.8	0.3	5.672	5.4	0.8	0.3	5.514
6.8	0.8	0.2	5.795	5.5	1.0	0.1	5.717	5.4	0.9	0.1	5.561
6.8	0.8	0.3	8.207	5.5	1.0	0.2	4.900	5.4	0.9	0.2	4.538
6.8	1.0	0.0	7.818	5.5	1.0	0.3	6.146	5.4	0.9	0.3	5.662
6.8	1.0	0.1	5.377	5.2	0.6	0.1	6.108	5.3	0.7	0.1	5.711
6.8	1.0	0.2	6.170	5.2	0.6	0.2	4.942	5.3	0.7	0.2	4.542
5.7	0.6	0.0	8.424	5.2	0.6	0.3	5.577	5.3	0.7	0.3	5.460
5.7	0.6	0.1	5.711	5.2	0.8	0.1	5.683	5.3	0.8	0.1	5.583
5.7	0.6	0.2	5.020	5.2	0.8	0.2	4.416	5.3	0.8	0.2	4.413
5.7	0.6	0.3	6.270	5.2	0.8	0.3	5.266	5.3	0.8	0.3	5.364
5.7	0.6	0.4	8.228	5.2	1.0	0.1	5.972	5.3	0.9	0.1	5.651
5.7	0.8	0.0	8.160	5.2	1.0	0.2	4.856	5.3	0.9	0.2	4.525
5.7	0.8	0.1	5.263	5.2	1.0	0.3	5.708	5.3	0.9	0.3	5.512
5.7	0.8	0.2	4.545	4.9	0.6	0.1	6.441				
5.7	0.8	0.3	6.014	4.9	0.6	0.2	5.045				
5.7	0.8	0.4	8.203	4.9	0.6	0.3	5.303				
5.7	1.0	0.0	8.411	4.9	0.8	0.1	6.017				
5.7	1.0	0.1	5.582	4.9	0.8	0.2	4.514				
5.7	1.0	0.2	4.985	4.9	0.8	0.3	4.923				
5.7	1.0	0.3	6.482	4.9	1.0	0.1	6.299				
4.6	0.0	0.0	12.348	4.9	1.0	0.2	4.932				
4.6	0.0	0.1	10.635	4.9	1.0	0.3	5.366				
4.6	0.0	0.2	9.691								
4.6	0.0	0.3	9.512								
4.6	0.0	0.4	9.886								
4.6	0.2	0.0	11.056								
4.6	0.2	0.1	9.073								
4.6	0.2	0.2	7.969								
4.6	0.2	0.3	7.777								
4.6	0.2	0.4	8.340								
4.6	0.4	0.0	10.027								
4.6	0.4	0.1	7.742								
4.6	0.4	0.2	6.416								
4.6	0.4	0.3	6.279								
4.6	0.4	0.4	7.055								
4.6	0.6	0.0	9.348								
4.6	0.6	0.1	6.804								
4.6	0.6	0.2	5.264								
4.6	0.6	0.3	5.148								
4.6	0.6	0.4	6.216								
4.6	0.8	0.0	9.099								
4.6	0.8	0.1	6.398								
4.6	0.8	0.2	4.741								
4.6	0.8	0.3	4.737								
4.6	0.8	0.4	5.973								
4.6	1.0	0.0	9.313								
4.6	1.0	0.1	6.659								
4.6	1.0	0.2	5.127								
4.6	1.0	0.3	5.148								
4.6	1.0	0.4	6.435								
3.5	0.6	0.0	10.558								
3.5	0.6	0.1	8.480								
3.5	0.6	0.2	6.876								
3.5	0.6	0.3	5.905								
3.5	0.6	0.4	5.707								
3.5	0.6	0.5	6.204								
3.5	0.8	0.0	10.315								
3.5	0.8	0.1	8.137								
3.5	0.8	0.2	6.473								
3.5	0.8	0.3	5.454								
3.5	0.8	0.4	5.317								
3.5	0.8	0.5	5.846								
3.5	1.0	0.0	10.483								
3.5	1.0	0.1	8.319								
3.5	1.0	0.2	6.679								
3.5	1.0	0.3	5.758								
3.5	1.0	0.4	5.626								
3.5	1.0	0.5	6.291								